Author/s:
Liu, Bingxin

Title:
Nontoxic Thermochromic Materials

Date:
2019

Persistent Link:
https://hdl.handle.net/11343/235597

Nontoxic Thermochromic Materials

Bingxin Liu

Submitted in total fulfilment of the requirements of the degree of Doctor of Philosophy

October 2019

Department of Chemical Engineering

The University of Melbourne

Abstract

Thermochromic products have had great commercial success in the past with colour changing products, the most well-known being the American Coor's beer can, which saw a spike in sales at its introduction. A large range of thermochromic materials and systems, such as liquid crystals, photonic crystals, gold or silver nanoparticles, leuco dye systems, polydiacetylene derivatives and aggregachromic dyes, have been developed for industrial applications. However, concerns about their safety have limited their application in the area of food packaging. Intelligent thermochromic food packaging has the potential to monitor food quality, trace thermal history and deter anticounterfeiting. The research presented here is aimed at the development of a nontoxic and versatile thermochromic material for the next generation of intelligent food packaging.

In this work, sulfonephthalein-solvent binary systems have been demonstrated to show clear and reversible colour change which is triggered by melting or freezing of the solvent component. This system comprises of a commercially available sulfonephthalein pH indicator dye, such as chlorophenol red, bromothymol blue, bromocresol purple, bromocresol green, bromophenol blue and thymol blue, dissolved in liquid linear chain esters, acids, alcohols or water. It was determined that the colour changing mechanism is based on π-π stacked aggregation or disaggregation of the sulfonephthalein dyes during the phase transition of solvent. Cell toxicity tests confirmed that the sulfonephthaleins are nontoxic.

With the choice of a nontoxic solvent, this binary system can form a nontoxic thermochromic material. To make this new material more broadly applicable, microencapsulation of the binary system into a practical and workable medium for applications in ink and film is necessary. Sulfonephthalein-water thermochromic system was then developed into a microcapsule form with silicone shells prepared via reaction between water and octadecyltrichlorosilane at the interface of a w/o emulsion. The obtained microcapsules also exhibited clear colour change with full reversibility and were successfully used as inks by screen printing and as additives in films. Nontoxicity of both microcapsules and films were demonstrated through cell cytotoxicity assays.

To show the thermochromic performance at ambient temperatures, a hybrid polymeric sensor containing dispersed sulfonephthalein-fatty acid particles was then developed. The obtained sensor exhibited potential as a time-temperature indicator according to its irreversible thermochromic behaviour from the dissolution and diffusion of the binary system in polymeric matrix. This sensor also showed obvious and irreversible halochromic behaviour in ammonia or bio-amines vapor.

These colour change functions coupled with the non-toxic nature of ingredients and ease of preparation, make these novel materials applicable for the next generation of intelligent food packaging materials.

Declaration

This is to certify that

(i) This thesis comprises only my original work towards the Ph.D. except where indicated in the Preface,

(ii) Due acknowledgement has been made in the text to all other material used,

(iii) This thesis is less than 100,000 words in length, exclusive of tables, figures, bibliography and appendices.

Bingxin Liu

October 2019

Preface

Cell toxicity tests described in Chapter 2 and Chapter 3 were carried out by Dr. Hadi Ranji-Burachaloo and Ms. Alicia Rasines Mazo, respectively.

Molecular dynamic simulations described in Chapter 2 were carried out by Dr. Eirini Goudeli.

3D-printed moulds described in Chapter 3 was prepared by Mr. Tom Pattison.

Acknowledgements

This work has been made possible through the support of many people. Firstly, I really thank my Supervisors Greg Qiao and Paul Gurr for providing the opportunity for me to work and study in the Polymer Science Group at The University of Melbourne. I appreciate your guidance and help no matter in the materials synthesis, theoretical explanation, writing papers and attending conferences. Without your support and the facilities of this group, I can't finish my work during the Ph.D. period. Also, I really appreciate my Chairman of Committee Dr. Daniel Heath, who always supported me firmly and provided practical advice so that I can finish all the work more efficiently in time.

Secondly, I want to thank all my colleagues and friends in Polymer Science Group, including Ms. Alicia Rasines Mazo, Ms. Wenlian Qiu, Dr. Fatemeh Karimi, Dr. Qiang Fu, Ms. Stephanie Allison, Dr. Hadi Ranjiburachaloo, Mr. Min Liu, Dr. Ke Xie, Dr. Amin Reyhani, Dr. Joel Scofield, Dr. Tom McKenzie and Mr. Tom Pattison. Your help and cooperation have enabled my work to be carried out and completed smoothly. The most important thing is that every time I was facing something difficult, I received all kind of advice and help from you guys, which is an invaluable experience.

I also acknowledge Dr. Eirini Goudeli for help on the molecular dynamic simulations, Prof. Jonathan White and Dr. Marc Antoine Sani for their assistance on the analysis of single crystals and solid NMR spectra respectively. I also thank Dr. Srinivas Mettu and Dr. Matthew Biviano for their suggestions on emulsion and microencapsulation techniques. My sincere thanks to Ms. Sioe See Volaric, a lovely lady, who allows me to perform all the ‘tedious’ experiments in her lab. Special thanks to my RPs and summer project students, including Jiaxi, Chuan, Shilin and Alvin, for all your assistance.

I wish to thank various funding sources that have made this work possible, including the Australian Research Council, The University of Melbourne, Department of Chemical Engineering and Particulate Fluids Processing Centre. Last but not least, my deepest thankyou to my parents and other family members for firmly supporting me study abroad. Also thankyou to other friends, including but not limited to Zhijian, Shuanglong, Yili, Fengjie, Sadegh, Ming, Jian, Liu, Kejie, Fan, Zhongyi, Jeroen, Yiran, Xiangyu, Tianshi, Ruixin, Hongjiao, Tao, Kai, Yiyuan, Xinyan, Jinguk, Shu, Shereen, Emma, Steven, Ignacio, Ross and Eric.

Publications

Peer-reviewed Journal Papers

Chapter 1

'π-π Stacking in Thermochromic Materials'

Bingxin Liu, Paul A. Gurr and Greg G. Qiao

Journal of Materials Chemistry C, in preparation.

Chapter 2

'A nontoxic reversible thermochromic binary system via π-π stacking of sulfonephthaleins'

Bingxin Liu, Hadi Ranji-Burachaloo, Paul A. Gurr, Eirini Goudeli and Greg G. Qiao

Journal of Materials Chemistry C, **2019**, 7, 9335-9345.

Chapter 3

'Reversible Nontoxic Thermochromic Microcapsules'

Bingxin Liu, Alicia Rasines Mazo, Paul A. Gurr and Greg G. Qiao

ACS Applied Materials & Interfaces, **2020**, 12 (8), 9782-9789.

Chapter 4

'A Nontoxic Dual Thermochromic and Halochromic Sensor'

Bingxin Liu, Paul A. Gurr and Greg G. Qiao

ACS Sensors, in preparation.

Conference Proceedings

'Thermochromism in Food Packaging Applications'

Bingxin Liu, Joel M. P. Scofield, Paul A. Gurr, and Greg G. Qiao

- Australian Research Council (ARC) Industrial Transformation Research Program (ITRP) launch (Melbourne, Australia), 25th February 2016 (Poster)

'Thermochromic Smart Packaging for the Food Industry'

Bingxin Liu, Wenlian Qiu, Paul A. Gurr and Greg G. Qiao

- Australian Institute of Food Science & Technology (AIFST) 50th Anniversary Convention (Sydney, Australia), 17th-18th July 2017 (Poster)

'A nontoxic reversible thermochromic binary system via π–π stacking of sulfonephthaleins'

Bingxin Liu, Hadi Ranji-Burachaloo, Paul A. Gurr, Eirini Goudeli and Greg G. Qiao

- 5th Edition International Smart Materials and Surfaces (SMS) (Lisbon, Portugal), 23rd-25th October 2019 (Oral)

'Microcapsules and films of a nontoxic thermochromic binary system via π-π stacking of sulfonephthaleins'

Bingxin Liu, Hadi Ranji-Burachaloo, Paul A. Gurr, Eirini Goudeli and Greg G. Qiao

- 37th Australasian Polymer Symposium (APS) (Sunshine Coast, Australia), 10th-13th November 2019 (Oral)

Table of Contents

List of Figures

Chapter 1

Chapter 2

Figure 2.1 The chemical structures of (A) sulfonephthalein dyes: chlorophenol red (CPR), bromothymol blue (BTB), bromocresol purple (BCP), bromocresol green (BCG), bromophenol blue (BPB), and thymol blue (TB); (B) comparative dyes: methyl green (MG), crystal violet (CV), crystal violet lactone (CVL), and dimethyl yellow (DMY); and (C) solvents: straight chain aliphatic esters, acids and alcohols.

Figure 2.2 (A) Photographic images of the colour change between solid (25 °C) and liquid (70 °C) states of six sulfonephthalein dyes (0.07 mol%) in DA. (B) Standard CIE 1931 chromaticity chart showing the x–y values of the colour transition between solid (25 °C) and liquid (70 °C) state of samples a–f. (C) Photographic images of solid (25 °C) and liquid (70 °C) states of MG, CVL, DMY and CV (0.07 mol%) in DA.

Figure 2.3 (A) Photographic images of the colour change between solid (25 °C) and liquid (70 °C) states of CPR (0.07 mol%) in (a) hexadecanoic acid, (b) methyl hexadecanoate and (c) hexadecanol. (B) The corresponding UV-vis absorption spectra of all solid CPR–solvent samples (a–c) at 25 °C, showing strong absorption peaks at 541 nm compared to liquid samples (a'–c') at 70 °C independent of the functionality of the solvent.

Figure 2.4 (A) Photographic images of CPR–HD (0.07 mol%), CPR–TD (0.07 mol%), CPR–DD (0.07 mol%) and CPR–DD (0.2 mol%) in the solid state (20 °C, a–d) and liquid state (70 °C, a'–d'). (B) The corresponding UV-vis absorption spectra of solid (20 °C) samples a–d and liquid (70 °C) samples a'–d' and microscopic image of solid sample 'a'. (C) Captured images from a microscopic video of the solidification of sample 'a' upon cooling.

Figure 2.5 (A) Plots of UV-vis absorbance at 541 nm of CPR–DA vs. time upon cooling from 70 °C to 35 °C. The concentrations of CPR in the binary systems were 0.07 mol%, 0.03 mol%, 0.02 mol%, 0.01 mol% and 0.007 mol%, respectively. (B) Plots of colour change equilibrium time vs. concentration of dye in the CPR–DA binary system.

Figure 2.6 (A) Cytotoxicity of CPR, cyanidin chloride and rhodamine B base toward NIH-3T3 cells incubated for 24 h. (B) Comparison of the IC_{50} values of CPR, cyanidin chloride and rhodamine B base in NIH-3T3 cells. *$P < 0.05$ and **$P < 0.01$.

Figure 2.7 (A) Digital pictures of CPR–MDD binary system with a concentration of 0.07 mol% after being treated with ammonium hydroxide or hydrochloride vapour for 1 minute at 25 °C and corresponding solids at 0 °C. (B) The corresponding UV-vis spectra of sample a, a', b and b' and ring-closed or ring-opened molecular structures of CPR.

Figure 2.8 XRD patterns of pure (a) 100% solid TD, (b) CPR–TD solid binary system with 10 mol% CPR, (c) CPR–TD solid binary system with 25 mol% CPR and (d) 100% solid CPR powder.

Figure 2.9 (A) The photographic images of CPR–methanol samples with a concentration of (α) 0.0001 mol%, (β) 0.1 mol% and (γ) 2 mol% at 25 °C and -196 °C. The corresponding UV-vis absorption spectra indicate only sample β shows thermochromism. (B) ^1H NMR spectra of CPR (0.1 mol% and 2 mol%) in CD_3OD showing an

upfield shift for peaks a, b, b' and c. (C) A schematic representation of CPR molecules in solvent in a diluted liquid state, concentrated liquid state and diluted solid state.

Figure 2.10 Absorbance spectra of 1 (red solid line), 2 (green solid line), 3 (black solid line) and 4 CPR molecules (blue solid line) at -196 °C and 8 CPR molecules at 25 °C (black broken line).

Figure 2.S1 Plot of UV-Vis absorbance at 541nm of CPR-DA (0.07 mol%) vs. temperature upon heating from 35 °C to 48 °C.

Figure 2.S2 Photographic images of the colour change between solid (0 °C) and liquid (25 °C) state of six sulfonephthalein dyes (0.07 mol%) in MDD and corresponding coordinates in standard CIE 1931 chromaticity chart.

Figure 2.S3 Cytotoxicity of BCP, CPR, BTB, BCG, BPB and TB toward NIH-3T3 cells incubated for 24 hours.

Figure 2.S4 FTIR spectra of CPR-TD (10 mol%) liquid sample at 70 °C, solid sample at 25 °C and base vapour (aq. NH_4OH) treated solid sample at 25 °C.

Figure 2.S5 Initial (t = 0 ns) configuration (top) of the 8 CPR molecules dispersed in 200 methanol molecules (depicted by grey spheres) simulated in the NVT ensemble at (A) 25 °C and (B) –196 °C.

Figure 2.S6 A) Snapshot of benzene rings connected to the sulfoxide group (highlighted pink atoms) obtained by MD simulations of eight CPR molecules in 200 methanol molecules at –196 °C. Three pairs of benzene rings are shown. B) The interplanar distance and angle of the three pairs.

Chapter 3

Figure 3.1 The schematic diagram of the fabrication of CPR-water based microcapsules with crosslinked silicone shells and their application in crosslinked PDMS films.

Figure 3.2 Photographic images of aqueous CPR solutions at different concentrations (10^{-2} M, 10^{-3} M, 10^{-4} M and 10^{-5} M) and their w/o emulsions in toluene (volume ratio of 1:10) at melted (25 °C) and frozen states (-196 °C). The colour differences between melted and frozen states are evaluated by ΔE according to CIE2000.

Figure 3.3 Encapsulation percentage of encapsulated core part of sample BX_1, BX_2, BX_3 and BX_4 with different core-shell feed mass ratios (320:1, 40:1, 20:1 and 10:1) when core is CPR aqueous solution and shell material is OTS and corresponding photographic images of capsules in tubes.

Figure 3.4 ATR-FTIR spectra of core CPR aqueous solutions and core-shell microcapsules at 25 °C.

Figure 3.5 A) The optical microscopic image of core-shell microcapsules from BX_3. B) The scanning electron microscopic image of core-shell microcapsule from BX_3. C) The size distribution of core-shell microcapsules calculated by ImageJ analysis software based on the optical microscopic image. D) The size distribution of core-shell microcapsules analysed by dynamic light scattering.

Figure 3.6 A) Photographic images of core-shell microcapsules from BX_3 in centrifuge tubes at i) 25 °C and i') -80 °C and their corresponding x-y coordinates represented in the standard CIE 1931 chromaticity chart. B) DSC heat flow curves (5 °C/min, blue) and ΔE value-temperature curve (red) of BX_3 microcapsules in temperature range between -60 °C and 20 °C when colour of microcapsules at 25 °C is set as reference. C) ΔE values of BX_3 microcapsules over 30 thermal cycles between 25 °C (●) and -80 °C (●).

Figure 3.7 Thermochromic prototypes prepared from BX_3 microcapsules A) cast into a 3D-printed mould and B) screen printed as ink onto paper.

Figure 3.8 A) Photographic images of film at j) 25 °C and j') -80 °C and corresponding x-y coordinates represented in standard CIE 1931 chromaticity chart. B) DSC heat flow curves (5 °C/min, blue) and ΔE value-temperature curve (red) of film in temperature range between -60 °C and 20 °C when colour of film at 25 °C is set as reference. C) ΔE values of film over 30 thermal cycles between 25 °C (●) and -80 °C (●).

Figure 3.9 Cytotoxicity of microcapsules (2 mg/mL) or films (20 wt.% microcapsules in film) toward NIH-3T3 cells incubated for 24h. *P <0.05. The cells were incubated only with fresh medium in the control samples.

Figure 3.S1 The UV-Vis spectra of w/o emulsion of CPR aqueous solution (10^{-3} M) in toluene (volume ratio of 1:10) at melted (25 °C) and frozen states (-196 °C).

Figure 3.S2 The DSC heat flow curve of CPR aqueous solution (0.001 M) in heating and cooling processes between -60 °C and 20 °C (5 °C/min).

Figure 3.S3 Optical microscopy images of NIH-3T3 fibroblast cells (A) control, (B) incubated with 2 mg/mL microcapsules after 24h and (C) incubated with films (20 wt.% microcapsules in film) after 24 h.

Chapter 4

Figure 4.1 A) Preparation scheme of the hybrid film with PDMS as the polymeric medium and dispersed chlorophenol red-dodecanoic acid (CPR-DA) binary system as the functional particles. B) The molecular structures of CPR and DA.

Figure 4.2 Photographic images CPR-DA binary system and film samples (F_1 to F_6) at 25 ºC and 70 ºC. ΔE values indicate the colour difference of samples between 25 ºC and 70 ºC.

Figure 4.3 UV-Vis absorption spectra of CPR-DA binary system and film samples at 25 ºC and 70 ºC.

Figure 4.4 The UV-Vis absorbance change at 541nm of CPR-DA binary system (thickness of 10 mm) as a function of time when binary system cools down (from 70 ºC to 25 ºC or from 70 ºC to 35 ºC) or heats up (from 25 ºC to 45 ºC or from 25ºC to 55 ºC).

Figure 4.5 Thermochromic response time of CPR-DA binary system and film F_2 in cooling (70 ºC to 25 ºC or 70 ºC to 35 ºC) and heating (25 ºC to 45 ºC or 25 ºC to 55 ºC) process.

Figure 4.6 A) Photographic images of CPR-DA binary system and F_2 during the first cycle of heating and cooling (25 ^oC-70 ^oC-25 ^oC, 30 minutes at each temperature). B) Corresponding UV-Vis absorption spectra of F_2 during the first cycle of heating and cooling. C) The schematic diagram of F_2 during the first cycle of heating and cooling.

Figure 4.7 A) The photographic image of F_2 (25 ^oC) in original state, after 10 cycles of heating (70 ^oC, 30 mins) and cooling (25 ^oC, 30 mins) and after 50 cycles of heating (70 ^oC, 30 mins) and cooling (25 ^oC, 30 mins). B) The corresponding optical microscopic images of cold F_2 (25 ^oC). C) The schematic diagram of migration of binary system in F_2.

Figure 4.8 A) The ΔE value of cold F_2 (25 ^oC) after being treated in two different ways: i) continuous heating at 45 ^oC; ii) intermittent cycles of heating at 45 ^oC for 30 minutes and cooling at 25 ^oC for 30 minutes. B) The ΔE values of cold F_1-F_6 (25 ^oC) after continuous heating at 45 ^oC.

Figure 4.9 A) The standard curve and equation of absorbance at 435nm vs. CPR concentration in aqueous solution (pH=3, light pathway length=10 mm). B) The weight percentage of leached CPR from F_2 and laminated F_2 to water (pH=3) as a function of time.

Figure 4.10 A) The photographic images of F_2 before and after being exposed in ammonia vapor (aq. NH_4OH) for one minute at 25 ^oC. B) Molecular structure change of CPR in the reaction with ammonia. C) Corresponding UV-Vis absorption spectra of F_2 at 25 ^oC.

Figure 4.11 Photographic images of F_2 placed with a&a') fresh fish or beef, b&b') fish or beef at 25 ^oC for 4 days, c&c') fish or beef at -18 ^oC for 4 days and d&d') sample F_2 after removal of fish or beef then left for 24 hours at 25 ^oC.

List of Tables

Chapter 1

Chapter 2

Chapter 3

Chapter 4

List of Abbreviations and Notations

ATCC	American type culture collection
BBS	4,4'-*bis*(2-benzoxazolyl) stilbene
BCG	Bromocresol green
BCP	Bromocresol purple
BDBn	1,3-*bis*(hydroxyalkylamino)-4,6-dinitrobenzenes
BPA	Bisphenol A
BPB	Bromophenol blue
BTB	Bromothymol blue
CAD	Computer-aided design
CCA	Crystalline colloidal arrays
CCK	Cell counting kit
CD	Cyanine dye
CD_3OD	Deuterated methanol
CLCs	Cholesteric liquid crystals
COPVs	Cyano substituted *oligo*(*p*-phenylene vinylene) derivatives dyes
CPR	Chlorophenol red
CV	Crystal violet
CVL	Crystal violet lactone
DA	Dodecanoic acid
DBCOT	Dibenzocyclooctatetraene
DD	Dodecanol
DDG	Dodecyl gallate
DDQ	2,3-Dichloro-5,6-dicyano-1,4-benzoquinone
DLS	Dynamic light scattering
DMEM	Dulbecco's modified Eagle's medium
DMTs	Dynamic molecular tweezers
DMY	Dimethyl yellow
DSC	Differential scanning calorimetry
DTPP	2,6-Diphenyl-4-2,4,6-(triphenyl-1-pyridinio)-phenolate
FBS	Fetal bovine serum
Fcc	Face-centred-cubic
FTIR	Fourier transform infrared
HLA	Hyaluronic acid
HA	Hexadecanoic acid
HD	1-Hexadecanol
HPC	Hydroxyl propyl cellulose
IC_{50}	Half-maximum inhibitory concentration
LCST	Lower critical solution temperature

LG	Lauryl gallate
Li-PCDA	Lithium salt of 10,12-pentacosadiynoic acid
LLDPE	Linear low-density polyethylene
MD	Molecular dynamics
MDD	Methyl dodecanoate
Methacrylate-PDMS	(Methacryloxypropyl)methylsiloxane-dimethylsiloxane copolymer
MG	Methyl green
MH	Methyl hexadecanoate
NG-NH_2	Amino-functionalized PNIPAM-*co*-PGMA microgels
NMR	Nuclear magnetic resonance
o/w	Oil in water
OD	1-Octadecanol
ODG	Octadecyl gallate
OG	Octyl gallate
OTS	Octadecyltrichlorosilane
PA	Polyamide
PAA-PIA	Poly(acrylic acid-*co*-itaconic acid)
PAA-PMA	Poly(acrylic acid-*co*-methacrylic acid)
PBMA	Poly(benzylmethacrylate)
PCFF	Polymer consistent force field
PDA/MA	Poly (10,12-pentacosdiynoic acid)/melamine
PDAs	Polydiacetylenes
PDMS	Poly(dimethylsiloxane)
PE	Polyethylene
PEG	Polyethylene glycol
PEI	Poly(ethylene imine)
PEO	Polyethylene oxide
PET	Poly(ethylene terephthalate)
PETG	Poly(ethylene terephthalate glycol)
PEVA	Poly(ethylene-*co*-vinyl alcohol)
PG	Propyl gallate
PGPR	Polyglycerol polyricinoleate
PIL	Polymeric ionic liquid
PLA	Polylactide
PLGA	Poly(lactic-*co*-glycolic acid)
PMMA	Poly(methylmethacrylate)
PNIPAM	Poly(*N*-isopropyl acrylamide)
PNIPAM-*co*-PAA	Poly(*N*-isopropylacrylamide-*co*-acrylic acid)
PNIPAM-*co*-PGMA	Poly(*N*-isopropylacrylamide-*co*-glycidylmethacrylate)
PNIPAM-*co*-PHEA	Poly(*N*-isopropylacrylamide-*co*-2-hydroxyethyl acrylate)

PO	Polyolefin
Poly[PheDOT-$(C_{12})_2$]	Poly[3,4-(4,5-didodecylphenylene) dioxythiophene]
PP	Polypropylene
PVA	Polyvinyl alcohol
PVC	Poly(vinyl chloride)
PVDF-PHFPP	Poly(vinylidene fluoride-co-hexafluoropropylene)
PVP	Polyvinyl pyrrolidone
PZPER	*N,N'-bis*(2-(1-piperazino)ethyl)-3,4,9,10-perylenetetracarboxylic acid diimide dichloride
QR	Quick response
RFID	Radio-frequency identification
R-Pery	*N,N'-bis*-(*R*)-(1'-phenylethyl)-perylene-3,4,9,10-tetracarboxyldiimide
SEM	Scanning electron microscopy
SPEEK	Sulfonated poly(ether ether ketone)
TB	Thymol blue
TD	1-Tetradecanol
TEM	Transmission electron microscopy
TTIs	Time-temperature indicators
UV-Vis	Ultraviolet-visible
Vinyl-PDMS	Vinylmethylsiloxane-dimethylsiloxane copolymer
w/o	Water-in-oil
w/o/w	Water-in-oil-in-water
XRD	X-ray diffraction

d_i	Distance
d	Doublet
dd	Doublet of doublets
f	Functionality
n	Refractive index
T_c	Colour change temperature
T_f	Freezing point
T_g	Glass transition temperature
T_m	Melting point
t	Triplet
θ	Angle
λ	Wavelength

Chapter 1. Introduction

1.1 Background

1.1.1 Food security

In every culture food plays a major role in tradition, community and family life as well as being a source of nourishment. The importance of food quality has always been a very important aspect of daily life, as it can protect people from disease, infection, malnourishment as well as enhance consumer health and well-being. Food quality and security is especially important in fast developing countries, where there is an increase in disposable income to be able to import high quality foods from developed countries. As the distance and time required for food to be transported increases, so does the need for packaging to protect as well as indicate the quality of the product it contains. Food packaging is essentially important because it slows down food quality deterioration and makes distribution and marketing more efficient.[1] A reliable food supply chain is the foundation of modern life in every country. Yet people who are living in some developing countries often suffer from problems caused by unsafe food due to poor quality or counterfeited brands. Many incidences relating to food security have been reported in relation to contaminated cooking oil, illegal and toxic food additives in food products such as baby formulas.[2] These incidents cause serious concern among consumers in these areas and make local food less trustworthy. As a result, consumers prefer to purchase food products from other countries which are generally regarded as safe but with the added burden of longer transport times and requiring longer shelf lives. In light of such contamination incidences and the challenges of transport and counterfeiting, food packaging can be used as a valuable tool in solving these problems.

1.1.2 Intelligent Food Packaging

Intelligent food packaging, which accurately and objectively gives an indication of the quality of internal food products is one way to ensure quality, safety and consumer confidence. However, the majority of food packages only provide simple information, such as food ingredients, date of manufacture and an estimation of shelf-life by use-by dates. Use-by dates are typically underestimated to ensure consumer safety as the quality of the food is also closely related to the environmental conditions during transport, storage and sale. Typically, consumers have to judge the current quality of food themselves based on this simple information, with perhaps only producers, distributors or suppliers having access to supply chain tracking, food testing protocols or counterfeit detection. Therefore, there is a growing desire for intelligent packaging technologies to inform customers of direct food quality giving them confidence in the product to make the correct decisions when choosing safe and reliable food.

In the field of intelligent packaging progress has already developed offering thermochromic labels, freshness indicators, gas indicators, barcodes, quick response (QR) or 2-dimensional (2D) barcodes, radio-frequency identification (RFID) and biosensors as typical examples of conveying food quality or the history of supply chain.

Freshness indicators provide direct information on the products' quality throughout storage and transportation regarding microbial growth or chemical changes.[3] Gas indicators monitor the inside atmosphere of packaging due to leakage, internal chemical reactions or microorganism metabolism.[4] Barcodes and QRs consist of patterns of parallel bars and spaces that encode information about the products contained in the packages and have been widely used due to its low cost.[5] RFID technology can verify the products' information where-by readers emit radio signals and receive feedback from the tags attached the product or container.[6] Other advanced technologies, such as holograms and high-resolution printing techniques have also been used on packages. These technologies enhance packaging abilities and provide functions not available in traditional packaging. However, some of these technologies require extra equipment and materials, which leads to increased production cost. Each technology has its limitations and the issue of toxicity has meant that some examples are only applied to particular products where potential contact with food for example is possible.

1.1.3 Thermochromic Food Packaging

Compared to other types of intelligent packaging, thermochromic packaging has drawn increasing interest from food suppliers, industrial manufacturers and retailers in recent years (Figure 1.1).[3, 7] Thermochromism is the colour changing property of materials in response to temperature change. Correspondingly, packages incorporated with thermochromic materials will show colour change simply based on thermal stimuli from their environment or human contact and the colour change phenomenon can be observed by the naked eye, without the need for extra equipment or devices.[1, 4] From a commercial perspective, it has been reported that thermochromic packaging alone can influence the consumers choice to purchase such products [8] Therefore, thermochromic packages as one of the mainstreams of intelligent packaging have the ability to protect the brands and guarantee the quality of internal products including food or healthcare products. In general, thermochromic packaging can provide three functions for food products in the following areas:

Food security: Secure transportation and storage of packaged food products before consumption are the main goals throughout the supply chain.[1] Thermochromic packages, such as time-temperature indicators (TTIs), can help consumers trace the food supply chain and alert consumers to the deterioration of internal food through exhibiting accumulative colour response to time and temperature in thermal history of products.[9]

Optimal temperature of consumption: Some food products should be stored at certain temperatures to preserve their flavour, for example cola, ice cream, chocolate, hot fries and chicken. Thermochromic packaging can help consumers to visualize if the food product is at the best consumption temperature for optimal enjoyment by displaying a specific colour at the appropriate temperature.

Anti-counterfeiting: Thermochromic packages showing different colours at specific temperature changes can identify authentic products and distinguish them from counterfeit products, who lack these features.[8]

Figure 1.1 Commercial examples of thermochromic packages and indicators.

1.2 Thermochromic Materials

To meet the requirements of food packaging usage, thermochromic materials should be nontoxic, low cost, accurately indicative, easily fabricated and processable.[1] In general, thermochromic materials can be divided into two types: reversibly thermochromic or irreversibly thermochromic (Figure 1.2). The colour of the reversibly thermochromic material is only related to the current temperature, regardless of thermal history of the material. Therefore, the colour will be recovered once the temperature reverts back to its original value. This type of material can be used as a tool for anti-counterfeiting packages where the product can repeatedly verify its authenticity.[8] In contrast, the colour of irreversibly thermochromic materials, alters as the temperature is increased, yet does not revert back to its original colour upon cooling. Therefore, the colour which remains is an indication of the temperature profile of the product and can be used to quantify possible food deterioration due to inappropriate temperature changes during transportation or storage.[9]

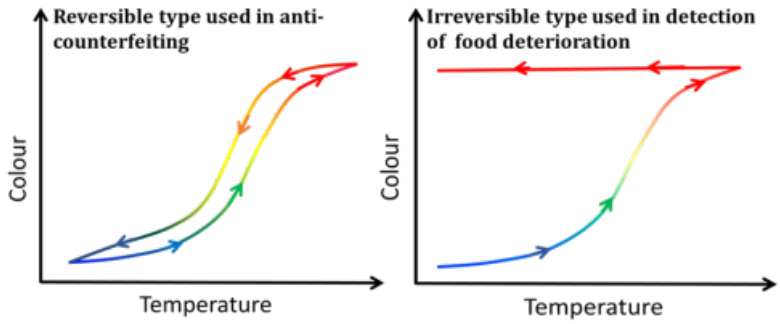

Figure 1.2 Reversible and irreversible types of thermochromism.

Scientists have developed various kinds of thermochromic materials based on different mechanisms, such as leuco dyes,[10] liquid crystals,[11] optical crystals,[12] dye-polymer mixtures,[13] conjugated polymers,[14] nanoparticles[15] and hydrogels[16]. To date, only cholesteric liquid crystals (CLCs) and leuco dye systems are widely applicable commercially among these materials.[17] In terms of scientific mechanisms, thermochromism can be divided into three main categories: reflection wavelength shift, absorption wavelength shift and surface plasmon resonance change.

Table 1.1 Classification of thermochromic materials.

Origin	Effect on light	System	Switch temperature
Change of optical path length in periodic structured materials	Reflection wavelength shift	Cholesteric liquid crystals	Various temperatures
		Bragg stacks	Lower critical solution temperature
		Crystalline colloidal arrays	Lower critical solution temperature or glass transition temperature
Structural change of chromophoric moieties	Absorption wavelength shift	Leuco dye system	Melting point
		Conjugated polymer	Various temperatures
		Inorganic-organic complex	Various temperatures
		Dye-hydrogel composite	Various temperatures
		Dye-polymer interaction composite	Glass transition temperature
		Pi-pi stacking	Glass transition temperature, melting point, lower critical solution temperature or various temperatures
Structural change of chromophoric moieties	Surface plasmon resonance change	A_u/A_g nanoparticles-polymer composite	Lower critical solution temperature or various temperatures

Bragg reflection wavelength shift is the most typical theory to explain thermochromism of CLCs and optical crystals or Bragg stacks. The reflected light from these materials usually follows the Bragg mirror reflection equation:

$$m\lambda = 2(\sum_i n_i d_i)$$

in which m is the order of diffraction while the reflection wavelength (λ) changes according to the change of distance (d_i) or refractive index (n_i) in the equation. The distance (d_i) could be spiral distance in CLCs or lamellar layer distance in stacks.[18] As a response to temperature changes, the reflection wavelength and refractive index shift due to expansion or contraction of the spiral structure or lamellar layers.

The molecular structures of dyes, some polymers and inorganic-organic complexes contain conjugated structures or unsaturated bonds, which absorb specific light at a corresponding wavelength.[19] These materials show colours if the corresponding wavelength is in visible range. At different temperatures, the absorption wavelength shifts as a result of configurational change of the conjugated structure or energy change of interactions in leuco dye systems, conjugated polymers, inorganic-organic complexes, dye-hydrogel composites and dye-polymer mixtures.

Surface plasmon resonance is the interaction between surface plasmon of nanoparticles and incident light when their frequencies match each other. Especially, the surface plasmon resonances of gold or silver nanoparticles are

in visible range and corresponding bands shift when the size, morphology, composition or shape of nanoparticles change.[15] Therefore, thermochromism occurs when gold or silver nanoparticles grow, agglomerate, change shape or change interparticle distance when they are incorporated into thermosensitive matrix.

1.2.1 Reflection wavelength shift

1.2.1.1 Cholesteric liquid crystals (CLCs)

Liquid Crystals, as the earliest thermochromic materials, was first found in 1888 by Reinitzer in a study of the properties of cholesterol esters, which led to the recognition of liquid crystals as distinct phases of matter.[20] The colour of CLCs is from reflection light, whose wavelength is dependent on the periodic spiral structure of the crystals (Figure 1.3). The periodic length of spiral structure in CLCs is called the 'pitch'. When the length of pitch and the wavelength of incident light meet the requirement of Bragg mirror reflection equation, this beam of light will be reflected by the liquid crystal.[21] Correspondingly, CLCs expand or contract its length of pitch at different temperatures leading to the shift of reflection wavelength and colour change.[22] In most cases, the basic requirement for a thermochromic liquid crystal includes a short-pitch chiral nematic phase with an underlying smectic phase. To date, only esters of cholesterol and ester derivatives of *(S)*-4-(2-methylbutyl)phenol have been successfully used as thermochromic liquid crystals.[22]

CLCs are still one of the commonly used thermochromic materials due to their fast and accurate response towards different temperatures.[17] In a review by Sage *et al.*, he outlined the most recent developments in material applications and devices of thermochromic liquid crystals.[22] White and co-workers looked at the unique dynamic colour changes observed in potential commercially available CLCs.[23] So far, thermochromic liquid crystals can be coated uniformly on the packaging substrates by flexographic, gravure, inkjet and screen-printing methods with highly specialized printing and handling techniques.[24] Aside from Flodberg's report which studied the level of migration of monomers and oligomers from poly(phydroxybenzoic acid-co-2-hydroxy-6-naphthoic acid) liquid crystalline polymer when it is used as the food packaging material, few studies have reviewed the toxicity of the components.[25] Results indicate the estimated daily intakes of those monomers exceed FDA approved thresholds at severe testing conditions making this polymer unavailable as a food packaging material. Therefore, toxicity, high cost and the weaken colour change effects of thermochromic liquid crystals limit their application to most commercial thermochromic products, especially the food packages.[17]

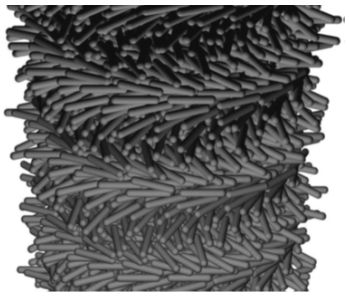

Figure 1.3 The schematic diagrams of spiral structure in thermochromic liquid crystals.[22]

1.2.1.2 Bragg stacks

The thermochromism of photonic crystals, including Bragg stacks and crystalline colloidal arrays, are usually dependent on the thermal sensitive properties of polymers such as poly(*N*-isopropyl acrylamide) (PNIPAM) [12] Poly(*N*-isopropyl acrylamide) (PNIPAM) is known to swell when hydrated at temperatures below its lower critical solution temperature (LCST, about 32°C) and when the temperature is above the LCST it dehydrates and shrinks.[26].

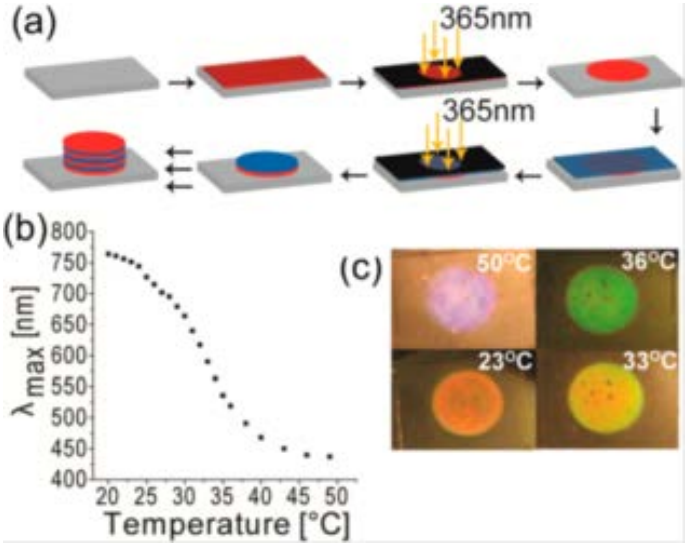

Figure 1.4 Schematic diagrams of layer by layer fabrication process and the resultant thermochromism.[27]

Bragg stacks are formed by at least two kinds of materials with different refractive indexes. The structure of Bragg stacks usually consists of alternate layers laminated together (Figure 1.4).[27] The incident light thus is reflected partially at each boundary between the two layers due to refractive index difference and the wavelength of reflection is determined by the refractive index difference and thickness of each layer according to Bragg's law.[28] If one of these materials is thermosensitive, the thickness and refractive index of corresponding layer varies upon a temperature change. As a result, the wavelength of reflection light changes accordingly and the stack exhibits colour change. Therefore, thermochromic Bragg stacks should contain at least one material that changes refractive index or layer thickness with temperature.

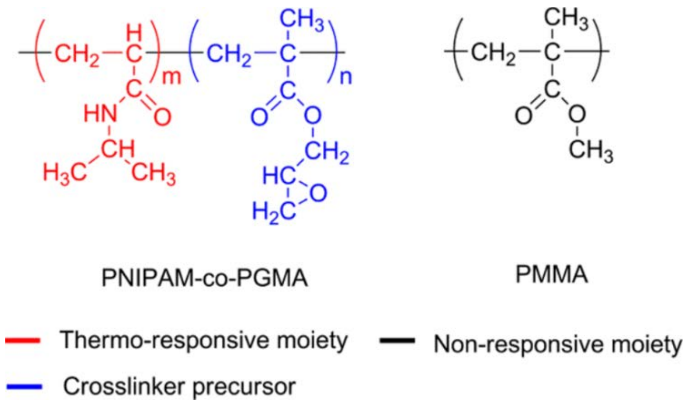

Figure 1.5 Thermosensitive structure in PNIPAM-*co*-PGMA and non-thermosensitive structure in PMMA.[18]

Accordingly, Wang reported a spin-coated thermochromic multilayer polymer film consisting of alternating layers of thermoresponsive poly(*N*-isopropylacrylamide-*co*-glycidylmethacrylate) (PNIPAM-*co*-PGMA) and nonthermoresponsive poly(methylmethacrylate) (PMMA) (Figure 1.5) which showed thermochromism as a result of thickness change of thermoresponsive layers upon a temperature change.[12] Matsubara and co-workers used 4-acryloylaminoazobenzene, *N*-isopropylacrylamide, and *N,N'*-methylenebisacrylamide to fabricate a copolymer gel matrix with multiple chromogenic effects that showed an improved local resolution of colour changing by temperature.[29] Although these thermochromic materials show reversible thermochromism in a short responsive time, they require solvation and may include realitvely toxic compoennts such as acrylamide monomers.

1.2.1.3 Crystalline colloidal arrays

Crystalline colloidal arrays (CCA) are three-dimension colloidal photonic crystals that consist of colloidal spheres or holes periodically. Therefore, the Bragg's law that crystalline colloidal arrays obey transform into:

$$m\lambda = 2nd_{hkl}sin\theta$$

where m is the order of diffraction. The wavelength of reflection light (λ) changes according to the change of interplanar spacing (d) of diffracting planes defined by the Miller indices (hkl) or mean refractive index (n) in the equation when the angle (θ) between the incident light and the planes is constant.[18] Asher *et al.* first reported this type of thermochromic photonic crystal in 1996 when his group used polystyrene spheres embedded into PNIPAM gel and found thermochromism due to the lattice space changing (Figure 1.6).[30]

Other researchers have reported thermochromic materials based on differences in refractive index, between thermochromic polymer matrixes and particles. Song *et al.* published a paper in 2013 reporting change of Bragg reflection intensity and wavelength of hydrogel samples consisting of poly(*N*-isopropylacrylamide-*co*-acrylic acid) (PNIPAM-*co*-PAA) thermoresponsive particles and poly(acrylamide/bisacrylamide) nonthermoresponsive matrix.[31] The contraction of thermoresponsive particles above their LCST resulted in larger refractive index contrast between particles and matrix, resulting into an increased reflection intensity. At the same time, the contraction of particles also leads to the declined volume of matrix, causing change of reflection wavelength due to a decreased lattice space.

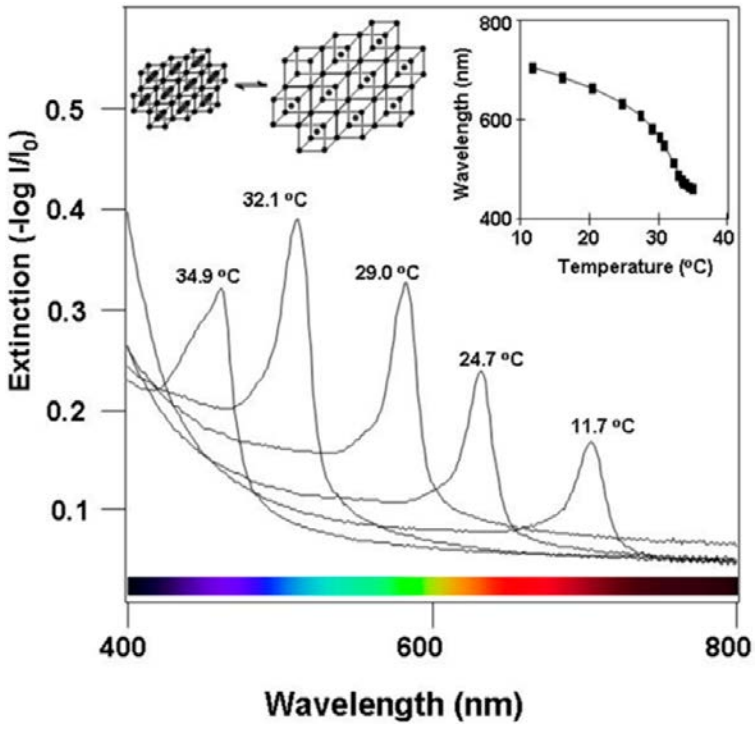

Figure 1.6 The diffraction wavelength shift of crystalline colloidal arrays using polystyrene spheres embedded into PNIPAM gel at different temperatures.[30]

In another example, thermoresponsive poly(*N*-isopropylacrylamide-*co*-2-hydroxyethyl acrylate) (PNIPAM-*co*-PHEA) copolymer nanoparticles were assembled and covalently crosslinked with a close-packed CCA. The sample changed colour from green to milky white at temperature above the LCST due to contraction of the nanoparticles, resulting in a loss of order and Bragg reflection.[32]

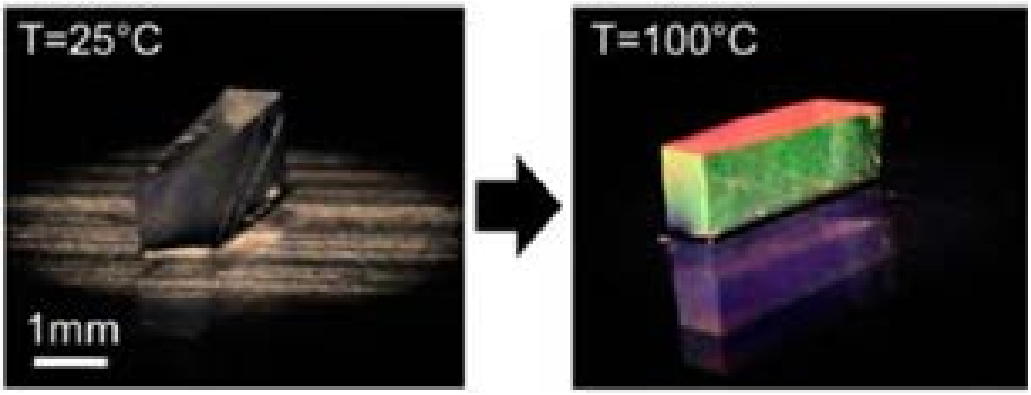

Figure 1.7 Photographic images of a polymer opal sample in matrix at 25 °C and 100 °C.[28]

Moreover, an industrially scalable method for manufacturing three-dimensional photonic crystals was reported, in which the core components of core-shell capsules assembled in a face-centred-cubic (fcc) structure within a thermoplastic matrix with the shell components of the capsules diffused into the matrix.[28] The core-shell capsules consisting of PMMA as core material and a mixture of poly(ethylacrylate) and poly(benzylmethacrylate) (PBMA) as the shell material. At room temperature, the refractive indexes of colloidal particles and matrix were

the same so that the sample was transparent (Figure 1.7). However, the refractive index of colloidal particles changed much less than that of the matrix when the temperature increased. Therefore, Bragg reflection occurred, and its intensity increased with temperature as a result of increased refractive index contrast between colloidal particles and matrix.

1.2.2 Absorption wavelength shift

1.2.2.1 Leuco dye systems

Leuco dye systems are the most commonly used and commercially available thermochromic material. The leuco dye system usually comprises of dye (with ring-opened or ring-closed structure), developer and solvent.[33] The developer interacts with the dye having a ring-opened structure which results in one colour of the leuco dye system. Upon a change in temperature, the dye converts to its ring-closed form with another colour as the developer coordinates with the solvent component. As shown in Figure 1.8, crystal violet lactone (CVL) molecules interact with lauryl gallate (LG) and open their rings to appear a dark colour at low temperature. As temperature increases, CVL molecules stop interaction with LG and close their rings to show a pale colour.[34] The colours of these systems can be varied by replacing the dye and developer components. Unlike liquid crystals, the leuco dye system shows a limited range of colours of the different dyes. Therefore, leuco dyes are usually used as a general indicator, which briefly shows 'high temperature' or 'low temperature', on products such as metallic containers, clothing and mugs. One famous example is from the 'Coors light' beer cans (Figure 1.2).

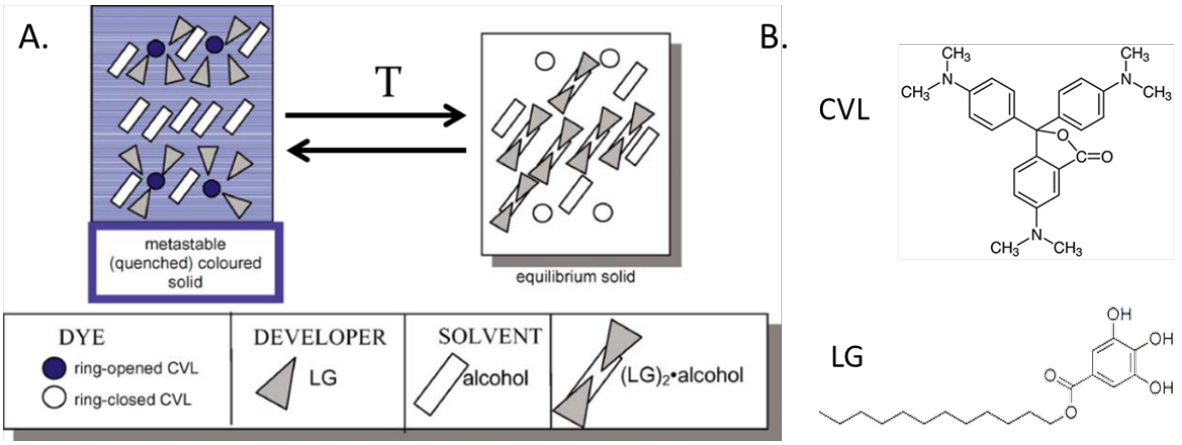

Figure 1.8 A) Schematic diagram indicating mechanism of thermochromism of crystal violet lactone-lauryl gallate-alcohol (CVL-LG-alcohol) leuco dye systems.[34] B) The molecular structures of CVL and LG.

The CVL–LG thermodynamic interaction potentials from a typical three-component (dye/developer/solvent) thermochromic leuco dye system were examined to reveal the thermochromic mechanism.[35] Through analysis of DSC results, microscopy, infrared and Raman spectroscopy, it is confirmed that LG:CVL forms a coloured complex in the ratio of 3:1, as an amorphous solid with ring-opened CVL. In a further paper, the metastability of coloured CVL-LG complex was found to be related to competition between dye-developer and developer-solvent interactions.[36] As a result, the rate of decolourisation can be achieved by adjusting the metastability of the leuco dye system via altering their developer-solvent interaction. In this context, the authors also used CVL with

different developers and solvents to study the developer-solvent interactions in the leuco dye systems and develop rules for reversibly thermochromic systems based on intermolecular interactions.[34] Propyl gallate (PG), octyl gallate (OG) and LG were used as alternative developer while 1-tetradecanol (TD), 1-octadecanol (OD) and 1-hexadecanol (HD) were used as alternative of solvent in the examined CVL-developer-solvent systems. It was found that high colour contrast and rapid decolorization rates could be achieved by using strongly attractive developer-solvent combinations that compete with attractive dye-developer complexes in the solid state. Similarly, the thermochromic behaviours of CVL-LG-alcohol three-component materials were investigated via changing the aliphatic chain length of alkyl alcohols.[37] Analysis reveals that orientationally disordered α-phase of the solvent with long enough chain is essential for the dye–developer complex generating colour change during cooling. On the other hand, solvents with too long chains will block the formation of coloured dye-developer complex during heating. Therefore, solvent with optimal chain length is required in leuco dye system. Furthermore, factors affecting thermochromic behaviours of CVL-developer-solvent leuco dye systems were studied via altering dodecyl gallate (DDG), octadecyl gallate (ODG), PG or OG as developer and TD, HD or OD as solvent.[38] The influence of alkyl chain length difference between developers and solvents on the thermochromic behaviour of these systems are summarized as: melt-darkened thermochromism was observed due to dominated developer-solvent interaction when the alkyl chain lengths match each other; melt-lightened thermochromism was observed due to dominated dye-developer interaction when the alkyl chain lengths are poorly matched. Besides, molar ratios of ternary components will be important to thermochromic behaviours when developer-solvent and dye-developer interaction strengths are very similar.

Although the leuco dye system is the most commonly used thermochromic material, its application towards food packaging area is still limited due to public concerns about toxic chemical migration. Bisphenol A (BPA), a very common chemical, is typically used as developer in leuco dye systems.[39-41] However, the toxicity of BPA has caused public concern and has affected the consumers' acceptance of thermochromic products using leuco dye systems.[42, 43] As a result, manufacturers try to avoid using BPA in the leuco dye system products and replace BPA with other chemicals. To date, numerous leuco dye systems have been prepared with triphenylmethane phthalides, rhodamine lactams, fluorans, phenothiazines, indolylphthalides, spiropyrans or leucoauramines as dye while thioureas, guanidines, benzothiazoles or benzothiazolyls as developer.[44] In general, the toxicity of most of these chemicals still remains unknown. Taking into account public concerns, an investigation about the attitude of those manufacturers was reported.[45] Results showed ink manufacturers reluctant to use leuco dye systems in any food application other than on glasses, metal or thick plastic where another layer of impermeable barrier is applied to separate the material from the food. Therefore, exploring alternative nontoxic components as substitutes in leuco dye systems posed a valid pursuit considering their current limitations.

1.2.2.2 Conjugated polymers

Conjugated polymers, e.g. polydiacetylenes (PDAs), polyacetylenes, poly (phenylene vinylidenes) and polythiophenes, contain conjugated structures with π electron clouds in polymer backbones.[18] Different conjugated structures absorb electromagnetic waves with different wavelengths. The colour of these materials can be observed by naked eye when the wavelength is in the visible range. Any conformational change of these

structures will lead to a shift of absorption wavelength. Therefore, conformational structure change of conjugated polymers at different temperatures can result in thermochromism.

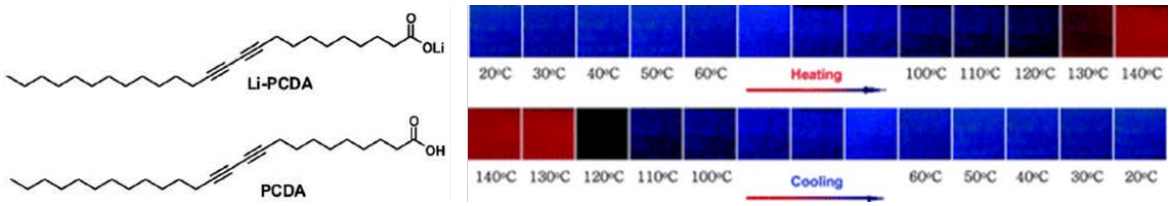

Figure 1.9 Molecular structures of Li-PCDA and PCDA and photographs of Li-PCDA solution embedded PVA films at different temperatures.[46]

The research of conjugated polymers has lasted for more than one hundred years, since Henry Letheby discovered polyaniline in the mid-19th century. Thermochromism of conjugated polymers also has been studied by lots of academics for decades to make continual progress. After studying the properties of poly(1,4-(2,5-dioctyloxyphenylene)-2,5-thiophene), poly(1,4-(2,5-dioctylphenylene)-2,5-furan), poly(1,4-(2,5-dioctylphenylene)-2,5-thiophene), poly(1,4-(2,5-dioctyloxyphenylene)-2,5-furan) and poly(1,4-(2,5-didodecyloxyphenylene)-2,5-(3,4- diethylenedioxythiophene)), Dufresne *et al.* found that subtle changes of conjugated structure would lead to completely different chromic behaviours of conjugated polymers. They also reported the conjugated polymers lost thermochromism when molecules steric interactions were too strong or too weak.[47] Furthermore, Yuan *et al.* reported a series of novel thermochromic PDAs, whose structures were connected by hydrogen bonding (H-bonding) on main chains.[48] In 2010, Balakrishnan *et al.* synthesised PDAs derived from lithium salt of 10,12-pentacosadiynoic acid (Li-PCDA) and found its reversible thermochromism (Figure 1.9).[46] Based on the theory that colour changing of PDAs was attributed to the changing of effective conjugation length of polymer backbone, researchers explained that the reversible thermochromism of Li-PCDA was owing to enhanced intermolecular head group interactions that recovered conjugation length of π-electron chromophores during temperature variation.[46] Guo *et al.* further introduced peptide amphiphilic molecules to the side chains of PDA fibres to make the reversible thermochromic speed ultrafast, which makes these fibres applicable to wearable electronics.[49]

1.2.2.3 Inorganic-organic complexes

Thermochromic inorganic-organic complexes are quite novel and have been reported by only a few researchers. These materials exhibit thermochromism based on the charge-transfer-complex formation (Figure 1.10). Jiang and co-workers fabricated a thermochromic polymer film consisting of $K_{12.5}N_{a1.5}[N_aP_5W_{30}O_{110}]$ ($N_aP_5W_{30}$) and poly(ethylene imine) (PEI) layers that would change its colour from yellow to blue in 30 minutes to 90 minutes when it was heated above 120 °C or from blue back to yellow in 180 minutes when it cooled down to room temperature and contacted to air.[50] The reversible colour change is attributed to charge transfer bridge formed by H-bond between $N_aP_5W_{30}$ and PEI.

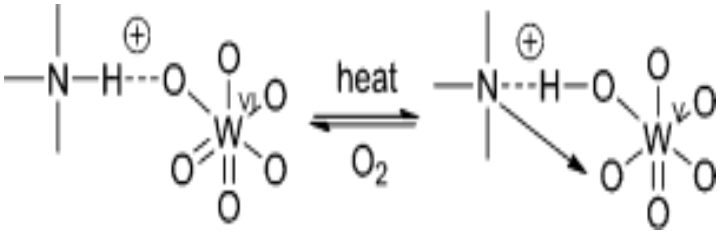

Figure 1.10 Structural change of an inorganic-organic ($N_aP_5W_{30}$-PEI) complexes towards temperature and oxygen.[50]

1.2.2.4 Dye-hydrogel composites

pH-indicators are known as colour changing dyes when pH of the solution changes. Similar to leuco dye, pH indicative dyes also absorb light with different wavelength and show different colour when the structure of chromophores convert at different protic or hydroxyl concentration in surrounding medium.[51] On the other hand, certain types of polymer-based hydrogels can provide an environment with variable protic concentration when temperature changes. Therefore, after being incorporated pH indicative dyes, those hydrogels would show thermochromism and the colour is dependent on the structure of corresponding dye molecules.

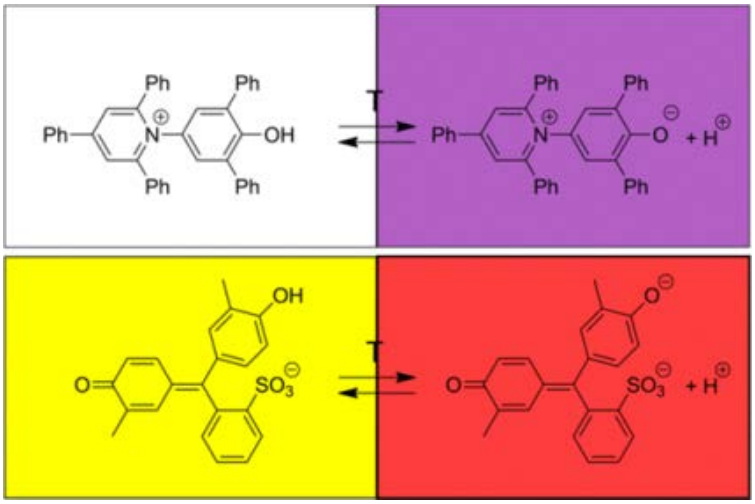

Figure 1.11 Molecular structural change of temperature dependent phenol−phenolate equilibria of DTPP and of cresol red.[18]

Seeboth *et al.* reported the first example of this type of thermochromic hydrogel with reversible thermochromism.[52] In this material, two dyes 2,6-diphenyl-4-2,4,6-(triphenyl-1-pyridinio)-phenolate (DTPP) and cresol red were incorporated into polyvinyl alcohol (PVA)-borax hydrogel, respectively. Both of these hydrogels showed colours due to the dye's deprotonated state when temperature heated to 80°C and fully reverted to their original colours when protonated upon cooling (Figure 1.11). Kriwanek *et al.* also investigated the thermochromism of phenol red-PVA-borax hydrogel and the influence of zwitterionic surfactant on chromogenic behaviour of this hydrogel.[53] Furthermore, it was indicated that only those pH-indicators with pK_a values between 7.0-9.4 showed thermochromism in the indicator-PVA-borax hydrogel system.[18] Naorem and co-workers published a paper in 2011 to illustrate the thermochromism of phenolphthalein-PVA-borax hydrogel when another polymer, such as polyvinyl pyrrolidone (PVP), hydroxyl propyl cellulose (HPC), polyethylene oxide

(PEO), gelatine A or agar, was mixed with PVA.[54] The disappearance of thermochromism was noted when the content of PVA in the blend was below 60% due to less formation of diol cross-links between borax and PVA.

1.2.2.5 Dye-polymer interaction composites

Some dyes, *e.g.* natural anthocyanin dyes with phenolic hydroxyl groups, can interact with polyesters via H-bonding. In this case, dye molecules change their structures and exhibit different colours when interaction starts or stops. Therefore, some scientists believe that different states of polyesters at different temperatures will result in different dye colours.[13] This kind of thermochromic composite is quite novel and only two reports have described this phenomenon.[13, 55]

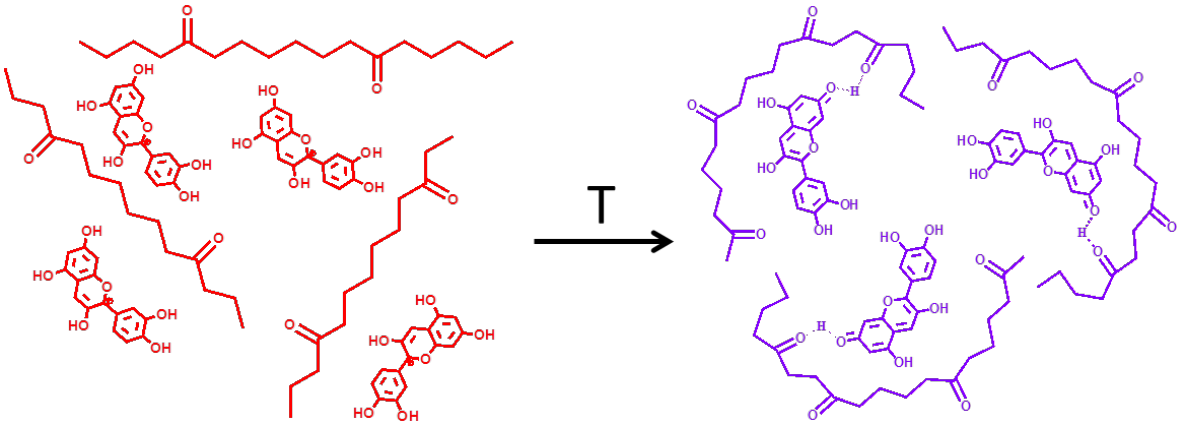

Figure 1.12 Schematic diagram indicating thermochromism of cyanidin chloride-polylactide blends during heating.

The first example of nontoxic dye-polymer thermochromic materials has been developed based on the interaction change between anthocyanidin dyes and polylactide (PLA).[13] The cyanidin chloride, dodecyl gallate, palmitic acid and PLA were mixed together and moulded into polymer sheets at 185 °C. The fabricated polymer sheets show colour change above or below certain temperatures. All the ingredients used in the system, including anthocyanidin dyes, fatty acids, dodecyl gallate and PLA, are all practically nontoxic making the polymer sheets entirely nontoxic. The colour change from wine red into violet during heating is ascribed to cyanidin dyes transforming molecular structures from neutral anhydro base form into anionic form, which interact with carbonyl groups of PLA through H-bond (Figure 1.12). The analysis reveals that it is more likely to form H-bonds with cyanidin dyes when the PLA is in a mobile amorphous state. Therefore, the colour transition temperature is directly related to the T_g of PLA. Although the system shows reversible colour change in the cooling process, the transition requires several days to reach equilibrium. Therefore, this system did not indicate instant temperature change. In another example, cyanidin chloride was replaced by pelargonidin chloride and delphinidin chloride to investigate the influence of dye structure on the thermochromic properties and the mechanism of PLA-dye composite materials.[55] Results indicate the hydroxyl group on 3'-position of anthocyanin dye molecules and its adjacent hydroxyl groups are essential for dye-polyester H-bond interaction, which leads to thermochromism (Figure 1.13). However, the stability of anthocyanidin dyes prevents this system being commercially available.[56] Therefore, other robust and cheap nontoxic natural dyes with phenol hydroxyl groups being incorporated into

polyesters with different T_g could be a promising way to synthesize thermochromic polymer sheets with adjustable responsive temperatures.

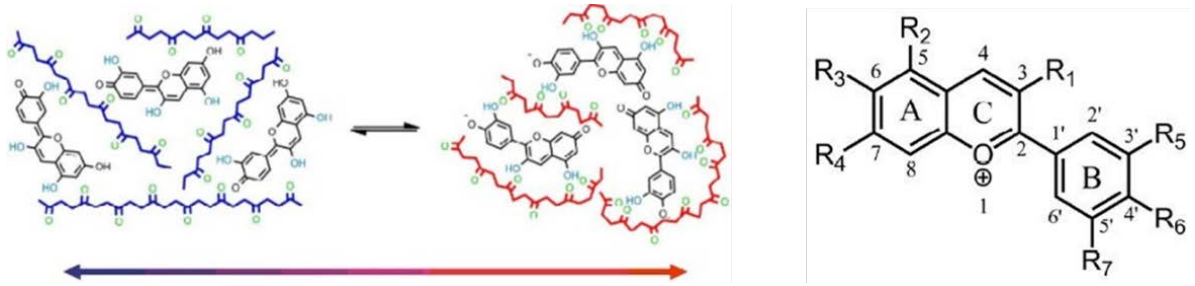

Figure 1.13 Schematic diagram indicating thermochromic mechanism of cyanidin-PLA composites and the molecular structure of anthocyanin.[55]

1.2.2.6 pi−pi stacking

pi−pi stacking describes the shared electron orbital interactions between adjacent aromatic rings and has been found in some aromatic compounds polymers and biological macro molecules.[57, 58] The geometric configurations of pi−pi stacking include face-to-face parallel shape, edge-to-face T-shape and face-to-face off-set shape, where parallel shape is the most unstable configuration and is consistent with a relative rarity in X-ray crystal data. The pi–pi stacking between two aromatic rings meets the requirements either (a) the distance between the aromatic ring centroids is less than 4.4 Å and the angle between the aromatic ring planes is less than 30° (face-to-face), or (b) the distance between the ring centroids is less than 5.5 Å and the angle between the aromatic ring planes is between 60° and 120° (edge-to-face).[59] pi−pi stacking, as a intermolecular interaction, its energy is much smaller than covalent bonds. However, the change of pi−pi stacking will still change in molecular energy which changes the absorption spectrum of material. Therefore, various types of thermochromic materials have been designed based on this mechanism of pi−pi stacking. According to the number of components, these materials are categorized into single-component, binary-components and multiple-components materials.

1.2.2.6.1 Single-component materials

Conjugated polymers, such as polythiophene, are consisted of coplanar repeating units of conjugated structure with π-orbitals. Conjugation relies upon overlap of the extended π systems, which is responsible for the optical properties of conjugated polymers.[47] The longer the conjugation length, which is determined by the number of coplanar rings, leads to lower separation between adjacent energy levels and longer absorption wavelength. On the contrary, twisting of the polymer backbone at increased temperature reduces the conjugation length and results in a shorter absorption wavelength. Due to strong interchain interactions and chain stiffness, the conjugated polymers are usually hard to process by solvents and thermoforming. Therefore, substitution by long and flexible side chains to conjugated polymer backbones is a common way to enhance the processability of these materials in solvents and thermo treatments and also introduce other properties, such as reversible thermochromism to these materials because of disordered side chain disrupting the planarity of backbones at higher temperature.[60] For example, the thermochromic behaviour of poly(3-alkylthiophene)s were studied since 1980s and its colour change was later proved to be related to twisting of the polymer backbone and disrupting conjugation.[61]

The derivatives of poly(3-alkylthiophene)s were the main research objects of thermochromic conjugated polymers in the past decade. It was commonly reported that poly(3-alkylthiophene)s show unusual two-step thermochromism, in which poly(3-alkylthiophene)s change colour from original into bright yellow after heating from room temperature to high temperature while their resultant colours dependent on different cooling speeds are different but the eventual colour after annealing is the same with original.[62-64] Therefore, poly(3-alkylthiophene)s at different temperatures are distinguished into three states: hot state, mesophase state and annealed state. Later, the effects of interchain phenomena of aggregation and crystallization of side chains on thermochromic behaviours of poly(3-alkylthiophene)s were verified via investigation of poly(3-alkylthiophene)s with very long *n*-alkyl side chains.[65] It was reported that pi-pi stacking of backbones is an important contributor to the thermochromism of these compounds while the interchain phenomena controls mesophase formation. The better conjugation and pi-pi interaction along the backbones results into lower energy of electronic transitions in annealed phase compared to hot phase, in which there is little conjugation and pi-pi interaction. The energy of mesophase is lower than hot phase but still higher than annealed phase, because the alkyl side chains are moderately ordered in mesophase leading to a reduction of pi-pi interaction between thiophene π systems on adjacent backbones.

Poly(3-hexylthiophene), as one of poly(3-alkylthiophenes), was deposited on a superhydrophobic surface comprised of poly(vinylidene fluoride-co-hexafluoropropylene) (PVDF-PHFPP) copolymer and SiO_2 nanocomposites to make temperature sensors for metal coatings simply by spray coating.[66] The thermochromic behaviour of poly(3-hexylthiophene) was enhanced due to the pi−pi interchain directional stacking (100) with uniform d-spacing was confined into a nanostructured surface texture. The thin composite film changed colour from red to yellow when temperature was escalated to 200°C from room temperature (Figure 1.14).

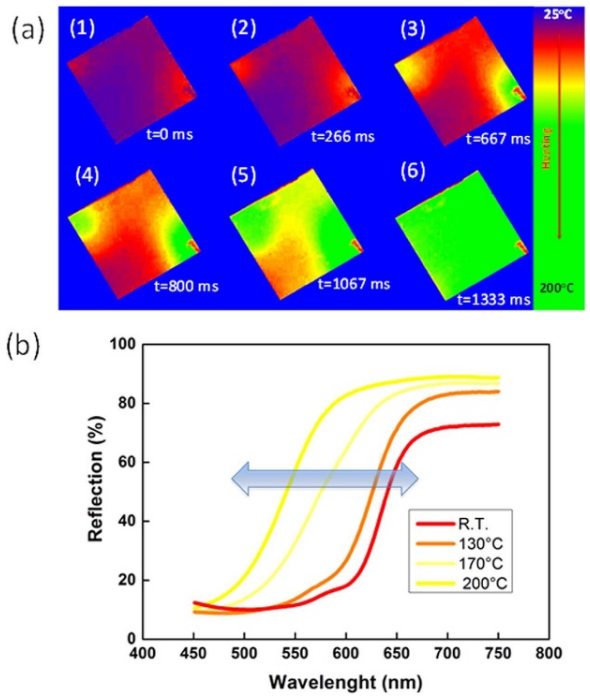

Figure 1.14 (a) High speed camera image sequences (600 fps) showing colour change of a thermochromic composite film during heating. (b) Corresponding surface reflection of the composite film during heating.[66]

In addition, some other conjugated molecules also show thermochromism based on pi-pi stacking change, such as derivatives of phenalenyl and 1,3-bis(hydroxyalkylamino)-4,6-dinitrobenzenes (BDBn, n = 2−5). The molecules of tri-*tert*-butylated phenalenyl form parallel pi-pi stacking structures in solid state due to its highly symmetrical and fully delocalized nature of electronic spin structure.[67] The first example of reversible thermochromism of solid crystal of diazaphenalenyl radical was reported in 2007, in which coexistence of a gabled σ-dimer and a pancake π-dimer was proved by X-ray crystal structure analyses.[68] The sample changed its colour between pale green and dark green when temperature switched between -170 °C and 150 °C. The colour change mechanism is ascribed to population difference between σ-dimers and π-dimers at different temperatures while π-dimers are responsible for the absorbance at 670 nm in polarized electronic spectra. Later, the valence tautomerization of two cyclo-biphenalenyl molecules with chair and boat conformations were examined by density functional theory.[69] Results show the molecule with chair conformation prefers σ-bonded structure while the one with boat conformation prefers π-π bonded structure although both conformations involve π−π bonded structure on their potential energy surfaces. The bond fluctuation between the π−π bonding and stretched σ-bonds makes these molecules possible to change colour, which is demonstrated by simulated UV−vis electronic spectroscopy, where chair conformation becomes darker and boat conformation becomes lighter with increasing temperature.

The example of BDBn (n = 2−5) was reported to exhibit both polymorphism and reversible thermochromic change between yellow and orange or red forms in the solid state.[70] Analysis revealed that the lattice expands in the stacking direction during heating, causing weakened pi−pi interaction between aromatic rings, enhanced oscillator strength and red shift of the absorption. At higher temperature, the second thermochromic change associated to intramolecular proton transfer of one amino proton to the nitro group occurs. Therefore, the thermochromic behaviour of these compounds is attributed to pi−pi interaction and intramolecular proton transfer.

1.2.2.6.2 Binary-components materials

Although solid and pure poly(3-alkylthiophene)s can change colour towards thermal stimuli, the solutions of poly(3-alkylthiophene)s are found to have thermochromic property as well. The example of poly[3,4-(4,5-didodecylphenylene)dioxythiophene] (poly[PheDOT-$(C_{12})_2$]) was synthesized and the thermochromic behaviour of its xylene solution was investigated.[71] The colour of solution changes from dark purple to red-orange during heating (Figure 1.15) due to the transition of poly[PheDOT-$(C_{12})_2$] molecules from π−π aggregates to isolated form with remained planar conformation, which is verified by the presence of vibronic features at high temperature. This thermochromic mechanism is different from that of solid poly(3-alkylthiophene)s, in which twisting polythiophene backbone of the conjugated polymer is responsible for colour change at high temperature. Another example is from a structurally well-defined “dumbbell-shaped” oligothiophene triblock copolymers, which form π−π aggregated complexation of the oligothiophene units in solution at low temperature.[72] As a result, the thermochromic phenomenon was observed when the solution of these copolymers cooled down due to lower solubility and the thermochromic behaviour was mainly dependent on the concentration or solubility.

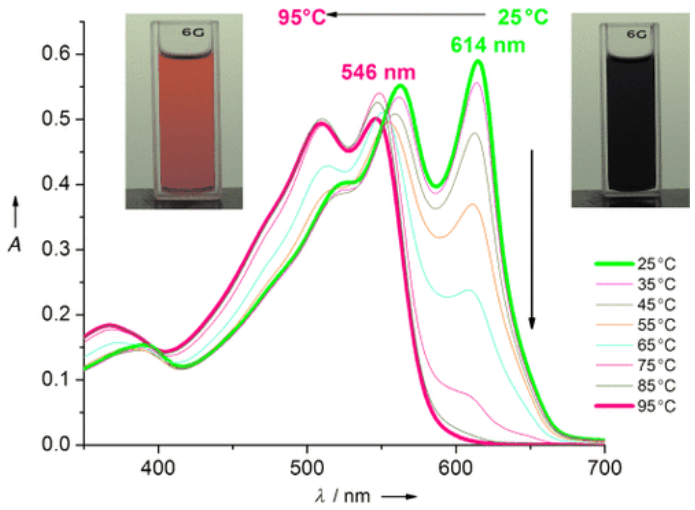

Figure 1.15 UV-Vis absorption spectra of poly[PheDOT-$(C_{12})_2$] (6×10^{-5} M, relative to the repeat unit) in xylenes at different temperatures and the photographic images of the solution at 95 °C (left) and 25 °C (right).[71]

The dyes with conjugated planar structures also exhibit similar phenomenon when they are incorporated into solvents or polymer matrix. pi−pi stacking change between dye molecules with conjugated aromatic structures in aggregation or disaggregation will lead to absorption wavelength change or fluorescent change.[73] These dyes are called as 'aggregachromic' dyes, which forms H- or J- aggregates by pi−pi stacking interactions among their planar aromatic backbones accompanied by charge transfer interactions within the dye aggregates or in conformational changes of the dye structure (Figure 1.16).[74] Polymer-aggregachromic dye blends with kinetically controlled thermochromic performances can be fabricated by dissolving the respective dye in the melted polymer followed by rapid cooling into the glassy state.[18] The aggregates of dye molecules are inhibited by viscosity of glassy polymer matrix during rapid cooling although the solubility of dye gets lower. However, the aggregates will gradually form from phase separation and crystallization of dye as a result of reduced viscosity of polymer matrix and increased mobility of dye molecules when the blends are heated above glass transition temperature (T_g). These materials are easy to fabricate with simple processing methods, like blending and melting extrusion and exhibit reversible fluorescence change or irreversible colour change when temperature is above T_g of polymer matrixes. Therefore, those polymer-aggregachromic dye blends form the largest category of binary-component thermochromic materials here.

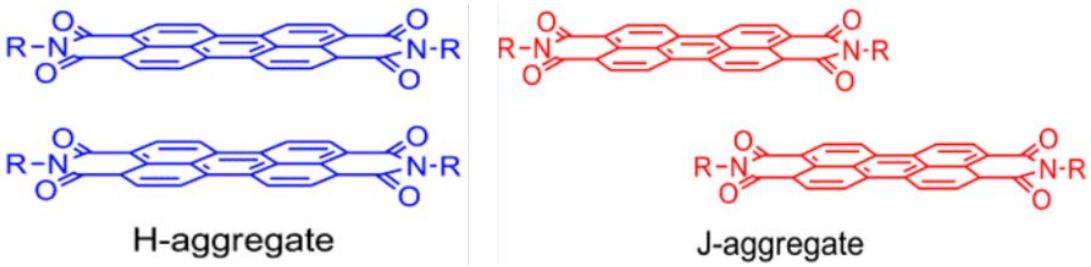

Figure 1.16 Schematic diagrams of transition dipole moment interactions in H-aggregates and J-aggregates.[74]

Cyano substituted oligo(p-phenylene vinylene) derivatives dyes (COPVs) (Figure 1.17) were mixed with melted poly(ethylene terephthalate glycol) (PETG), poly(ethylene terephthalate) (PET) or linear low-density

polyethylene (LLDPE) resin (0.5–2 wt.%) in the rotating twin-screw extruder to form thermochromic films.[75] These films changed colour from yellow to orange irreversibly when annealing at temperatures above T_g of polymer matrix. In the practical usage, the different response time of thermochromism of these materials will lead them into different application areas. Therefore, thermochromic polymer-COPVs blends with small amount (0.6–2.3 wt.%) of COPVs were fabricated and their irreversible thermo responsive colour and fluorescence change were investigated.[76] It revealed that aggregation rate is associated to annealing temperature, dye concentration and length of rigid core of dye. The threshold temperature of colour change can be adjusted via compositional variation of polymer matrix, making them potential for visual indicators or time-temperature indicators.

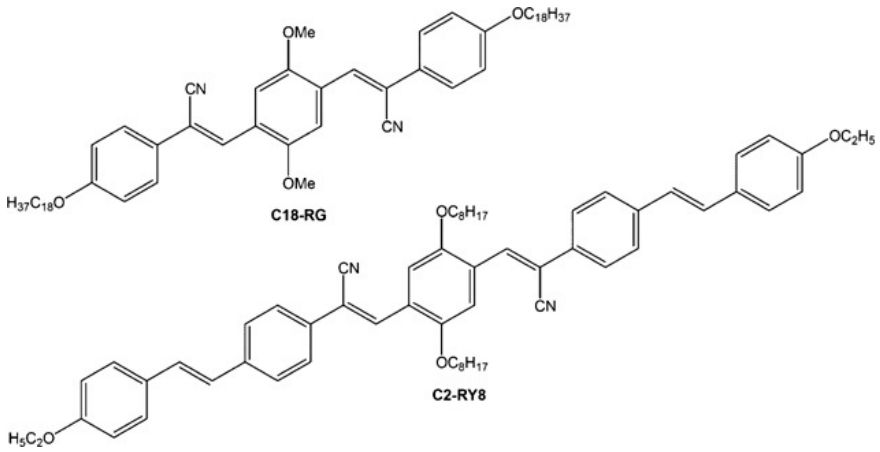

Figure 1.17 Molecular structures of COPVs.[75]

As another aggregachromic dye, *N,N'-bis*(2-(1-piperazino)ethyl)-3,4,9,10-perylenetetracarboxylic acid diimide dichloride (PZPER) (Figure 1.18) was synthesized and thermochromic behaviour of its aqueous solution and PVA or poly(ethylene-*co*-vinyl alcohol) (PEVA) blends were investigated.[77] H-type π−π aggregates of PZPER, which is influenced by H-bonds in solution and polymer matrix, were confirmed in absorption and emission chromophore features. Contrary to hydrophobic COPVs, hydrophilic PZPER prefers disperses in isolated monomeric form rather than aggregates in water or vinyl alcohol containing polymers when temperature increases. The chiral molecule of *N,N'-bis*-(R)-(1'-phenylethyl)-perylene-3,4,9,10-tetracarboxyldiimide (R-Pery) dye has similar core structure with PZPER. Therefore, the thermochromic and thermo-responsive fluorescence change of R-Pery/LLDPE blended films (0.01-0.1 wt.%) were studied.[78] The supramolecular aggregates of R-Pery from pi−pi stacking among perylene nuclei was verified by UV-Vis absorption, fluorescence and ^{1}H NMR spectra. The UV-Vis absorption and fluorescence spectra of these films changed during heating due to reduction of R-Pery aggregates and increasing R-Pery monomeric forms.

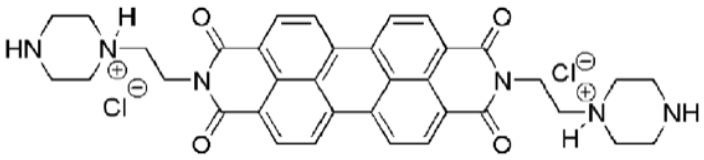

Figure 1.18 Molecular structure of the *N,N'-bis*(2-(1-piperazino)ethyl)-3,4,9,10-perylenetetracarboxylic acid diimide dichloride (PZPER).[77]

There are also some fluorescent dyes-polymer blends which exhibit irreversible aggregachromic properties when the temperature is above the T_g of the polymer matrix.[79-83] For example, nontoxic 4,4'-*bis*(2-benzoxazolyl)stilbene/PLA (BBS/PLA) blended films show obvious fluorescence change when temperature is above T_g of PLA due to induced aggregation of BBS.[81] Furthermore, a fluorescent dye-polymer blend, namely COPVs-poly(cyclooctene), shows reversibly fluorescence change towards temperature alternations due to solubility-dependent aggregation and disaggregation of dye.[84] However, these films only show thermo-responsive fluorescence change rather than thermochromism that can be observed by naked eye. Therefore, these fluorescent examples are not described in detail here.

Another type of thermochromic material which shows colour change arising from pi-pi stacking conformational change, when water molecules are either obtained or lost at different temperatures. One example is from sulfonated poly(ether ether ketone) (SPEEK) film, which changes its colour into yellow when temperature increases to its T_g due to molecular rearrangement from hydrogen-bonded networks to pi−pi stacking clusters. [85] At high temperature about 190°C, pi–pi stackings among aromatic rings dominate in SPEEK chains while the hydrogen bond networks between the sulfonated groups and the hydrated water molecules disappear due to the loss of water. The film recovers clear colour when it cools down to room temperature and forms hydrogen-bond again with ambient water, which plays essential role during the recovery step (Figure 1.19).

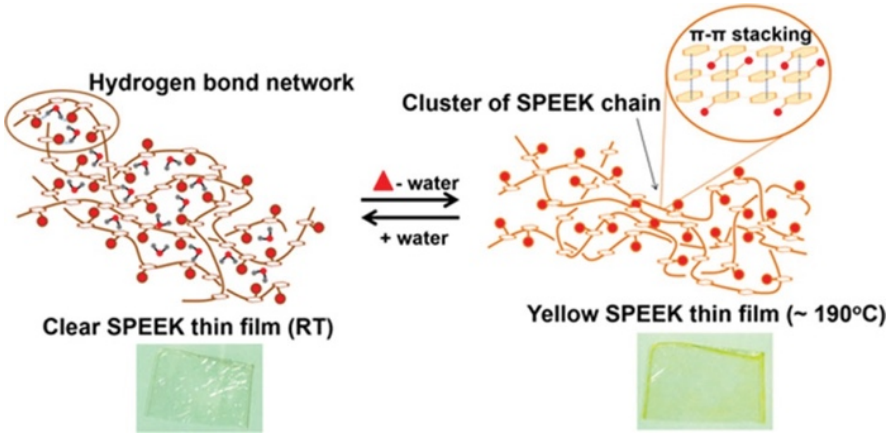

Figure 1.19 Schematic diagrams of reversible thermochromic SPEEK thin film at molecular level and the photographic images of this film at room temperature and 190 °C.[85]

The thermochromic behaviours of PDAs were always irreversible until the first reversibly thermochromic example of PDAs was reported.[14] In the report, a binary thermochromic material consisted of poly (10,12-pentacosdiynoic acid)/melamine (PDA/MA) lath-like cocrystals with lamellar structure was synthesized. The crystal structure, in which MA molecules are sandwiched by PDA molecules through H-bond while MA molecules form pi−pi stacking, was verified via DSC, XRD, FTIR and molecular dynamic simulation by density functional theory at B3LYP/6-31G** level (Figure 1.20). The colour change between blue and red of reversible sample between 25°C and 90°C is believed to be attributed to reversible conformation changes in PDA.

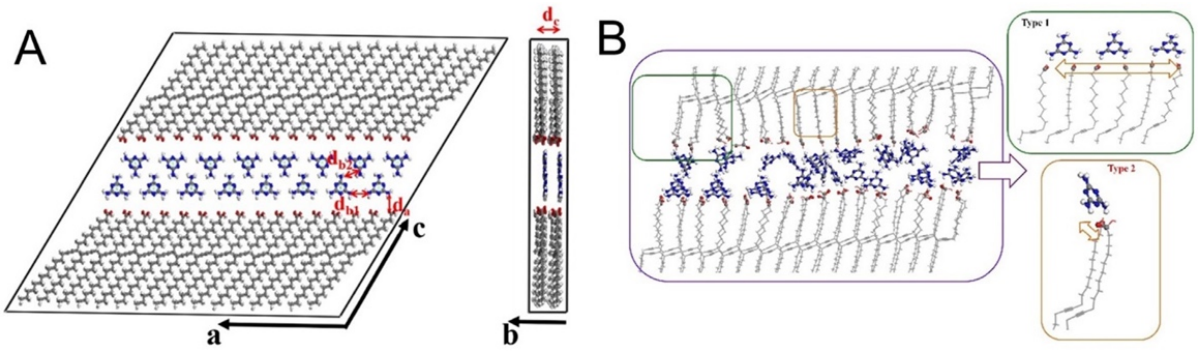

Figure 1.20 (A) Initial structure for simulation and (B) equilibrated structure of PDA/MA in molecular dynamic simulation during the annealing process.[14]

1.2.2.6.3 Multiple-components materials

Host–guest interaction in supramolecular chemistry has been attracting attention for decades. The first thermochromic phenomenon of host-guest complexion in solution based on dynamic molecular recognition was reported in 2009.[86] As the host molecule, cleft-shaped dynamic molecular tweezers (DMTs) (Figure 1.21) consisted of cyclacene and two tub-shaped dibenzocyclooctatetraene (DBCOT) units with different substituents on both the terminal benzene rings and two COT units were designed and synthesized. Analysis of UV-Vis absorption and ^{1}H NMR spectra indicate the *syn*-isomers of DMTs form 1:1 complex with 2,3-dichloro-5,6-dicyano-1,4-benzoquinone (DDQ), a planar π-system guest molecule, between the two benzene rings. The binding ability of DMTs with DDQ is dependent on electron-donating substituents on COT and length of the terminal alkoxy chains of the DMTs. The complex of DMTs/DDQ in chloroform solution changes colour from green to yellow via heating and from green to blue via cooling (Figure 1.21) ascribed to molar ratio of complex to free DDQ at different temperature.

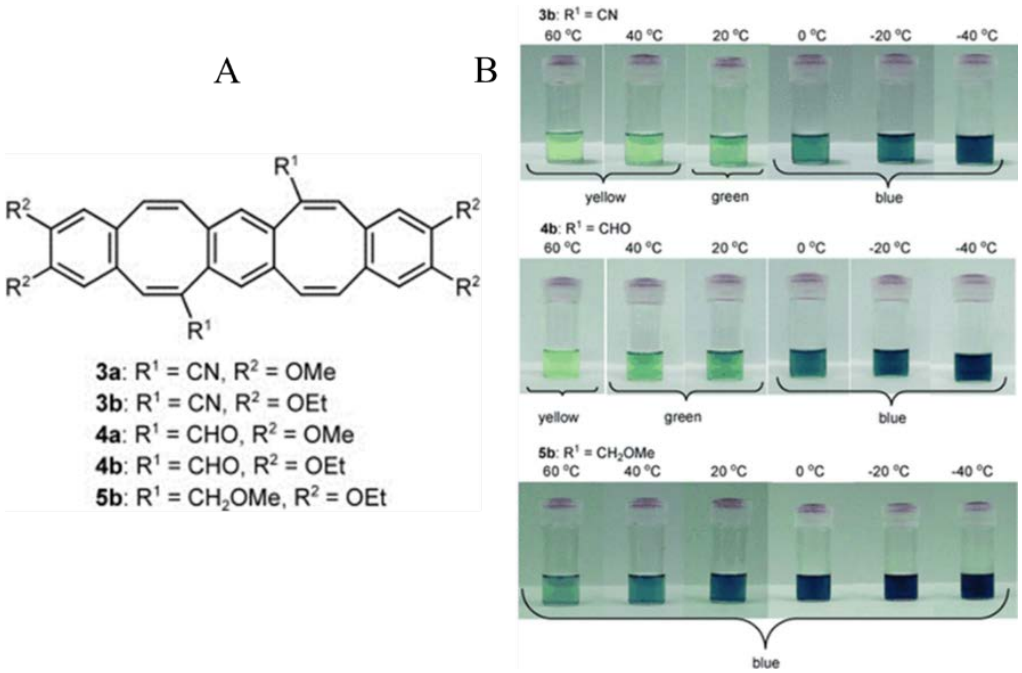

Figure 1.21 (A) The molecular structures of DMTs with different substituents; (B) The photographic images of solutions of 3b, 4b, and 5b with DDQ in $CHCl_3$ (DDQ: 1 mM, DMTs: 1 mM) at different temperatures (60 °C to −40 °C).[86]

Another example comes from the complex of cyanine dye-hyaluronic acid (CD-HLA) (Figure 1.22) in methanol-water solution.[87] As the temperature drops from 50 °C to 0 °C, the solution shows obvious colour change with blue-shifted peak in UV-Vis absorption spectra due to molecular switching of monomer-to-R-chiral dimer and R-chiral-to-S-chiral dimer transition of CD. The colour change phenomenon is reversible with an increase in temperature.

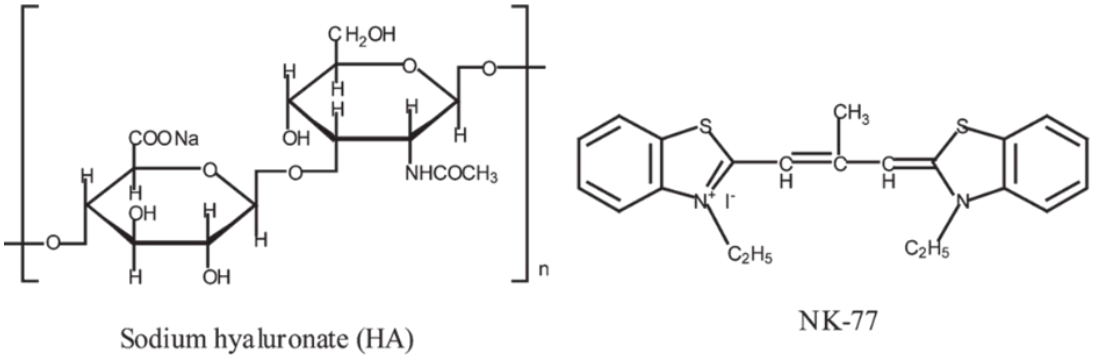

Figure 1.22 The molecular structures of hyaluronic acid (HLA) and cyanine dye (CD) NK-77.[87]

1.2.3 Surface plasmon resonance change

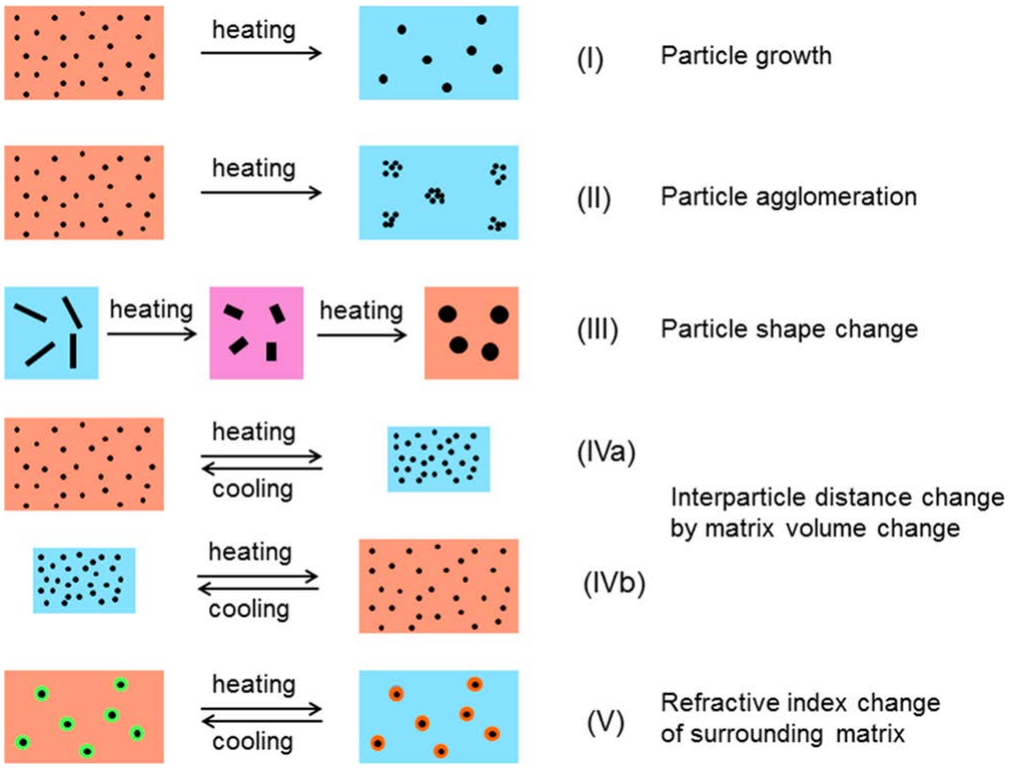

Figure 1.23 Schematic diagrams of structural change of nanoparticles showing reversible or irreversible thermochromic effects based on surface plasmon resonance.[18]

Plasmon is quantized wave of free electrons oscillating around their equilibrium positions.[18] Plasmons can couple with photons when their frequencies match each other. The surface plasmon of some certain metal nanoparticles, e.g. gold and silver, can couple with visible light and the corresponding wavelength is rely on the size, shape or surrounding medium of these nanoparticles. In this context, thermochromic materials based on surface plasmon resonance are synthesized by incorporating gold or silver nanoparticles in thermosensitive matrix. Therefore, the thermochromic behaviour of these materials could be reversible due to change of interparticle distance or refractive index of surrounding matrix[15] or irreversible due to growth, agglomeration and shape change of nanoparticles[88, 89] (Figure 1.23).

So far, scientists have fabricated thermochromic nanoparticle-polymer blends via incorporating gold or silver nanoparticles into polymers with LCST or polymers with distinct volume variation at T_g.[90, 91] For example, thermochromic behaviours of hybrid microgels, which are consisted of PNIPAM-*co*-PGMA matrix and Au or Au/Ag core-shell nanoparticles with various structures, were investigated.[92] The samples were synthesized via *in situ* reaction between HA_uCl_4 and amino-functionalized PNIPAM-*co*-PGMA microgels (NG-NH_2) with or without A_gNO_3 in acidic aqueous solution (Figure 1.24). Due to the thermosensitive swelling/deswelling property of microgels in water, these samples show slight colour change between 25°C and 40°C with absorption peak shifts (Figure 1.25) based on surface plasmon resonance change from interparticle interactions of nanoparticles. The samples of NG-NH_2-A_u/A_u and NG-NH_2-A_u/A_g show reversible thermochromic behaviour while the sample of NG-NH_2-A_u/A_g/A_u show irreversible thermochromic phenomenon. The difference is resulted from the fact that larger nanoparticles are prone to agglomerate due to less intermediate polymer matrix among them.

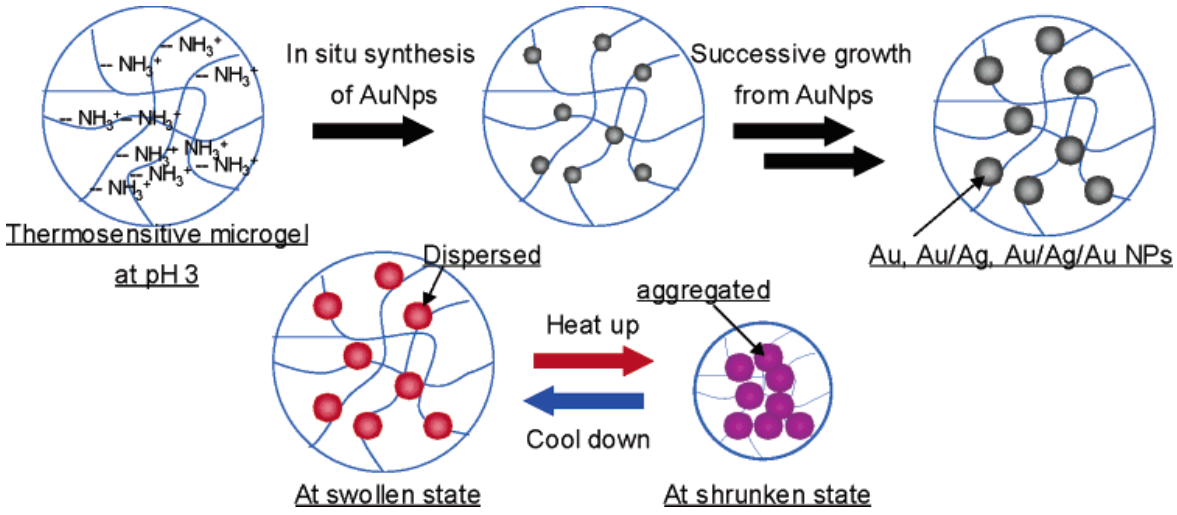

Figure 1.24 Schematic diagram of synthesis of thermosensitive microgels and corresponding thermochromic behaviour.[92]

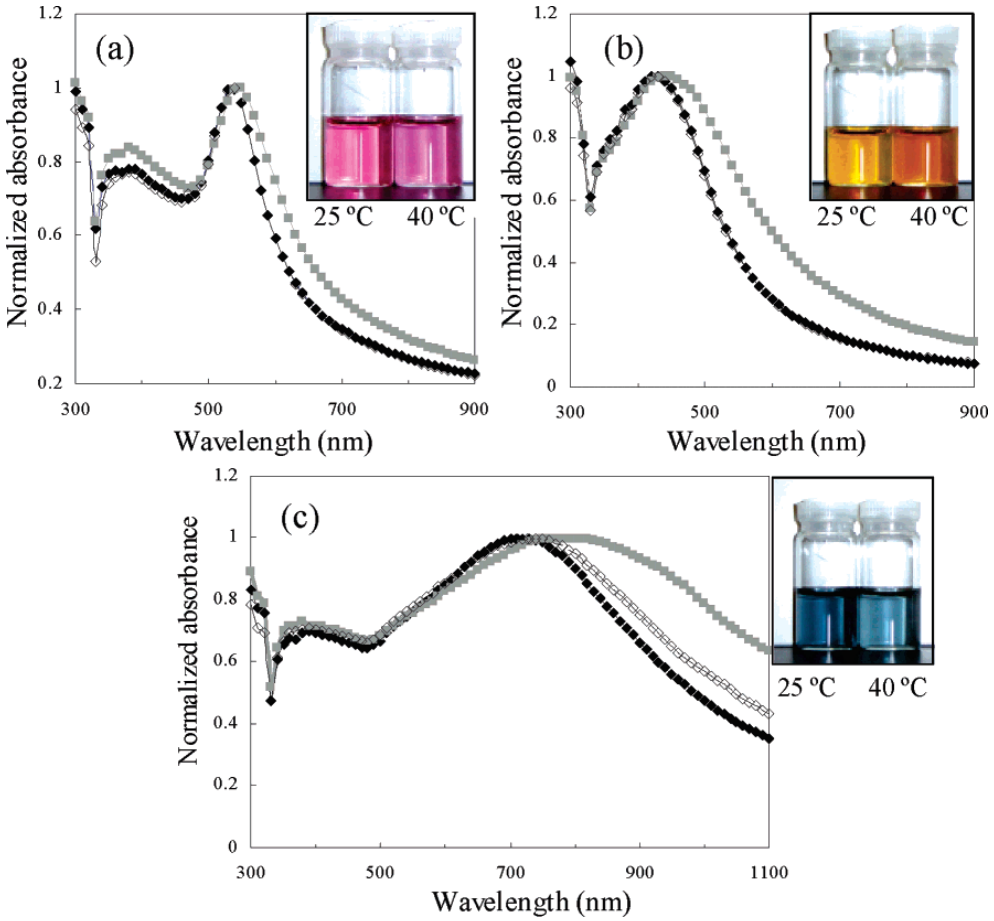

Figure 1.25 UV-vis absorption spectra and photographic images of (a) NG-NH_2-A_u/A_u, (b) NG-NH_2-A_u/A_g and (c) NG-NH_2-A_u/A_g/A_u microgels measured at 25 °C (black square), 40 °C (grey square), and 25 °C after 10 heating& cooling cycles (empty square).[92]

Another example comes from poly(1-vinyl-3-ethylimidazolium)bis-(trifluoromethanesulfonimide) based polymeric ionic liquid (PIL) composite films incorporated by gold or silver nanorods.[93] The PIL/A_u nanocomposite film shows irreversible colour change from violet (25 °C) to blue (160 °C) and finally to pink (200 °C) while the PIL/A_g nanocomposite film shows irreversible colour change from purple (25 °C)/red (130 °C) through orange (155 °C) to yellow (190 °C) (Figure 1.26A&B). The analysis of transmission electron microscopy (TEM) images and UV-Vis absorption spectra indicate the irreversible thermochromism is ascribed to surface plasmon resonance change from shape change of nanorods to nanospheres during heating (Figure 1.26C). Therefore, the expansion of the colour range as well as expanding the range of colour transition temperature can be achieved via using nanorods of additional metals.

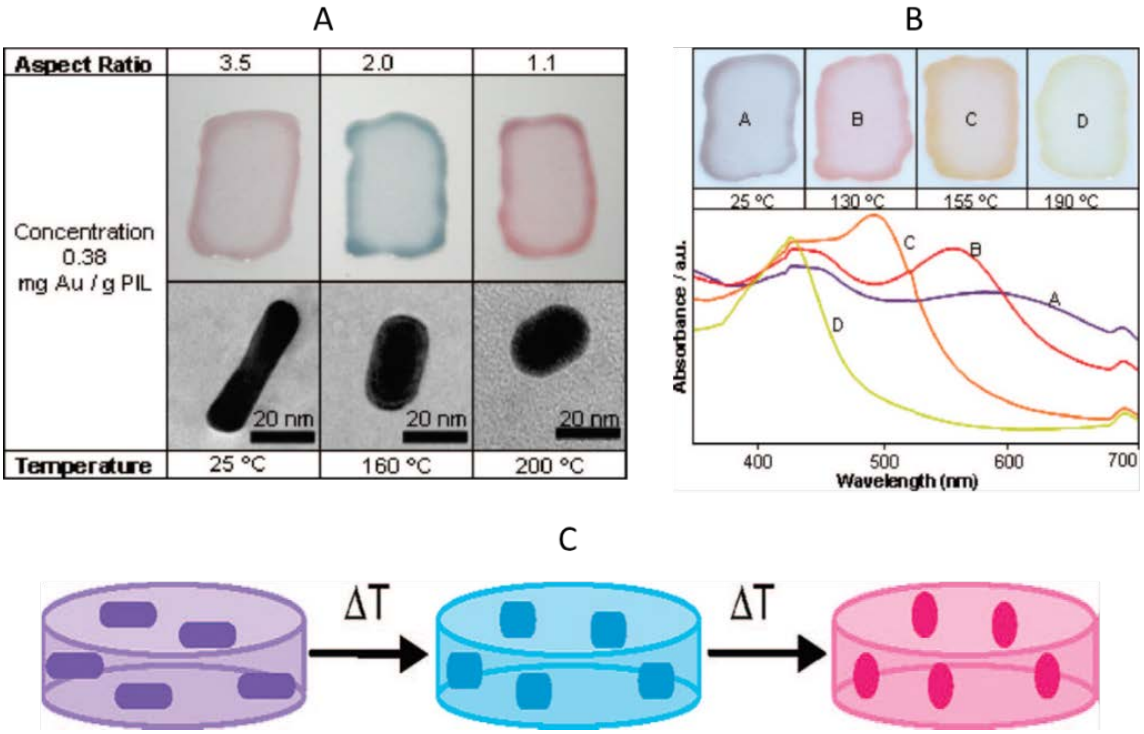

Figure 1.26 (A) Photographic images of gold nanorods/poly(1-vinyl-3-ethylimidiazolium) bis(trifluoromethanesulfonimide) films at different temperatures and TEM images of corresponding gold nanocomposite samples; (B) Photographic images of silver nanorods/poly(1-vinyl-3-ethylimidiazolium) bis(trifluoromethanesulfonimide) films at different temperatures and UV-Vis absorption spectra of corresponding silver nanocomposite samples. C) Schematic diagram of irreversible thermochromism due to shape change of nanoparticles in polymer matrix.[93]

1.3 Commercial Challenges and Solutions

1.3.1 Key issues in application

To date, some package suppliers have applied thermochromic materials to food packaging for commercial purposes (Figure 1.2). For example, thermochromic ink has been printed on the metallic cans of Coors Light Beer that turns into deep blue colour at icy temperature, which is the optimal consumption temperature for consumers. Another example is the CoolVu label (Figure 1.27), which indicates the freshness of the food products by displaying different occupied silvery areas based on a temperature dependent dissolution process of a fine aluminium layer.[94] Pizza Hut also has used thermochromic 'hot spot' pizza boxes for home delivery to help customers differentiate this brand from others while indicate the temperature of pizzas within.

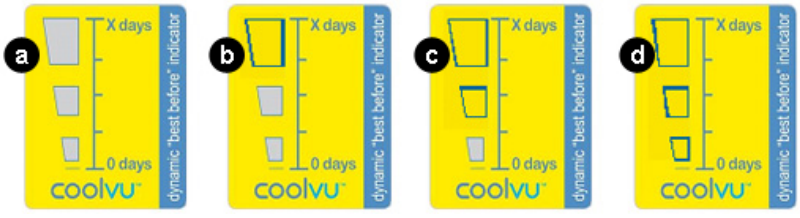

Figure 1.27 Commercial examples of CoolVu labels: a) freshly activated label; b) early mid-life label; c) late mid-life label; d) expired label.[94]

Although thermochromic packages have been commercially available for many years, there are still some problems that need to be solved before these materials can be widely applicable to all types of food packaging. The first problem is the added cost of thermochromic materials on packages and manufacturing equipment, which limits its broad acceptance from food suppliers.[95] Package suppliers would incorporate the added cost of thermochromic materials by including the technology innovation, intellectual property, machine maintenance and changes on manufacturing process, to guarantee their products are still commercially competitive to traditional packages. The value for money would also have to be justified by the food manufacturers and suppliers, and currently this cost is not warranted. In addition, retailers are concerned about the low accuracy or false indications of food quality by thermochromic materials, which would decrease their sales and affects their acceptance of thermochromic packages.[95]

Compared to the cost and accuracy problems, the toxicity of thermochromic materials seems the most serious factor affecting their implementation. Dye-developer-solvent leuco dye systems are the most commonly used commercial thermochromic materials so far.[17] However, leuco dye systems usually contain toxic dyes, such as triphenylmethane phthalides, rhodamine lactams, fluorans, phenothiazines, indolylphthalides, spiropyrans and leucoauramines, and toxic developers, such as bisphenol A, thioureas, guanidines, benzothiazoles and benzothiazolyls.[44] As a result, the use of leuco dye systems is limited to non-food applications or food packaging articles where significant barriers exist, such as glass, metal or thick plastic layers so that direct food contact may be avoided.[96]

1.3.2 Solutions

To address the concerns regarding the toxicity of existing thermochromic materials we have attempted to either remove or substitute relatively toxic components with non-toxic ones. In addition, we aim to incorporate these materials into inks as microencapsulated materials as well as laminated materials to avoid potential chemical migration.

1.3.2.1 Microencapsulation

Food ingredients, cells and other additives can be entrapped by the shells of capsules via various microencapsulation technologies to protect the encapsulated materials from moisture, heat or other extreme conditions.[97, 98] Therefore, microencapsulation technologies can also be applied to protect thermochromic materials and avoid leaking to contaminate packages.[99-104] In general, interfacial deposition, spray drying, emulsion-solvent evaporation/extraction, *in situ* polymerization and phase separation-coacervation have all been considered.[105]

1.3.2.1.1 Microencapsulation for hydrophobic components

The two most commonly used thermochromic systems are leuco dye systems and CLCs.[17] Oil-in-water (o/w) emulsion and *in situ* polymerization are used for microencapsulation of leuco dye systems due to their hydrophobic components. Typically, the shell components utilize urea/ melamine and formaldehyde as water-

soluble monomers, with resorcinol as an accelerating agent and poly(acrylic acid-*co*-methacrylic acid) (PAA-PMA) or poly(acrylic acid-*co*-itaconic acid) (PAA-PIA) as stabilizers (Figure 1.28).[103] Firstly, hydrophilic water-soluble stabilizers, urea, melamine and resorcinol are dissolved in water at 50 °C followed by pH adjustment; then the melted and hydrophobic (oil phase) leuco dye system is added to aqueous solution and stirred with a homomixer at high speed to emulsify. Finally, formalin is added to the emulsion at 60 °C under low speed stirring and crosslinking of the urea/melamine-formaldehyde shell occurs. These obtained microcapsules are chemical resistant, commercially available and consisting of dense shells to avoid leakage of the core materials.[106, 107] However, formaldehyde has relatively high toxicity and has therefore been replaced with less toxic monomers as shell materials, such as methyl methacrylate, methacrylic acid, amino-aldehyde prepolymers and styrene.[102, 108, 109].

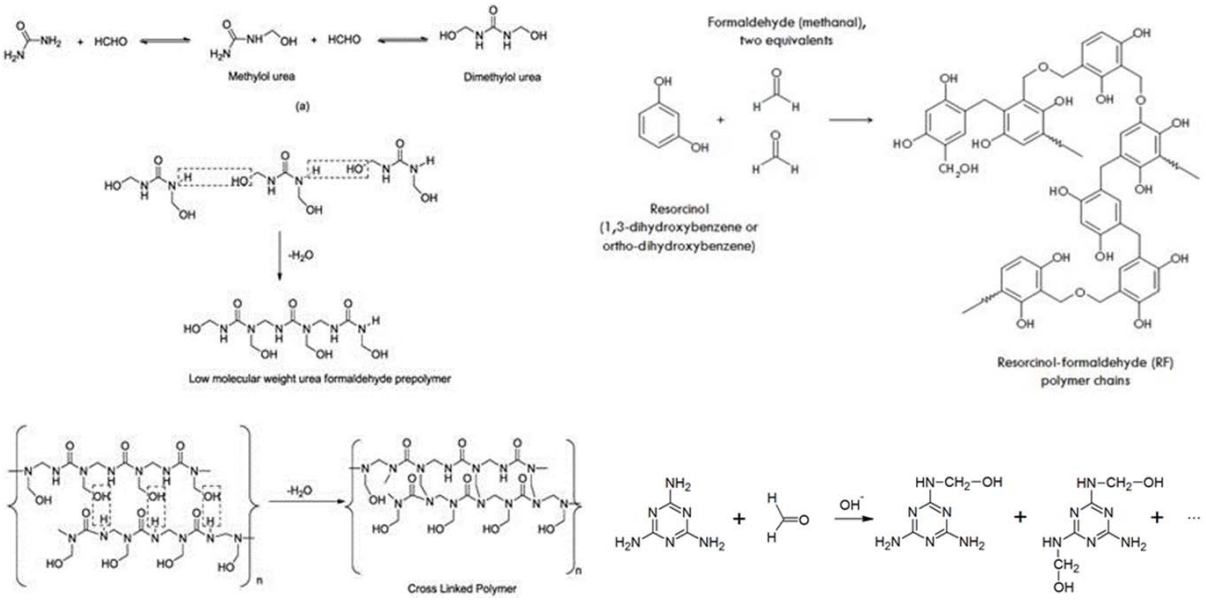

Figure 1.28 Crosslinking schemes of urea/melamine-formaldehyde polymers.[110, 111]

The second example of hydrophobic encapsulation is the preparation of CLCs. A typical microencapsulation process for CLCs is carried out by the complex coacervation of gelatine and gum acacia as a negative-ion colloid.[22] Similar to leuco dye systems, CLCs are hydrophobic and also can be o/w emulsified in aqueous gelatine and gum acacia (Figure 1.29). Gelatine is a nontoxic water-soluble protein with an isoelectric point and is also a surfactant.[112] After adjustment of pH by adding acetic acid, the gum acacia and gelatine polymer chains carry opposite charges. As a result, phase separation occurs and a complex coacervate surrounds on the surface of CLCs droplets spontaneously. At last, glutaraldehyde solution is added to crosslink the shells of microcapsules at low temperature.[113] The microcapsules of CLCs are obtained after removing contaminant and excess water. However, the coacervation shell is not compact enough to prevent contamination from external small molecules.[22] Another disadvantage is that extremely sticky coacervate layers would frequently stick each other before complete phase separation.[105]

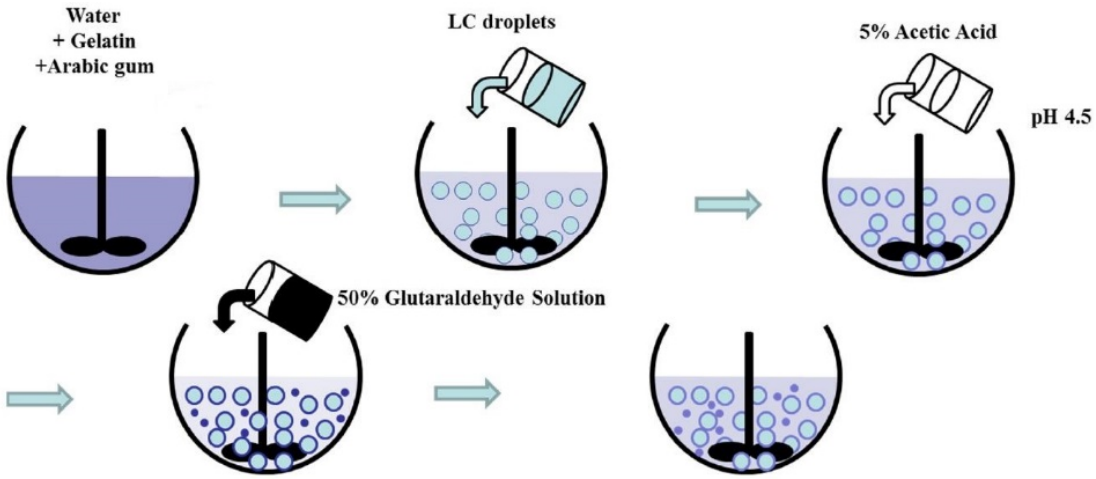

Figure 1.29 Preparation schemes of CLCs microcapsules via complex coacervation of gelatine and Arabic gum.[112]

1.3.2.1.2 Microencapsulation for hydrophilic components

Most hydrophilic drugs, peptides and proteins are microencapsulated via water-in-oil-in-water (w/o/w) double emulsion methods (Figure 1.30).[114-117] In this method, the hydrophilic components are dissolved in aqueous solution at first followed by the step of water-in-oil (w/o) emulsification of the aqueous solution in organic continuous phase by high speed homogenizers or sonication. The shell materials have been pre-dissolved in the organic phase before the w/o emulsification. Then the w/o emulsion is transferred into large amount of water under vigorous stirring to form w/o/w double emulsion. At last, the organic solvent will be removed by either evaporation or extraction process.[105] The dissolved shell materials will spontaneously coat on the surface of hydrophilic core components to form core-shell structured microcapsules. Various of shell materials such as chitosan, xanthan gum, cellulose, gum Arabic, poly(ethylene glycol-*co*-lactide), PLA and poly(lactic-*co*-glycolic acid) (PLGA) have been used to encapsulate insulin, caffeic acid, L-ascorbic acid, anthocyanins or bovine haemoglobin.[117-123]

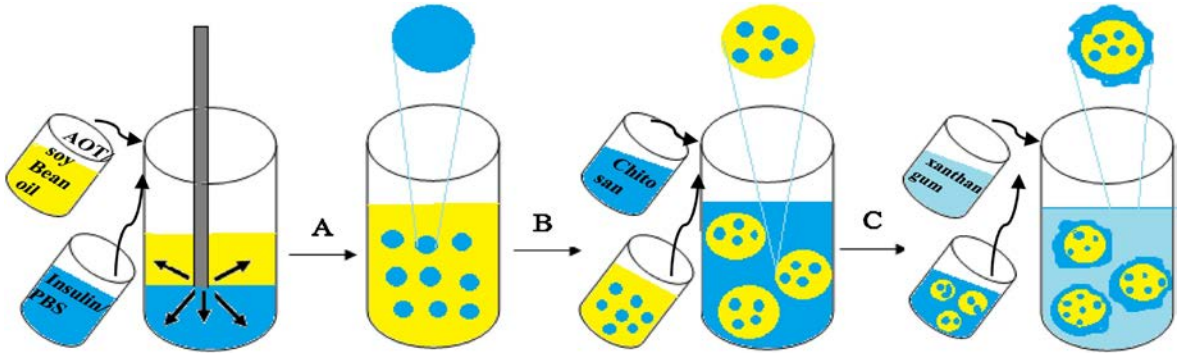

Figure 1.30 Schematic diagram of microencapsulation for hydrophilic insulin: A) Emulsify; B) Re-emulsify primary emulsion to produce a w/o/w double emulsion; C) Stabilize the double emulsion droplets with polymers shells by adding Xanthan Gum.[117]

Additionally, the microencapsulation of hydrophilic components have also been successfully carried out through w/o/w double emulsion in collaboration with spray drying or complex coacervation methods.[124-126] In general,

the encapsulation efficiency of core-shell microcapsules is dependent on different encapsulation methods, composition of shell materials, concentration of stabilizer, reaction condition and core-shell ratio.[117, 118, 125]

1.3.2.1.3 Printing application

There are several types of printing methods available for different needs, including offset printing, flexographic printing, digital printing, gravure printing, screen printing and others.[127] In offset printing, inked image area of content on the aluminium printing plate is transferred from the plate onto rollers or rubber blankets before going onto the printing surface. Therefore, offset printing is widely used for printing on substrates such as papers, plastics, cardboards and any media with rough surfaces. In flexographic printing, the inked image area of content on photopolymer printing plates is transferred onto the printing surface when the plates are quickly rotating. Flexographic printing is mainly used for packaging and labels with substrates of plastics, cellophane and metals. In gravure printing, the image area of content is engraved into a printing cylinder at first. Then the inked cylinder transfers the image of content onto paper during printing. Therefore, gravure printing is suitable for high volume work such as publication printing. Digital printing mainly relies on inkjet printers and laser printers. To create the images, inkjet printers spray ink droplets from the nozzles onto substrates while laser printers transfer toner particles from selective areas on drum cylinder with electrical charge onto substrates. From the economic perspective, digital printing is suitable for printing in small numbers. The screen printing is conducted on a fine fabric mesh with open apertures forming image of content. The ink could transfer onto substrates beneath the screen only through the open apertures to the form corresponding image when a blade is moving across the screen.[128] The surface of substrate does not have to be flat so that screen printing is widely used for printing on textiles, glass, ceramics and metals.

After microencapsulation, thermochromic materials, mainly leuco dye systems, can be used in thermochromic inks for printing application. For microcapsules intended to be used in ink applications, the size range needs to be well controlled.[11] For examples, digital printing is not usually used for printing with microcapsules due to nozzle clogging issues unless the size of microcapsules is smaller than 1 micron.[127] So far, the thermochromic microcapsules including encapsulated leuco dye systems and liquid crystals are approximately micron sized.[129, 130] For printing applications, their size is typically around several microns, which is 10-times larger than ordinary non-thermochromic pigment particles.[131] Smaller microcapsules have better mechanical properties and can bear high shearing forces so that they are more favoured as offset inks, while larger ones have better thermochromic performance and are more suited for screen printing.[11, 132] Screen printing technology also can obtain the highest quantity of microcapsules in the prints.[127]

1.3.2.2 Film fabrication and polymerization

Laminated packages, such as metal coated polymeric films, are believed to prevent chemical migration. The laminated package is generated layer by layer via co-extrusion of polymeric material or vacuum-deposition of metal materials, mostly aluminium.[133] These individual layers combine together by suitable adhesive to create a laminated structure as a better barrier due to additional interfaces between the layers significantly reducing the chemical migration.[134] In general, PET,[133] polyamide (PA),[135] polyethylene (PE),[136] poly(vinyl

chloride) (PVC),[137] polypropylene (PP)[138] and polyolefin (PO)[139] are commonly used polymeric resins for laminated packages. In addition to preventing chemical migration, these polymeric or metal layers also protect thermochromic materials from external moisture or chemicals.

In most cases, it is difficult to fabricate thermochromic materials into flexible films without polymer matrix if thermochromic materials are consisted of small molecules or particles. In view of this situation, an approach of using polymer matrix for thermochromic materials has been identified to fabricate flexible films inside laminated packages.

1.3.2.2.1 Film fabrication

A number of different methods are used to prepare polymeric films, such as phase inversion, moulding, casting, spin coating and interfacial polymerization. Phase inversion has been widely used for preparing the commercial polymeric films. In this process, the polymer solution is precipitated by immersion in a nonsolvent coagulant bath, cooling, evaporation or vapor adsorption. In a typical phase inversion process induced by immersion precipitation, the polymer solution is cast onto a substrate before being immersed into a coagulation bath to prepare an asymmetric film with a dense top layer and a porous sublayer.[140] A film can be easily fabricated through casting method, in which polymer solution is cast on a substrate before solvent evaporating at an appropriate temperature.[137] In moulding method, the melted polymer resin with or without other additives is extruded followed by compression moulding at an appropriate temperature to obtain the polymeric flat sheets.[141] A film with uniform thickness can be deposited on a planar solid substrate via spin coating, in which a polymer solution is dropped on a rotating substrate and the liquid drop will be flattened by the radial and hydrodynamic forces before solvent evaporation.[142] In the interfacial polymerization method, limited reactive monomers from two immiscible phases polymerize on the surface to create an extreme thin film with nanoscales.[143]

1.3.2.2.2 Chain-growth polymerization

The thermochromic films not only can be prepared through mixing thermochromic materials with polymer resin before moulding, coating or casting but also can be created via mixing thermochromic materials with reactive monomers before polymerization. Polymerization reactions can be divided into chain-growth polymerization and step-growth polymerization according to classification based on reaction kinetics.[144]

The olefins, including monosubstituted or 1,1-disubstituted mono-olefins and conjugated dienes, are the main monomers for chain-growth polymerization. The π-bonds in olefinic molecules are weaker than σ-bonds so that are easily broken to undergo chain-growth polymerization.[145] However, this polymerization does not automatically occur under normal conditions unless with participation of the initiators or applied energy. The initiators 'I' easily decompose homolytically or heterolytically due to weak bonds. There will be two free radicals 'R●' with a lone pair of electrons after homolytic decomposition. But in the case of heterolytic decomposition, there will be an anion $B^{\ominus}$ unilaterally owning a pair of electrons from the covalent bond and an electron-deficient cation $A^{\oplus}$. These active species, including free radicals, anions and cations, can respectively initiate free radical polymerization, anionic polymerization and cationic polymerization. In general, free radical polymerization involves initiation, propagation, chain transfer and termination (Figure 1.31).[146, 147]

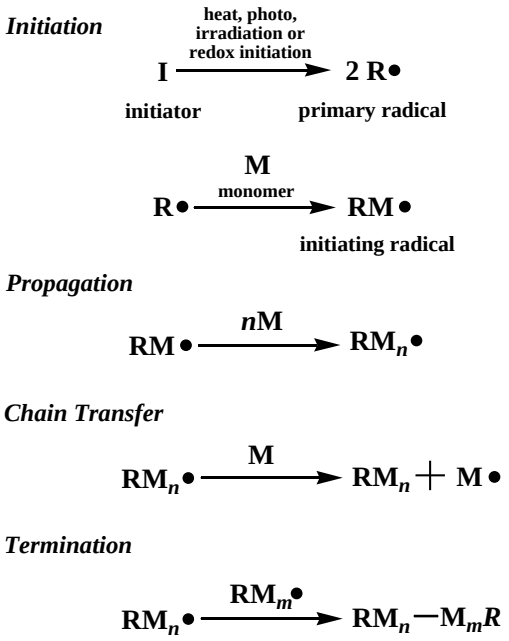

Figure 1.31 Mechanisms of conventional free radical polymerization.

Initiation is a process where the primary free radical 'R●' is formed and is then involved in formation of a monomeric radical 'RM●'. The monomeric free radicals continue to open the π-bonds of other olefinic molecules to cause the polymer chain growth in propagation process, when the active centre is always at the end of the active chain. The growing active chain 'RM_n●' may transfer activity to monomers, solvents, etc. to form a new active species 'M●' while the chain itself terminates in a chain transfer process. The living chain can also be terminated into a 'dead' polymer by another living chain. Many of these elementary reactions constitute the free radical polymerization.[147]

The elementary reactions of ion polymerization and coordination polymerization differ from that of free radical polymerization. Different kinds of ethylenic monomers have different selectivity for radical polymerization, anionic polymerization and cationic polymerization.[145] Among chain-growth polymerizations, the mechanism and kinetics of free radical polymerization have been well studied. On the other hand, important industrial polymer products, such as PE, polystyrene, PVC, poly(tetrafluoroethylene), polyvinyl acetate, polymethacrylate, polyacrylonitrile, poly(styrene-*co*-butadiene), neoprene and poly(acrylonitrile-*co*-butadiene-*co*-styrene) are synthesized through free radical polymerization.[146]

1.3.2.2.3 Step-growth polymerization

Polyester, polyamide, phenolic resin, epoxy resin and alkyd resin are mostly synthesized by step-growth polymerization, which plays an important role in polymer synthesis. Step-growth polymerization is a reaction between groups and can be categorized into polycondensation and others. A wide range of products involve polyimide, polycarbonate, poly(phenylene sulphide), polysiloxanes, cellulose, nucleic acid and proteins are from polycondensation. Apart from polycondensation, aryl nucleation of polysulfone, polyaddition of polyurethane, oxidative coupling of polyphenylene ether, ring-opening polymerization of caprolactam and Diels-Alder addition reaction are also accounted as step-growth polymerization.[148]

The polycondensation reaction repeats the condensation step to form a product. These reactions occur between functional groups from different monomers or different groups from same monomers. In this polymerization process, two monomers condense into a dimer, which may form a trimer with monomer or form a tetramer with another dimer. These oligomers further react with monomers, dimers or other oligomers by the same condensation reaction. The degree of polymerization increases as condensation continues until the reaction terminates. As a result, by-products usually appear in polycondensation reactions making the polydispersity of final product broad.[149]

Functionality (*f*) is dependent on the polymerizable groups in polymerization. For example, *f* of phenol is 1 in a general reaction but will change into 3 when phenol reacts with formaldehyde due to the *ortho* and *para* hydrogens of the phenolic hydroxyl group are the participating groups in the reaction. Generally, the polycondensation formula of difunctional monomers can be expressed as:

$$n\mathrm{A{-}A} + n\mathrm{B{-}B} \longrightarrow \left(\mathrm{A{-}AB{-}B}\right)_n$$

$$n\mathrm{A{-}B} \longrightarrow \left(\mathrm{A{-}B}\right)_n$$

where A and B represent two different types of functional groups. Therefore, linear polymer is obtained from polymerization of difunctional monomers while cross-linked polymers can be obtained from polymerization of monomers with $f \geq 3$. The controlling of molecular weight is the key to linear polymerization while controlling of gel point is the key to crosslinking polymerization.[150]

Typical functional groups for step-growth polymerization such as -OH, $-NH_2$, -COOH, -COOR, -COCl, $-(CO)_2O$, -Cl, $-SO_3H$, $-SO_2Cl$ can form characteristic bonds such as -OCO-, -O-, -NHCO-, -NHCOO-, $-SO_2-$ in polymers. Therefore, the performance, crystallinity, melting point and flexibility of polymer can be adjusted through changing the functional groups or composition of monomers.[149]

1.4 Objectives and approaches

In order to apply thermochromic materials to the packages of food or health care products, low toxic or even non-toxic thermochromic materials need to be developed for film or ink applications. So far, the only published nontoxic examples of thermochromic material were mixtures of anthocyanidin dyes, fatty acids, dodecyl gallate and PLA. However, the stability of anthocyanidin dyes prevent this system being commercially available.[56] Due to the widespread usage and production of leuco dye systems in current thermochromic products, we aimed to replace the toxic dyes or developers with low-toxic or even non-toxic ingredients. In this case, low-toxic dyes, such as sulfonephthaleins, and low-toxic developers, such as phenols, alkyl gallates, were tried in dye-developer-solvent triple systems with non-toxic solvents, such as long chain esters, acids or alcohols.

The cytotoxicity of each ingredient was first considered and after initial screening a selection of components were tested for their thermochromism. The materials were required to show clear colour change that is visible to the

naked eye in response to temperature change. The colour transition temperature was targeted to be adjustable to cover a practical and versatile range. It was desirable to attain both reversible and irreversible thermochromic systems, since reversible systems could be used as validation or proof of authenticity in anti-counterfeiting as well as a visual cue for optimal consumption at a given storage temperature; while irreversible systems could be used to trace the thermal history of supply chains acting as TTIs or to indicate product quality.

To protect such materials and make their thermochromic performances reversible, microencapsulation techniques will be applied to encapsulate them into core-shell structured microcapsules. According to the hydrophilic or hydrophobic nature of these core materials, appropriate microencapsulation technique chosen from interfacial deposition, spray drying, emulsion-solvent evaporation/extraction, in situ polymerization and phase separation-coacervation will be applied. After microencapsulation, tests of the thermochromic behaviour of obtained microcapsules will be conducted. The possibility of using these microcapsules as inks or film additives will also investigated.

As an alternative use, core materials lacking the shell structures will be dispersed into polymeric medium directly to obtain flexible hybrid films. Biocompatible polymers, such as silicones, polylactide, polyacrylates, PVA or polyethylene glycol (PEG) derivatives, will be used as candidate materials for polymeric matrix. The obtained film may exhibit thermochromic behaviour due to the presence of the core material, meanwhile, its colour change effect might be irreversible due to the diffusion effect of the core material into polymeric matrix. Therefore, the correlation of the colour of obtained film towards temperature and time should be investigated to check its potential as TTI. Other smart responsive properties of the film in response to external stimuli, such as pressure, light, pH, magnetic and electric fields or exposure to moisture and chemical compounds could also be checked.

1.5 Thesis outline

In **Chapter 2**, a new class of reversible and nontoxic dye–solvent binary thermochromic materials is reported. Dye-solvent binary systems including sulfonephthaleins, triarylmethane, leuco dye and azo dye in aliphatic chain esters, acids and alcohols were screened based on the appearance of thermochromism. The effect of dye concentration and solubility on thermochromic performance of selected sulfonephthalein-solvent binary systems was examined. The toxicity of sulfonephthaleins towards NIH-3T3 (noncancerous fibroblasts) cells were compared to rhodamine B base and cyanidin chloride, which are the representatives of thermochromic leuco dyes and food dyes. The mechanism study of the thermochromism is further investigated using various analytical techniques including ^{1}H NMR, UV-vis absorption spectroscopy, XRD, DSC and ATR-FTIR analysis as well as molecular dynamics simulations.

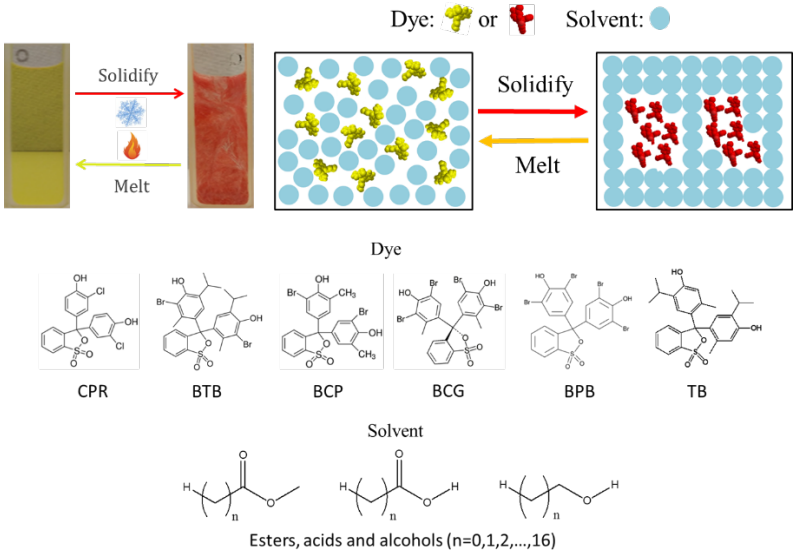

Figure 1.32 Thermochromic performance and mechanism of a dye-solvent binary system upon melting/freezing and the molecular structures of dyes and solvents.

Chapter 3 explores the method of microencapsulation towards dye-solvent binary thermochromic systems. Chlorophenol red (CPR), the best candidate of sulfonephthaleins as outlined in **Chapter 2**, was used as the dye while water was used as solvent. The thermochromic performance of CPR-water binary system was demonstrated in solution and emulsion. This phenomenon was in consistent with sulfonephthalein-aliphatic long chain solvent binary systems from **Chapter 2**. The core-shell structured microcapsules were prepared from the hydrolysis of trichlorosilane and subsequent crosslinking on surface of a w/o emulsion to form stable silicone shells encapsulating nontoxic CPR-water binary system. The composition and structure of the microcapsules were verified by ATR-FTIR and SEM analysis, while size distribution of microcapsules was conducted by DLS and ImageJ analysis software. Subsequently, these microcapsules were incorporated into a crosslinked PDMS matrix via photo free radical polymerization. The colour transition temperature of both microcapsules and films were measured in an acetone-dry ice cooling bath. In addition, the microcapsules were tested as potential thermochromic printing material using screen printing methods. The toxicity of both microcapsules and films towards NIH-3T3 (noncancerous fibroblasts) cell were also checked.

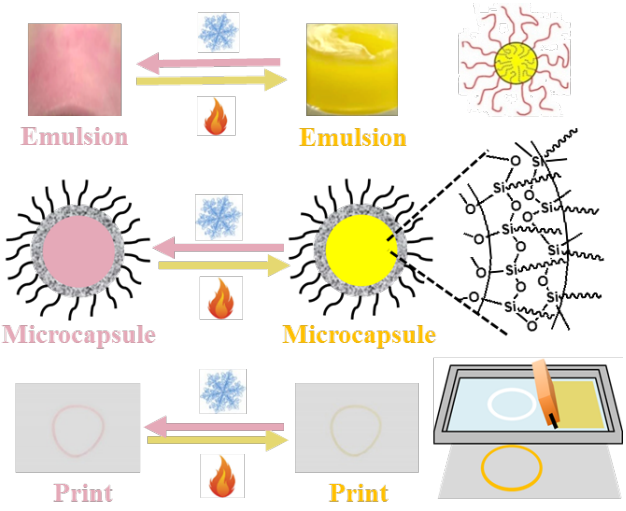

Figure 1.33 Thermochromic performances of core CPR-water emulsion in toluene, core-shell structured microcapsules and prints from screen printing using these microcapsules as inks.

Chapter 4 presents a dual functional sensor that shows clear and irreversible colour change towards temperature and base. Nontoxic solid CPR-dodecanoic acid (CPR-DA) particles, as an example of sulfonephthalein-solvent binary systems, were directly dispersed into a crosslinked PDMS matrix via photo free radical polymerization to obtain the sensor. The thermochromic performance between the hot and cold sensor were examined by UV-vis absorption spectroscopy and quantitively indicated by ΔE values. The diffusion of melted CPR-DA in PDMS matrix, which led to irreversible thermochromic behaviour of the obtained sensor, was characterized by optical microscopy. The property of cold sensor as a TTI was investigated through comparison of ΔE values of cold sensor after continuous heating or intermittent heating. Furthermore, the colour change performance of this sensor in response to base was investigated in the atmosphere of ammonia or biogenic amines. At last, leakage of dye from this sensor was carried out by an experiment where sensors with or without lamination were stirred with water.

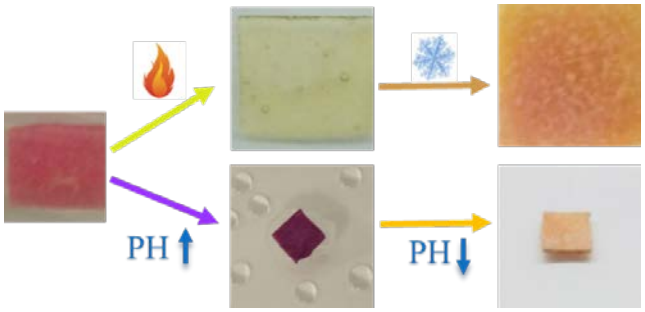

Figure 1.34 Irreversible colour change of the dual functional sensor towards temperature and basic vapour.

In **Chapter 5**, concluding remarks are presented along with some proposed future perspectives for the work outlined in this thesis.

1.6 References

1. Ghaani, M.; Cozzolino, C. A.; Castelli, G.; Farris, S., An overview of the intelligent packaging technologies in the food sector. *Trends in Food Science & Technology* **2016,** 51, 1-11.
2. Liu, A.; Shen, L.; Tan, Y.; Zeng, Z.; Liu, Y.; Li, C., Food integrity in China: Insights from the national food spot check data in 2016. *Food Control* **2018,** 84, 403-407.
3. Siró, I., Active and intelligent packaging of food. *Progress in food preservation* **2011**, 23-48.
4. Yam, K. L.; Takhistov, P. T.; Miltz, J., Intelligent packaging: concepts and applications. *Journal of food science* **2005,** 70 (1), R1-R10.
5. Han, J., A review of food packaging technologies and innovations. *Innovations in food packaging* **2014**, 3-12.
6. Kumar, P.; Reinitz, H.; Simunovic, J.; Sandeep, K.; Franzon, P., Overview of RFID technology and its applications in the food industry. *Journal of Food Science* **2009,** 74 (8), R101-R106.
7. De Jong, A.; Boumans, H.; Slaghek, T.; Van Veen, J.; Rijk, R.; Van Zandvoort, M., Active and intelligent packaging for food: Is it the future? *Food Additives and Contaminants* **2005,** 22 (10), 975-979.
8. Torrico, D. D.; Fuentes, S.; Viejo, C. G.; Ashman, H.; Gurr, P. A.; Dunshea, F. R., Analysis of thermochromic label elements and colour transitions using sensory acceptability and eye tracking techniques. *LWT* **2018,** 89, 475-481.
9. Galliani, D.; Mascheroni, L.; Sassi, M.; Turrisi, R.; Lorenzi, R.; Scaccabarozzi, A.; Stingelin, N.; Beverina, L., Thermochromic Latent-Pigment-Based Time–Temperature Indicators for Perishable Goods. *Advanced Optical Materials* **2015,** 3 (9), 1164-1168.
10. Yumiko, S.; Satoshi, T.; Takeshi, G.; Kenji, S., Molecular Structures of the Coloring Species of a Leuco Dye with Phenolic Color Developers. *Chemistry Letters* **2007,** 36 (8), 1010-1011.
11. Guan, Y.; Zhang, L.; Wang, D.; West, J. L.; Fu, S., Preparation of thermochromic liquid crystal microcapsules for intelligent functional fiber. *Materials & Design* **2018,** 147, 28-34.
12. Wang, Z.; Zhang, J.; Xie, J.; Wang, Z.; Yin, Y.; Li, J.; Li, Y.; Liang, S.; Zhang, L.; Cui, L., Polymer Bragg stack as color tunable photonic paper. *Journal of Materials Chemistry* **2012,** 22 (16), 7887-7893.
13. Seeboth, A.; Lötzsch, D.; Ruhmann, R., First example of a non-toxic thermochromic polymer material–based on a novel mechanism. *Journal of Materials Chemistry C* **2013,** 1 (16), 2811-2816.
14. Guo, J.; Fu, K.; Zhang, Z.; Yang, L.; Huang, Y.-C.; Huang, C.-I.; Zhu, L.; Chen, D., Reversible thermochromism via hydrogen-bonded cocrystals of polydiacetylene and melamine. *Polymer* **2016,** 105, 440-448.
15. Mitsuishi, M.; Koishikawa, Y.; Tanaka, H.; Sato, E.; Mikayama, T.; Matsui, J.; Miyashita, T., Nanoscale actuation of thermoreversible polymer brushes coupled with localized surface plasmon resonance of gold nanoparticles. *Langmuir* **2007,** 23 (14), 7472-7474.
16. Chung, W. Y.; Lee, S. M.; Koo, S. M.; Suh, D. H., Surfactant-free thermochromic hydrogel system: PVA/borax gel networks containing pH-sensitive dyes. *Journal of applied polymer science* **2004,** 91 (2), 890-893.

17. Zhang, Y.; Hu, Z.; Xiang, H.; Zhai, G.; Zhu, M., Fabrication of visual textile temperature indicators based on reversible thermochromic fibers. *Dyes and Pigments* **2019,** 162, 705-711.
18. Seeboth, A.; Lötzsch, D.; Ruhmann, R.; Muehling, O., Thermochromic Polymers—Function by Design. *Chemical Reviews* **2014,** 114 (5), 3037-3068.
19. Gürses, A.; Açıkyıldız, M.; Güneş, K.; Gürses, M. S., Dyes and pigments: their structure and properties. In *Dyes and Pigments*, Springer: **2016**, pp 13-29.
20. Reinitzer, E., quoted by Lehmann, OZ: Physik. *Chemie* **1889,** 4, 462-472.
21. Li, Q.; Li, Y.; Ma, J., Smart photochromic chiral nematic liquid crystal window. In Google Patents: 2015.
22. Sage, I., Thermochromic liquid crystals. *Liquid crystals* **2011,** 38 (11-12), 1551-1561.
23. White, T. J.; McConney, M. E.; Bunning, T. J., Dynamic color in stimuli-responsive cholesteric liquid crystals. *Journal of Materials Chemistry* **2010,** 20 (44), 9832-9847.
24. Clayton, T. S.; Owen, T. J.; Small, L., Small scale microencapsulated pigments and uses thereof. U.S. Patent US8883049B2, **2017**.
25. Flodberg, G.; Höjvall, L.; Hedenqvist, M. S.; Gedde, U. W., Migration of monomers from liquid crystalline poly (p-hydroxybenzoic acid-co-2-hydroxy-6-naphthoic acid). *Food Additives & Contaminants* **2002,** 19 (5), 492-501.
26. Pham, Q.-T.; Yao, Z.-H.; Chang, Y.-T.; Wang, F.-M.; Chern, C.-S., LCST phase transition kinetics of aqueous poly (N-isopropylacrylamide) solution. *Journal of the Taiwan Institute of Chemical Engineers* **2018,** 93, 63-69.
27. Chiappelli, M. C.; Hayward, R. C., Photonic Multilayer Sensors from Photo-Crosslinkable Polymer Films. *Advanced Materials* **2012,** 24 (45), 6100-6104.
28. Sussman, J.; Snoswell, D.; Kontogeorgos, A.; Baumberg, J. J.; Spahn, P., Thermochromic polymer opals. *Applied Physics Letters* **2009,** 95 (17), 173116.
29. Matsubara, K.; Watanabe, M.; Takeoka, Y., A thermally adjustable multicolor photochromic hydrogel. *Angewandte Chemie International Edition* **2007,** 46 (10), 1688-1692.
30. Weissman, J. M.; Sunkara, H. B.; Tse, A. S.; Asher, S. A. *Thermally Switchable Periodicities and Diffraction from Novel Mesoscopically Ordered Materials*; DTIC Document: **1996**.
31. Song, W.; Guan, Y.; Zhang, Y.; Zhu, X., Mutual interaction between embedded microgel particles and the surrounding hydrogel matrix. *Soft Matter* **2013,** 9 (9), 2629-2636.
32. Hu, Z.; Lu, X.; Gao, J., Hydrogel opals. *Advanced Materials* **2001,** 13 (22), 1708-1712.
33. Bašnec, K.; Perše, L. S.; Šumiga, B.; Huskić, M.; Meden, A.; Hladnik, A.; Podgornik, B. B.; Gunde, M. K., Relation between colour- and phase changes of a leuco dye-based thermochromic composite. *Scientific Reports* **2018,** 8 (1), 5511.
34. MacLaren, D.; White, M., Design rules for reversible thermochromic mixtures. *Journal of Materials Science* **2005,** 40 (3), 669-676.
35. MacLaren, D. C.; White, M. A., Dye–developer interactions in the crystal violet lactone–lauryl gallate binary system: implications for thermochromism. *Journal of Materials Chemistry* **2003,** 13 (7), 1695-1700.

36. MacLaren, D. C.; White, M. A., Competition between dye–developer and solvent–developer interactions in a reversible thermochromic system. *Journal of Materials Chemistry* **2003,** 13 (7), 1701-1704.
37. Tang, H.; MacLaren, D. C.; White, M. A., New insights concerning the mechanism of reversible thermochromic mixtures. *Canadian Journal of Chemistry* **2010,** 88 (11), 1063-1070.
38. Bourque, A. N.; White, M. A., Control of thermochromic behaviour in crystal violet lactone (CVL)/alkyl gallate/alcohol ternary mixtures. *Canadian Journal of Chemistry* **2014,** 93 (1), 22-31.
39. Seeboth, A.; Lötzsch, D.; Potechius, E.; Vetter, R., Thermochromic effects of leuco dyes studied in polypropylene. *Chinese journal of polymer science* **2006,** 24 (04), 363-368.
40. Panák, O.; Držková, M.; Kaplanová, M., Insight into the evaluation of colour changes of leuco dye based thermochromic systems as a function of temperature. *Dyes and Pigments* **2015,** 120, 279-287.
41. Panák, O.; Držková, M.; Kaplanová, M.; Novak, U.; Gunde, M. K., The relation between colour and structural changes in thermochromic systems comprising crystal violet lactone, bisphenol A, and tetradecanol. *Dyes and Pigments* **2017,** 136, 382-389.
42. Biedermann, S.; Tschudin, P.; Grob, K., Transfer of bisphenol A from thermal printer paper to the skin. *Analytical and bioanalytical chemistry* **2010,** 398 (1), 571-576.
43. Geens, T.; Goeyens, L.; Kannan, K.; Neels, H.; Covaci, A., Levels of bisphenol-A in thermal paper receipts from Belgium and estimation of human exposure. *Science of the Total Environment* **2012,** 435, 30-33.
44. Yoshikawa, K.; Fukuo, H.; Kuroda, J., Thermochromic compositions. U.S. Patent US4620941A, **1986**.
45. Smithers, P., Thermochromic inks and reducing household food waste. **2013**.
46. Balakrishnan, S.; Lee, S.; Kim, J.-M., Thermochromic reversibility of conjugated polymers derived from a diacetylenic lipid containing lithium salt. *Journal of Materials Chemistry* **2010,** 20 (12), 2302-2304.
47. Dufresne, G.; Bouchard, J.; Belletête, M.; Durocher, G.; Leclerc, M., Thermochromic and solvatochromic conjugated polymers by design. *Macromolecules* **2000,** 33 (22), 8252-8257.
48. Yuan, Z.; Lee, C. W.; Lee, S. H., Reversible Thermochromism in Hydrogen-Bonded Polymers Containing Polydiacetylenes. *Angewandte Chemie International Edition* **2004,** 43 (32), 4197-4200.
49. Guo, H.; Zhang, J.; Porter, D.; Peng, H.; Löwik, D. W.; Wang, Y.; Zhang, Z.; Chen, X.; Shao, Z., Ultrafast and reversible thermochromism of a conjugated polymer material based on the assembly of peptide amphiphiles. *Chemical Science* **2014,** 5 (11), 4189-4195.
50. Jiang, M.; Wang, E.; Xu, L.; Kang, Z.; Lian, S., The first example of multilayer films with thermochromic properties. *Journal of Solid State Chemistry* **2004,** 177 (4), 1776-1779.
51. De Meyer, T.; Hemelsoet, K.; Van Speybroeck, V.; De Clerck, K., Substituent effects on absorption spectra of pH indicators: An experimental and computational study of sulfonphthaleine dyes. *Dyes and Pigments* **2014,** 102, 241-250.
52. Seeboth, A.; Kriwanek, J.; Vetter, R., The first example of thermochromism of dyes embedded in transparent polymer gel networks. *Journal of Materials Chemistry* **1999,** 9 (10), 2277-2278.

53. Kriwanek, J.; Lötzsch, D.; Vetter, R.; Seeboth, A., Influence of a zwitterionic surfactant on the chromogenic behavior of a dye-containing aqueous PVA–polyether gel network. *Polymers for Advanced Technologies* **2003,** 14 (2), 79-82.

54. Naorem, H.; Devi, S. D., Gelling Behavior of PVA or its Blends with Other Polymers in Presence of Borax and Thermochromism in Such Gel Network Materials. *Journal of Surface Science and Technology* **2011,** 27 (3-4), 233-243.

55. Detlef, L., Ralf, R., Arno, S., Thermochromic biopolymer based on natural anthocyanidin dyes. *Open Journal of Polymer Chemistry* **2013,** 3, 43-47.

56. Dao, L. T.; Takeoka, G. R.; Edwards, R. H.; Berrios, J. D. J., Improved Method for the Stabilization of Anthocyanidins. *Journal of Agricultural and Food Chemistry* **1998,** 46 (9), 3564-3569.

57. Sinnokrot, M. O.; Valeev, E. F.; Sherrill, C. D., Estimates of the ab initio limit for π− π interactions: The benzene dimer. *Journal of the American Chemical Society* **2002,** 124 (36), 10887-10893.

58. McGaughey, G. B.; Gagné, M.; Rappé, A. K., π-Stacking interactions alive and well in proteins. *Journal of Biological Chemistry* **1998,** 273 (25), 15458-15463.

59. Sivaramakrishnan, V.; Ilamathi, M.; Ghosh, K.; Sathish, S.; Gowda, T.; Vishwanath, B.; Rangappa, K.; Dhananjaya, B., Virtual analysis of structurally diverse synthetic analogs as inhibitors of snake venom secretory phospholipase A2. *Journal of Molecular Recognition* **2016,** 29 (1), 22-32.

60. Perepichka, I. F.; Besbes, M.; Levillain, E.; Sallé, M.; Roncali, J., Hydrophilic oligo (oxyethylene)-derivatized poly (3, 4-ethylenedioxythiophenes): Cation-responsive optoelectroelectrochemical properties and solid-state chromism. *Chemistry of Materials* **2002,** 14 (1), 449-457.

61. Wu, Z.; Petzold, A.; Henze, T.; Thurn-Albrecht, T.; Lohwasser, R. H.; Sommer, M.; Thelakkat, M., Temperature and molecular weight dependent hierarchical equilibrium structures in semiconducting poly (3-hexylthiophene). *Macromolecules* **2010,** 43 (10), 4646-4653.

62. Garreau, S.; Leclerc, M.; Errien, N.; Louarn, G., Planar-to-nonplanar conformational transition in thermochromic polythiophenes: a spectroscopic study. *Macromolecules* **2003,** 36 (3), 692-697.

63. Wang, Y.; Archambault, N.; Marold, A.; Weng, L.; Lucht, B. L.; Euler, W. B., Observation of two-step thermochromism in poly (3-docosylthiophene): DSC and reflection spectroscopy. *Macromolecules* **2004,** 37 (14), 5415-5422.

64. Ewbank, P. C.; Stefan, M. C.; Sauvé, G.; McCullough, R. D., Synthesis, characterization and properties of regioregular polythiophene-based materials. *Handbook of Thiophene-Based Materials* **2009**, 157-217.

65. Wang, Y.; Archambault, N.; Belcher, A. M.; Busse, D.; Damon, D. B.; Mills, A.; Riddle, A. E.; Samardjiev, I. J.; Lucht, B. L.; Euler, W. B., Mesophase Formation in Regioregular Poly (3-alkylthiophene) s Containing Long Chain Alkyl Groups. *Macromolecules* **2008,** 41 (19), 7115-7121.

66. Cataldi, P.; Bayer, I. S.; Cingolani, R.; Marras, S.; Chellali, R.; Athanassiou, A., A thermochromic superhydrophobic surface. *Scientific reports* **2016,** 6, 27984.

67. Suzuki, S.; Morita, Y.; Fukui, K.; Sato, K.; Shiomi, D.; Takui, T.; Nakasuji, K., Aromaticity on the pancake-bonded dimer of neutral phenalenyl radical as studied by MS and NMR spectroscopies and NICS analysis. *Journal of the American Chemical Society* **2006,** 128 (8), 2530-2531.

68. Morita, Y.; Suzuki, S.; Fukui, K.; Nakazawa, S.; Kitagawa, H.; Kishida, H.; Okamoto, H.; Naito, A.; Sekine, A.; Ohashi, Y., Thermochromism in an organic crystal based on the coexistence of σ-and π-dimers. *Nature Materials* **2008,** 7 (1), 48.

69. Huang, J.; Sumpter, B. G.; Meunier, V.; Tian, Y.-H.; Kertesz, M., Cyclo-biphenalenyl biradicaloid molecular materials: Conformation, tautomerization, magnetism, and thermochromism. *Chemistry of Materials* **2010,** 23 (3), 874-885.

70. Naumov, P.; Lee, S. C.; Ishizawa, N.; Jeong, Y. G.; Chung, I. H.; Fukuzumi, S., New Type of Dual Solid-State Thermochromism: Modulation of Intramolecular Charge Transfer by Intermolecular π− π Interactions, Kinetic Trapping of the Aci-Nitro Group, and Reversible Molecular Locking. *The Journal of Physical Chemistry A* **2009,** 113 (42), 11354-11366.

71. Grenier, C. R.; Pisula, W.; Joncheray, T. J.; Müllen, K.; Reynolds, J. R., Regiosymmetric Poly (dialkylphenylenedioxythiophene) s: Electron-Rich, Stackable π-Conjugated Nanoribbons. *Angewandte Chemie International Edition* **2007,** 46 (5), 714-717.

72. Apperloo, J. J.; Janssen, R. A.; Malenfant, P. R.; Fréchet, J. M., Concentration-dependent thermochromism and supramolecular aggregation in solution of triblock copolymers based on lengthy oligothiophene cores and poly (benzyl ether) dendrons. *Macromolecules* **2000,** 33 (19), 7038-7043.

73. Lee, C.; Sung, Y. W.; Park, J. W., Multiple equilibria of phenothiazine dyes in aqueous cyclodextrin solutions. *The Journal of Physical Chemistry B* **1999,** 103 (5), 893-898.

74. Donati, F.; Pucci, A.; Cappelli, C.; Mennucci, B.; Ruggeri, G., Modulation of the optical response of polyethylene films containing luminescent perylene chromophores. *The Journal of Physical Chemistry B* **2008,** 112 (12), 3668-3679.

75. Kunzelman, J.; Crenshaw, B. R.; Kinami, M.; Weder, C., Self-Assembly and Dispersion of Chromogenic Molecules: A Versatile and General Approach for Self-Assessing Polymers. *Macromolecular rapid communications* **2006,** 27 (23), 1981-1987.

76. Crenshaw, B. R.; Kunzelman, J.; Sing, C. E.; Ander, C.; Weder, C., Threshold temperature sensors with tunable properties. *Macromolecular Chemistry and Physics* **2007,** 208 (6), 572-580.

77. Donati, F.; Pucci, A.; Ruggeri, G., Temperature and chemical environment effects on the aggregation extent of water soluble perylene dye into vinyl alcohol-containing polymers. *Physical Chemistry Chemical Physics* **2009,** 11 (29), 6276-6282.

78. Pucci, A.; Donati, F.; Nazzi, S.; Barretta, G. U.; Pescitelli, G.; Di Bari, L.; Ruggeri, G., Association phenomena of a chiral perylene derivative in solution and in poly (ethylene) dispersion. *Reactive and Functional Polymers* **2010,** 70 (12), 951-960.

79. Crenshaw, B. R.; Weder, C., Phase Separation of Excimer-Forming Fluorescent Dyes and Amorphous Polymers: A Versatile Mechanism for Sensor Applications. *Advanced Materials* **2005,** 17 (12), 1471-1476.

80. Kinami, M.; Crenshaw, B. R.; Weder, C., Polyesters with built-in threshold temperature and deformation sensors. *Chemistry of materials* **2006,** 18 (4), 946-955.

81. Pucci, A.; Signori, F.; Bizzarri, R.; Bronco, S.; Ruggeri, G.; Ciardelli, F., Threshold temperature luminescent indicators from biodegradable poly (lactic acid)/poly (butylene succinate) blends. *Journal of Materials Chemistry* **2010,** 20 (28), 5843-5852.

82. Donati, F.; Pucci, A.; Boggioni, L.; Tritto, I.; Ruggeri, G., New cyclic olefin copolymer for the preparation of thermally responsive luminescent films. *Macromolecular Chemistry and Physics* **2009,** 210 (9), 728-735.

83. Pucci, A.; Di Cuia, F.; Signori, F.; Ruggeri, G., Bis (benzoxazolyl) stilbene excimers as temperature and deformation sensors for biodegradable poly (1, 4-butylene succinate) films. *Journal of Materials Chemistry* **2007,** 17 (8), 783-790.

84. Kunzelman, J.; Chung, T.; Mather, P. T.; Weder, C., Shape memory polymers with built-in threshold temperature sensors. *Journal of Materials Chemistry* **2008,** 18 (10), 1082-1086.

85. Jarumaneeroj, C.; Tashiro, K.; Chirachanchai, S., Shifting from Hydrogen Bond Network to π–π Stacking: A Key Mechanism for Reversible Thermochromic Sulfonated Poly (Ether Ether Ketone). *Macromolecular rapid communications* **2014,** 35 (16), 1397-1401.

86. Nishiuchi, T.; Kuwatani, Y.; Nishinaga, T.; Iyoda, M., Dynamic Molecular Tweezers Composed of Dibenzocyclooctatetraene Units: Synthesis, Properties, and Thermochromism in Host–Guest Complexes. *Chemistry–A European Journal* **2009,** 15 (28), 6838-6847.

87. Sagawa, T.; Tobata, H.; Ihara, H., Exciton interactions in cyanine dye–hyaluronic acid (HA) complex: reversible and biphasic molecular switching of chromophores induced by random coil-to-double-helix phase transition of HA. *Chemical Communications* **2004**, (18), 2090-2091.

88. Uhlenhaut, D. I.; Smith, P.; Caseri, W., Color switching in gold—polysiloxane elastomeric nanocomposites. *Advanced Materials* **2006,** 18 (13), 1653-1656.

89. Liu, Y.; Mills, E. N.; Composto, R. J., Tuning optical properties of gold nanorods in polymer films through thermal reshaping. *Journal of Materials Chemistry* **2009,** 19 (18), 2704-2709.

90. Karg, M.; Pastoriza-Santos, I.; Pérez-Juste, J.; Hellweg, T.; Liz-Marzán, L. M., Nanorod-Coated PNIPAM Microgels: Thermoresponsive Optical Properties. *Small* **2007,** 3 (7), 1222-1229.

91. Carotenuto, G.; Nicolais, F., Synthesis of polymer-embedded metal, semimetal, or sulfide clusters by thermolysis of mercaptide molecules dissolved in polymers. *Recent Patents on Materials Science* **2008,** 1 (1), 1-11.

92. Suzuki, D.; Kawaguchi, H., Hybrid microgels with reversibly changeable multiple brilliant color. *Langmuir* **2006,** 22 (8), 3818-3822.

93. Tollan, C. M.; Marcilla, R.; Pomposo, J. A.; Rodriguez, J.; Aizpurua, J.; Molina, J.; Mecerreyes, D., Irreversible thermochromic behavior in gold and silver nanorod/polymeric ionic liquid nanocomposite films. *ACS applied materials & interfaces* **2008,** 1 (2), 348-352.

94. El Deen, M. M. K., The Intelligent Colorimetric Timer Indicator Systems to develop label Packaging Industry in Egypt. *International Design Journal* **2014,** 4 (2).

95. Dainelli, D.; Gontard, N.; Spyropoulos, D.; Zondervan-van den Beuken, E.; Tobback, P., Active and intelligent food packaging: legal aspects and safety concerns. *Trends in Food Science & Technology* **2008,** 19, S103-S112.

96. Report, W. R. A. P. *Thermochromic inks and reducing household food waste*; Waste & Resources Action Programme: Oxon, United Kingdom, **2013**.

97. F. Gibbs, S. K., Inteaz Alli, Catherine N. Mulligan, Bernard, Encapsulation in the food industry: a review. *International journal of food sciences and nutrition* **1999,** 50 (3), 213-224.

98. Nedovic, V.; Kalusevic, A.; Manojlovic, V.; Levic, S.; Bugarski, B., An overview of encapsulation technologies for food applications. *Procedia Food Science* **2011,** 1, 1806-1815.

99. Pielichowska, K.; Pielichowski, K., Phase change materials for thermal energy storage. *Progress in materials science* **2014,** 65, 67-123.

100. Sarier, N.; Onder, E., Organic phase change materials and their textile applications: an overview. *Thermochimica Acta* **2012,** 540, 7-60.

101. Li, W.; Zhang, X.-X.; Wang, X.-C.; Niu, J.-J., Preparation and characterization of microencapsulated phase change material with low remnant formaldehyde content. *Materials Chemistry and Physics* **2007,** 106 (2-3), 437-442.

102. Tözüm, M. S.; Aksoy, S. A.; Alkan, C., Microencapsulation of Three-Component Thermochromic System for Reversible Color Change and Thermal Energy Storage. *Fibers and Polymers* **2018,** 19 (3), 660-669.

103. Fukuo, H.; Onoguchi, T., Microcapsule manufacture. U.S. Patent US4753759A, **1988**.

104. Geng, X.; Li, W.; Yin, Q.; Wang, Y.; Han, N.; Wang, N.; Bian, J.; Wang, J.; Zhang, X., Design and fabrication of reversible thermochromic microencapsulated phase change materials for thermal energy storage and its antibacterial activity. *Energy* **2018,** 159, 857-869.

105. Park, J.; Ye, M.; Park, K., Biodegradable polymers for microencapsulation of drugs. *Molecules* **2005,** 10 (1), 146-161.

106. Su, J.-F.; Huang, Z.; Ren, L., High compact melamine-formaldehyde microPCMs containing n-octadecane fabricated by a two-step coacervation method. *Colloid and Polymer Science* **2007,** 285 (14), 1581-1591.

107. Geng, X.; Li, W.; Wang, Y.; Lu, J.; Wang, J.; Wang, N.; Li, J.; Zhang, X., Reversible thermochromic microencapsulated phase change materials for thermal energy storage application in thermal protective clothing. *Applied energy* **2018,** 217, 281-294.

108. Bašnec, K.; Perše, L. S.; Šumiga, B.; Huskić, M.; Meden, A.; Hladnik, A.; Podgornik, B. B.; Gunde, M. K., Relation between colour-and phase changes of a leuco dye-based thermochromic composite. *Scientific reports* **2018,** 8 (1), 5511.

109. Kim, I. J.; Ramalingam, M.; Son, Y.-A., Investigation of reversible self-thermochromism in microencapsulated fluoran-based materials. *Dyes and Pigments* **2018,** 151, 64-74.

110. Thanawala, K.; Mutneja, N.; Khanna, A.; Raman, R., Development of self-healing coatings based on linseed oil as autonomous repairing agent for corrosion resistance. *Materials* **2014,** 7 (11), 7324-7338.

111. Gupta, R.; Kandasubramanian, B., Hybrid caged nanostructure ablative composites of octaphenyl-POSS/RF as heat shields. *RSC Advances* **2015,** 5 (12), 8757-8769.

112. Chen, C. P.; Kim, D. S.; Jhun, C. G., Electro-Optical Effects of a Color Polymer-Dispersed Liquid Crystal Device by Micro-Encapsulation with a Pigment-Doped Shell. *Crystals* **2019,** 9 (7), 364.

113. Kim, D. S.; Yeo, D. B.; Heo, K. C.; Gwag, J. S.; Jhun, C. G., Color Polymer Dispersed Liquid Crystal Device with Colored Core-Shell Structure. *Molecular Crystals and Liquid Crystals* **2015,** 613 (1), 39-44.

114. Okochi, H.; Nakano, M., Preparation and evaluation of w/o/w type emulsions containing vancomycin. *Advanced drug delivery reviews* **2000,** 45 (1), 5-26.

115. Crotts, G.; Park, T. G., Protein delivery from poly (lactic-co-glycolic acid) biodegradable microspheres: release kinetics and stability issues. *Journal of microencapsulation* **1998,** 15 (6), 699-713.

116. Sinha, V.; Trehan, A., Biodegradable microspheres for protein delivery. *Journal of controlled release* **2003,** 90 (3), 261-280.

117. Mutaliyeva, B.; Grigoriev, D.; Madybekova, G.; Sharipova, A.; Aidarova, S.; Saparbekova, A.; Miller, R., Microencapsulation of insulin and its release using w/o/w double emulsion method. *Colloids and Surfaces A: Physicochemical and Engineering Aspects* **2017,** 521, 147-152.

118. Paulo, F.; Santos, L., Microencapsulation of caffeic acid and its release using aw/o/w double emulsion method: Assessment of formulation parameters. *Drying Technology* **2019,** 37 (8), 950-961.

119. Taguchi, Y.; Suzuki, T.; Saito, N.; Yokoyama, H.; Tanaka, M., Preparation of soft microcapsules containing multiple core materials with interfacial dehydration reaction using the (W/O)/W emulsion. *Journal of microencapsulation* **2017,** 34 (8), 744-753.

120. Huang, Y.; Zhou, W., Microencapsulation of anthocyanins through two-step emulsification and release characteristics during in vitro digestion. *Food chemistry* **2019,** 278, 357-363.

121. Meng, F.; Ma, G.; Liu, Y.; Qiu, W.; Su, Z., Microencapsulation of bovine hemoglobin with high bio-activity and high entrapment efficiency using a W/O/W double emulsion technique. *Colloids and surfaces B: Biointerfaces* **2004,** 33 (3-4), 177-183.

122. Iwata, M.; McGinity, J., Preparation of multi-phase microspheres of poly (D, L-lactic acid) and poly (D, L-lactic-co-glycolic acid) containing a W/O emulsion by a multiple emulsion solvent evaporation technique. *Journal of microencapsulation* **1991,** 9 (2), 201-214.

123. Sah, H., Microencapsulation techniques using ethyl acetate as a dispersed solvent: effects of its extraction rate on the characteristics of PLGA microspheres. *Journal of controlled release* **1997,** 47 (3), 233-245.

124. Pagano, A. P. E.; Khalid, N.; Kobayashi, I.; Nakajima, M.; Neves, M. A.; Bastos, E. L., Microencapsulation of betanin in monodisperse W/O/W emulsions. *Food research international* **2018,** 109, 489-496.

125. Souza, C. J.; Comunian, T. A.; Kasemodel, M. G.; Favaro-Trindade, C. S., Microencapsulation of lactase by W/O/W emulsion followed by complex coacervation: Effects of enzyme source, addition of potassium and core to shell ratio on encapsulation efficiency, stability and kinetics of release. *Food research international* **2019,** 121, 754-764.

126. Adachi, S.; Imaoka, H.; Ashida, H.; Maeda, H.; Matsuno, R., Preparation of microcapsules of W/O/W emulsions containing a polysaccharide in the outer aqueous phase by spray-drying. *European journal of lipid science and technology* **2004,** 106 (4), 225-231.

127. Milošević, R.; Kasikovic, N.; Pavlović, Ž.; Stankovielesini, U.; Urbas, R., *Microcapsules properties and their application using different printing techniques*. **2016**.

128. Khan, S.; Lorenzelli, L.; Dahiya, R. S., Technologies for printing sensors and electronics over large flexible substrates: a review. *IEEE Sensors Journal* **2014,** 15 (6), 3164-3185.

129. Zhu, X.; Liu, Y.; Li, Z.; Wang, W., Thermochromic microcapsules with highly transparent shells obtained through in-situ polymerization of urea formaldehyde around thermochromic cores for smart wood coatings. *Scientific reports* **2018,** 8 (1), 4015.

130. Lee, S. S.; Kim, B.; Kim, S. K.; Won, J. C.; Kim, Y. H.; Kim, S. H., Robust microfluidic encapsulation of cholesteric liquid crystals toward photonic ink capsules. *Advanced Materials* **2015,** 27 (4), 627-633.

131. Kulčar, R.; Gunde, M. K.; Friškovec, M., Thermochromic inks–dynamic colour possibilities. *Dyes and Pigments* **2010,** 86, 271-277.

132. Kulčar, R.; Klanjšeg Gunde, M.; Knešaurek, N., Dynamic colour possibilities and functional properties of thermochromic printing inks. *Acta graphica: znanstveni časopis za tiskarstvo i grafičke komunikacije* **2012,** 23 (1-2), 25-36.

133. Jesdinszki, M.; Struller, C.; Rodler, N.; Blondin, D.; Cassio, V.; Kucukpinar, E.; Langowski, H.-C., Evaluation of adhesion strength between thin aluminum layer and poly (ethylene terephthalate) substrate by peel tests—A practical approach for the packaging industry. *Journal of Adhesion Science and Technology* **2012,** 26 (20-21), 2357-2380.

134. Gårdebjer, S.; Gebäck, T.; Andersson, T.; Fratini, E.; Baglioni, P.; Bordes, R.; Viridén, A.; Nicholas, M.; Lorén, N.; Larsson, A., The impact of interfaces in laminated packaging on transport of carboxylic acids. *Journal of Membrane Science* **2016,** 518, 305-312.

135. Guo, Z.; Fan, Y.; Du, S., Influence of lithium hexafluorophosphate/ethylene carbonate/dimethyl carbonate electrolyte soaking on heat seal strength of polyamide 6/aluminum/cast-polypropylene laminates used as lithium-ion battery packaging. *Journal of Plastic Film & Sheeting* **2018,** 34 (1), 10-26.

136. Olafsson, G.; Hildingsson, I., Sorption of fatty acids into low density polyethylene and its effect on adhesion with aluminum foil in laminated packaging material. *Journal of agricultural and food chemistry* **1995,** 43 (2), 306-312.

137. Liu, B.; Chen, J.; Du, X.; Xue, L., Poly (vinyl chloride)/montmorillonite hybrid membranes for total-heat recovery ventilation. *Journal of membrane science* **2013,** 443, 83-92.

138. Wang, Z.; Yang, H.; Pan, N.; Li, W.; Xie, Y.; Liu, Z.; Fang, Y., Effect of Polyethylene Film Lamination on the Water Absorbency of Hydrophilic-finished Polypropylene Non-woven Fabric. *Fibers and Polymers* **2019,** 20 (7), 1404-1410.

139. Lazić, V.; Budinski-Simendić, J.; Gvozdenović, J.; Simendić, B., Barrier properties of coated and laminated polyolefin films for food packaging. *Acta Physica Polonica A* **2010,** 117 (5), 855-858.

140. Ismail, A. F.; Khulbe, K. C.; Matsuura, T., Membrane Fabrication/Manufacturing Techniques. In *Gas Separation Membranes*, Springer: **2015**; pp 193-220.
141. Zia, J.; Paul, U. C.; Heredia-Guerrero, J. A.; Athanassiou, A.; Fragouli, D., Low-density polyethylene/curcumin melt extruded composites with enhanced water vapor barrier and antioxidant properties for active food packaging. *Polymer* **2019,** 175, 137-145.
142. Danglad-Flores, J.; Eickelmann, S.; Riegler, H., Deposition of polymer films by spin casting: A quantitative analysis. *Chemical Engineering Science* **2018,** 179, 257-264.
143. Seman, M. A.; Khayet, M.; Hilal, N., Nanofiltration thin-film composite polyester polyethersulfone-based membranes prepared by interfacial polymerization. *Journal of membrane science* **2010,** 348 (1-2), 109-116.
144. Nicholson, J., *The chemistry of polymers*. Royal Society of Chemistry: **2017**.
145. Seymour, R. B.; Carraher, C. E., *Polymer chemistry*. Marcel Dekker New York: **2000**; Vol. 181.
146. Matyjaszewski, K.; Davis, T. P., *Handbook of radical polymerization*. John Wiley & Sons: **2003**.
147. Moad, G.; Solomon, D. H., *The chemistry of radical polymerization*. Elsevier: **2006**.
148. Rogers, M. E.; Long, T. E., *Synthetic methods in step-growth polymers*. John Wiley & Sons: 2003.
149. Odian, G., *Principles of polymerization*. John Wiley & Sons: **2004**.
150. Koltzenburg, S.; Maskos, M.; Nuyken, O.; Mülhaupt, R.; Matyjaszewski, K., *Polymer Chemistry*. Springer: **2017**.

Chapter 2. A nontoxic reversible thermochromic binary system via π-π stacking of sulfonephthaleins

2.1 Chapter perspective

Toxic ingredients limit the use of current leuco dye systems, which is a triple system consisted of dye, developer and solvent, to non-food applications or food packaging articles with significant barriers. In this chapter, dye-solvent binary systems with less toxic dyes and solvents will be prepared to demonstrate the thermochromic performance. Cell toxicity tests of these dyes towards NIH-3T3 cells will also be conducted to compare the toxicity of an anthocyanin, the bench mark of the current only known nontoxic food dye with thermochromism. The mechanism of thermochromic behaviour of these binary systems will further be investigated.

This chapter is an article published in *Journal of Materials Chemistry C*, 2019, 7, 9335

Journal of Materials Chemistry C

PAPER

View Article Online
View Journal | View Issue

Cite this: J. Mater. Chem. C, 2019, 7, 9335

A nontoxic reversible thermochromic binary system *via* π–π stacking of sulfonephthaleins†

Bingxin Liu, Hadi Ranji-Burachaloo, Paul A. Gurr, Eirini Goudeli and Greg G. Qiao *

Received 18th April 2019,
Accepted 1st July 2019

DOI: 10.1039/c9tc02071c

rsc.li/materials-c

The mechanisms of thermochromic materials are mostly based on Bragg reflection, surface plasmon absorption, molecular structure changes, conformational stretching or aggregation. Here, a simple class of dye–solvent binary systems with clear and reversible thermochromism around ambient temperatures is reported with an alternative mechanism. This system comprises commercially available sulfonephthaleins dissolved in liquid linear chain esters, acids or alcohols, which demonstrate colour changes at different temperatures when the solvents transition from solid to liquid states. The colour changing mechanism is based on π–π stacked aggregation or disaggregation of the sulfonephthalein dyes. Cell toxicity tests confirmed that the sulfonephthalein dyes are less toxic to NIH-3T3 cells than cyanidin chloride, which is the only reported nontoxic food dye affording thermochromism, while this is based on an alternative mechanism. With the choice of a nontoxic solvent, this binary system can form a nontoxic thermochromic material.

1. Introduction

There are many examples of commercial products that change colour under an external stimulus, such as pressure (piezochromic), light (photochromic), temperature (thermochromic) and changes in pH. Thermochromism was first discovered in 1888 by Reinitzer[1] with the discovery of the properties of cholesteryl benzoate liquid crystals. Thermochromic products have had great commercial success in the past with colour changing products such as beer cans, coffee mugs, nail polish, costumes and hair dyes. To date, scientists have developed a large range of thermochromic materials and systems with a number being applied in industrial applications.[2] Examples of thermochromic materials include liquid crystals,[3,4] photonic crystals,[5] gold or silver nanoparticles,[6] leuco dye systems,[7] polydiacetylene derivatives[8] and aggregachromic dyes.[9] Bragg reflection,[5,10] surface plasmon absorption,[6] ring-opening and -closing of molecular structures,[7] protonation and deprotonation of dye materials[11] and conformational stretching of spiral structures[4] have been used to explain the mechanisms of these thermochromic materials. Nevertheless, few reports mention the relative toxicity of these thermochromic materials and concerns about their safety have limited their application in the areas of food or health care product packaging.[12]

Currently, the most utilized commercial thermochromic products are based on leuco dye systems. The leuco dye system consists of three-components, dye, developer and solvent.[13] The thermochromic mechanism of the leuco dye system relies on the molecular structure of the dye component switching between two isomeric forms in the presence of a developer, and this process is triggered by a phase change of the solvent.[14] The solvent components of the system are typically relatively nontoxic long chain esters, alcohols or fatty acids.[15] The dye components are one of the following class of compounds including triphenylmethane phthalides, rhodamine lactams, fluorans, phenothiazines, indolylphthalides, spiropyrans and leucoauramines, while the developers are typically phenolic compounds, such as thioureas, guanidines, benzothiazoles or benzothiazolyls.[16] Due to concerns over the toxicity of the dyes and developers, industry is reticent to use these formulations on food product labels without significant barriers between the dye system and the food itself. A common consensus in the packaging area is that these leuco dye materials are recommended to only be applied to glass, metal or thick plastic substrate surfaces to avoid direct food contact.[12] Hence, solving the toxicity issue of dyes and developers is key to reducing the toxic limitations associated with the leuco dye system.

Sulfonephthalein dyes manifest low toxicity according to their material safety data sheets. These commercially available dyes are well-known pH indicators, which change colour reversibly, based on pH triggered ring-opening and ring-closing of their chemical structures.[17] Based on their low toxicity and pH-chromogenic properties, sulfonephthalein dyes

Department of Chemical Engineering, The University of Melbourne, VIC 3010, Australia. E-mail: gregghq@unimelb.edu.au

† Electronic supplementary information (ESI) available. See DOI: 10.1039/c9tc02071c

have been applied in colour changing hydrogels[18,19] and time-temperature indicators for monitoring food quality.[20] Recently, they have been used to fabricate thermochromic systems, for example, one sulfonephthalein dye (bromocresol purple) was used as a colour former in a three-component thermochromic system, in which stearic acid was the developer and long-chain alcohols were described as solvents with the reversible ring-opening mechanism similar to that of the leuco dye system.[21]

π–π stacking, a non-covalent interaction between molecules, has been reported to be the source of reversible thermochromism in conjugated polymers[22,23] and crystals.[24–26] It has also been used to explain the colour changing phenomenon of aggregachromic dyes with highly conjugated planar structures,[9,27] such as triphenylenes[28] and perylene bisimides,[29] which form dimers or other agglomerates in solution with an increase in dye concentration. Theoretical models were developed to explain or predict these aggregation behaviours using UV-vis and ^{1}H NMR spectroscopy.[30] Based on π–π stacking theory, aggregachromic dye–polymer binary systems have been extensively studied with regard to their thermoresponsive colour changing properties.[31–36] There are two main areas in aggregachromic dye–polymer studies. The first involves mixing fluorescent dyes into polymer matrices to fabricate binary systems that show a reversible or irreversible fluorescence change at different temperatures. However, these colour changes can only be observed under applied conditions, such as UV light.[31–33,35,36] The second area involves dye–polymer binary systems that show thermochromism observable by the naked eye. However, their colour changes are irreversible and only occur above the glass transition temperatures of the polymer matrix.[37–39] Hence, there is a need for thermochromic materials that are both fully reversible and are observable by the naked eye for applications in the food packaging and health care industries, which can be observed by the consumer.

Herein, we report the first example of a dye–solvent binary system that shows clear reversible thermochromism near room temperature resulting from the solubility-dependent π–π stacked agglomeration of sulfonephthalein dyes controlled by melting/crystallisation processing of the solvent. This simple binary thermochromic system is based purely on dye (sulfonephthalein) and solvent (linear chain esters, acids or alcohols). We further demonstrate that this thermochromic binary system is nontoxic. The mechanism study of the thermochromism is further investigated using various analytical techniques including NMR, UV-vis absorption, XRD and FTIR-ATR analysis as well as molecular dynamics simulations.

2. Results and discussion

2.1 Thermochromism of binary sulfonephthalein and model dye systems

In the study of the proposed binary systems, we firstly used a dye dissolved in either aliphatic linear chain acids, esters or alcohols. Six sulfonephthalein 'dyes', chlorophenol red (CPR), bromothymol blue (BTB), bromocresol purple (BCP), bromocresol green (BCG), bromophenol blue (BPB) and thymol blue (TB), and 'solvents' with varying end group functionality (ester, alcohol, or acid) and melting points were then used and their structures are shown in Fig. 1A and C, respectively. In addition, examples of charged triarylmethane dyes, methyl green (MG) and crystal violet (CV); a leuco dye, crystal violet lactone (CVL); and an azo dye, dimethyl yellow (DMY), were used for comparison in a binary system (Fig. 1B).

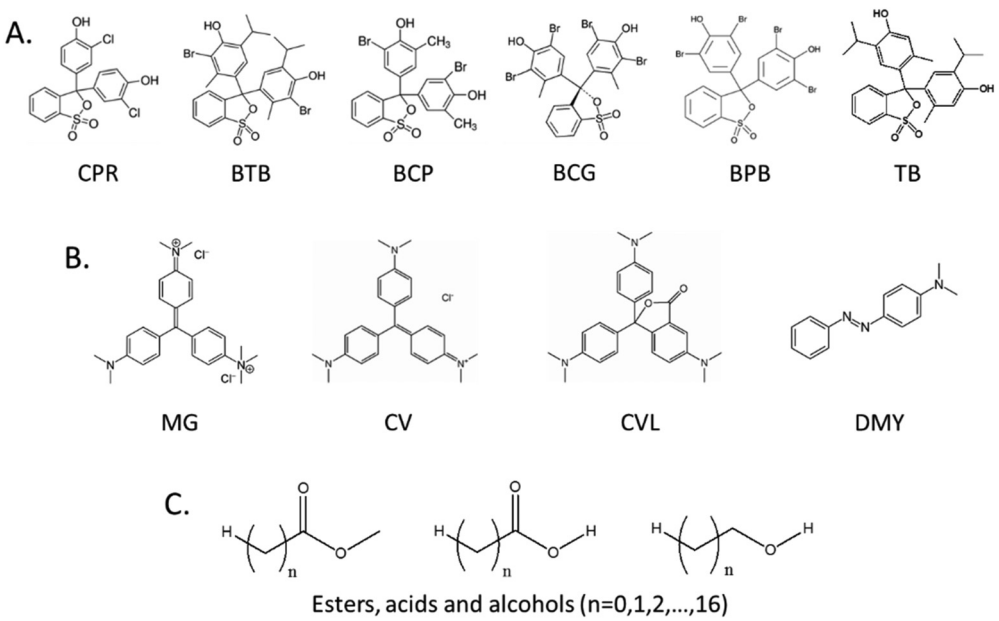

Fig. 1 The chemical structures of (A) sulfonephthalein dyes: chlorophenol (CPR), bromothymol blue (BTB), bromochloro purple (BCP), bromocresol green (BCG), bromophenol blue (BPB), and thymol blue (TB); (B) comparative dyes: methyl green (MG), crystal violet (CV), crystal violet lactone (CVL), and dimethyl yellow (DMY); and (C) solvents: straight chain aliphatic esters, acids and alcohols.

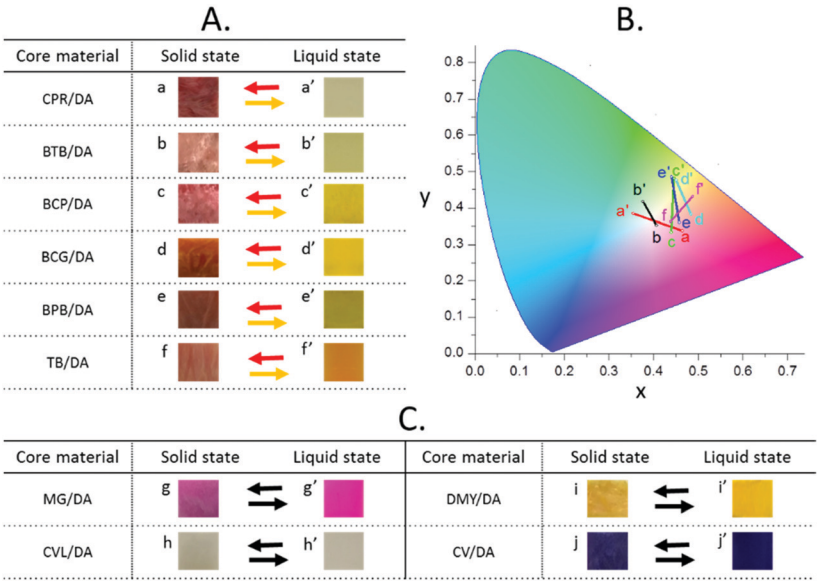

Fig. 2 (A) Photographic images of the colour change between solid (25 °C) and liquid (70 °C) states of six sulfonephthalein dyes (0.07 mol%) in DA. (B) Standard CIE 1931 chromaticity chart showing the x–y values of the colour transition between solid (25 °C) and liquid (70 °C) state of samples a–f. (C) Photographic images of solid (25 °C) and liquid (70 °C) states of MG, CVL, DMY and CV (0.07 mol%) in DA.

The dyes were dissolved in heated dodecanoic acid (DA) at 70 °C at typical concentrations of 0.07 mol%, to form homogenous solutions showing different colours depending on the dye, as shown in Fig. 2A and C. Upon cooling to 25 °C, distinct colour changes were observed for the sulfonephthalein samples resulting in non-uniform crystalline materials (Fig. 2A). Quantification of the colour change according to CIE2000[40] indicates the sample containing CPR (Fig. 2A, sample 'a') had a significantly high $\Delta E = 37.8$, with a distinctive contrast in colour. For this reason, the subsequent investigations used CPR as an example. The colour changes occur between the melted state and the solid state of solvents. Therefore, the threshold temperature of colour change is dependent on the melting point or freezing point of the solvent in the system. A plot of the absorbance (541 nm) *versus* temperature of CPR–DA (0.07 mol%) upon heating (Fig. S1, ESI†) shows a steep decrease in intensity to a constant value around 43–44 °C. The red colour disappearance is accompanied by the melting process of DA occurring at its melting point of 43.77 ± 0.03 °C. The CIE chromaticity chart (Fig. 2B) illustrates the colour shift of six sulfonephthalein dye–DA samples (Fig. 2A, samples a–f). Similarly, six sulfonephthalein dye–methyl dodecanoate (MDD) samples (Fig. S2, ESI†) also show a colour change between solid (0 °C) and liquid (25 °C) states. In contrast, four common dyes (MG, CV, CVL and DMY) when combined in a binary system (Fig. 2C, samples g–j) showed no colour change between solid and liquid states. The chemical structure of the sulfonephthalein dyes is therefore important in the thermochromism of the binary system.

The functionality of the solvent molecules and their importance in the thermochromism were studied using acid, alcohol and ester moieties of linear chain hexadecane, with CPR as the dye molecule. Fig. 3 shows the colour change between solid (25 °C) and liquid (70 °C) states and the corresponding UV-vis absorption spectra of samples of CPR–hexadecanoic acid (CPR–HA) (a–a′), CPR–methyl hexadecanoate (CPR–MH) (b–b′) and CPR–hexadecanol (CPR–HD) (c–c′). It is interesting that CPR exhibits a slightly different colour in each liquid solution due to a solvatochromism phenomenon,[41] yet all yellow liquid solutions turned red upon solidification at 25 °C, whether the solvent is an acid, ester or alcohol. Correspondingly, the UV-vis

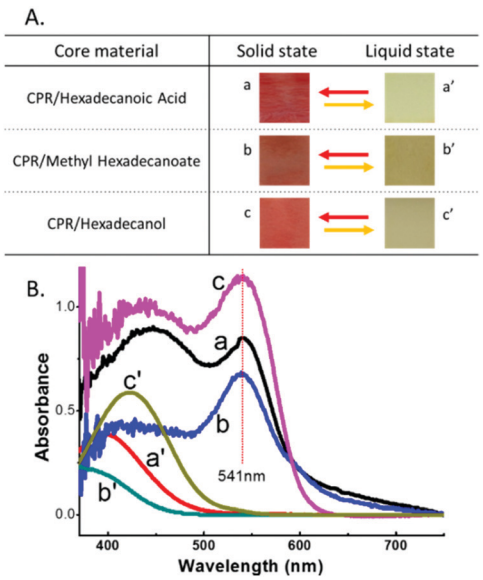

Fig. 3 (A) Photographic images of the colour change between solid (25 °C) and liquid (70 °C) states of CPR (0.07 mol%) in (a) hexadecanoic acid, (b) methyl hexadecanoate and (c) hexadecanol. (B) The corresponding UV-vis absorption spectra of all solid CPR–solvent samples (a–c) at 25 °C, showing strong absorption peaks at 541 nm compared to liquid samples (a′–c′) at 70 °C independent of the functionality of the solvent.

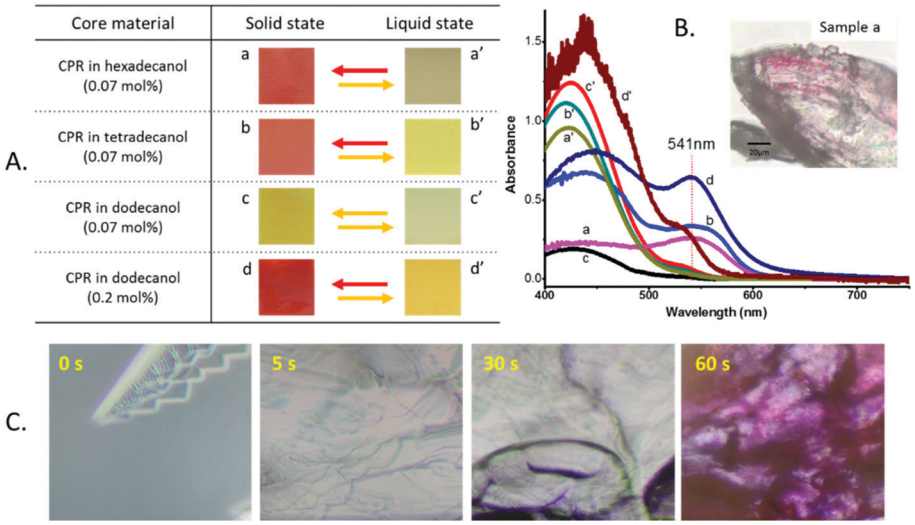

Fig. 4 (A) Photographic images of CPR–HD (0.07 mol%), CPR–TD (0.07 mol%), CPR–DD (0.07 mol%) and CPR–DD (0.2 mol%) in the solid state (20 °C, a–d) and liquid state (70 °C, a′–d′). (B) The corresponding UV-vis absorption spectra of solid (20 °C) samples a–d and liquid (70 °C) samples a′–d′ and microscopic image of solid sample 'a'. (C) Captured images from a microscopic video of the solidification of sample 'a' upon cooling.

absorption peak or shoulder of the liquid CPR–hexadecanoic acid, CPR–methyl hexadecanoate and CPR–hexadecanol solutions is at 396 nm, 385 nm and 423 nm, respectively. After solidifying at 25 °C, a peak at 541 nm appears in the UV-vis spectra of all three samples, which is indicative of the emerging red colour.

In order to investigate the effect of hydrophobicity and hence solubility on the thermochromic nature of the binary system, a series of mixtures containing CPR (0.07 mol%) in hexadecanol (HD), tetradecanol (TD) or dodecanol (DD) was prepared. As the aliphatic chain length increases along with an increase in hydrophobicity, the solubility of the hydrophilic CPR in the solvent decreases, leading to phase separation. At a CPR concentration of 0.07 mol%, the solid binary systems of CPR–HD and CPR–TD are heterogeneous and exhibit a strong red appearance with λ_{max} = 541 nm (Fig. 4A and B: a and b). At this concentration however, CPR is fully solubilized in DD, even below its freezing point (24 °C) and shows no thermochromism (Fig. 4A and B: c). As the concentration of CPR is increased to 0.2 mol% in DD, phase separation occurs in the solid state and the characteristic red colour at λ_{max} = 541 nm is observed (Fig. 4A and B: d). Microscopic images of sample 'a' in the solid state show strong red coloured regions of aggregated dye within the crystalline hydrophobic solvent regions. Video analysis (Fig. 4C) monitoring the thermochromism of sample 'a' upon cooling (ESI†) reveals agglomeration of the dye compounds forming between the regions of crystalline growth of the solvent. These observations reveal that the thermochromic behaviour of this binary system is dependent on the solubility of the dye in the solvent matrix. For effective thermochromism in this system, the concentration of the dye must be such that the dye is able to agglomerate below the freezing point of the solvent and be fully dissolved above the melting point of the solvent.

The concentration of dye in the binary system plays a very important role in its thermochromic behaviour; therefore, the effect of dye concentration on the colour changing time of this binary system is also examined. Here, CPR–DA solutions with five different CPR concentrations of 0.07, 0.03, 0.02, 0.01 and 0.007 mol% were cooled from 70 °C to 35 °C under the same conditions. The freezing points of these binary systems at varying concentrations are very similar (Fp. 41.7 ± 0.1 °C, Table S1, ESI†) with the change in CPR concentration having little effect. However, the effect of concentration on the time for the colour to change upon cooling is significant. A plot of the absorbance (541 nm) *versus* colour changing time of these samples upon cooling (Fig. 5A) shows a steep increase in intensity to a constant value. The colour change equilibrium time was taken as the intersection of the extrapolated baseline and the tangent to the plot at the inflection point (Fig. 5A). From the comparison of colour change equilibrium time of each sample (Fig. 5B), it is clear that the higher concentration CPR–DA solution showed a faster colour change upon the same rate of cooling. This phenomenon can be explained as follows: the solubility of the dye in the solvent decreases as the temperature drops, with the dye being excluded from the solvent phase; as a result, the more concentrated solution reaches its saturation faster, forming a more coloured solid than those at lower concentrations. Therefore, the colour changing speed of this binary system can be adjusted by varying the dye concentration.

2.2 Cell toxicity testing

The relative cytotoxicity of these six sulfonephthalein dyes was examined using the CCK-8 approach.[42] NIH-3T3 (noncancerous fibroblasts) cell lines were incubated with different concentrations of dyes for 24 hours and then processed with fresh medium containing CCK-8 solutions for a further 3 hours to determine cell viability. As shown in Fig. S3 (ESI†), TB is more toxic to NIH-3T3 cells than other sulfonephthalein dyes and the viability of cells decreases to 70% at a concentration of 200 μg mL^{-1} TB. Except for TB, a negligible cytotoxicity effect on NIH-3T3 was

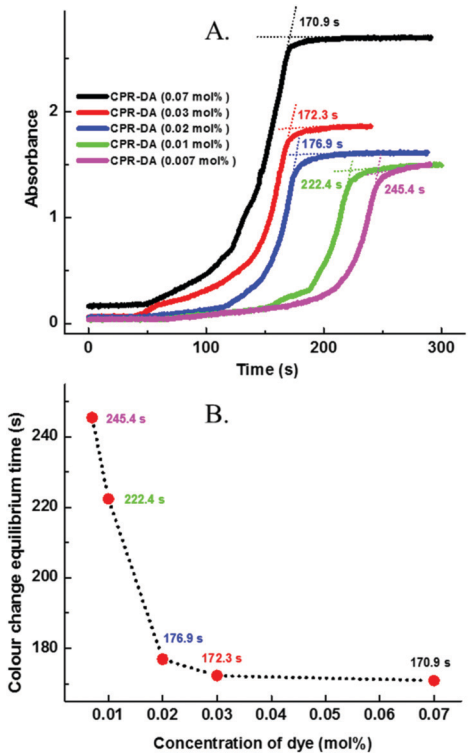

Fig. 5 (A) Plots of UV-vis absorbance at 541 nm of CPR–DA *vs.* time upon cooling from 70 °C to 35 °C. The concentrations of CPR in the binary systems were 0.07 mol%, 0.03 mol%, 0.02 mol%, 0.01 mol% and 0.007 mol%, respectively. (B) Plots of colour change equilibrium time *vs.* concentration of dye in the CPR–DA binary system.

observed when the concentration of all sulfonephthalein dyes ranges from 0 to 200 μg mL^{-1}, and all viabilities are more than 90% after 24 hour incubation. Notably, the toxic effects of BTB, BCP and CPR on cells were only seen at very high concentrations (>500 μg mL^{-1}).

Triarylmethane flourans such as rhodamine B have been studied as colour formers in leuco dye systems for decades and it is one of the most commonly used ingredients in current thermochromic products.[43–46] On the other hand, food dyes are usually regarded as safe additives[47] and have gradually been used in the thermochromic area.[48] Therefore, it is necessary to compare the relative toxicities of the leuco dyes, food dyes and sulfonephthaleins used in this work. Three dyes were chosen from the three classes, namely rhodamine B base, cyanidin chloride and chlorophenol red (CPR), respectively.

As shown in Fig. 6A, both cyanidin chloride and rhodamine B base are statistically toxic to NIH-3T3 cells in the concentration range of 0–1000 μg mL^{-1}. The viability of cells decreases to 45% and 36% at a concentration of 200 μg mL^{-1} cyanidin chloride and rhodamine B base, respectively. These results indicate that all sulfonephthalein dyes including TB are less toxic to NIH-3T3 cells than cyanidin chloride or rhodamine B base. The calculated half-maximum inhibitory concentration (IC_{50}) values for cyanidin chloride and rhodamine B base were 172 and 163 μg mL^{-1}, respectively, which were significantly lower than that of CPR, which was 786 μg mL^{-1} (Fig. 6B). Cyanidin chloride had a surprisingly similar IC_{50} to that of rhodamine B base, which may inhibit its use in commercial applications. Considering the low toxicity and very low dosage of sulfonephthalein, this binary thermochromic system can be regarded as nontoxic when it is used with a non-toxic solvent, *e.g.*, dodecanoic acid,[49,50] and has potential to be applied to real commercial food or health care product packaging.

2.3 Mechanism study

Sulfonephthaleins are commonly used as pH indicators due to their strong colour and transition over a wide pH range. The mechanism for this equilibrium is well-known with the opening of the sulfoxide ring leading to the highly coloured resonance structure shown in Fig. 7.[17,51] For example, CPR has a characteristic purple colour above pH 10 in the ring-opened form and a yellow colour below pH 4.6 in the ring-closed form.[52] In order to investigate the chemical structure of CPR in this binary system, melted CPR–methyl dodecanoate

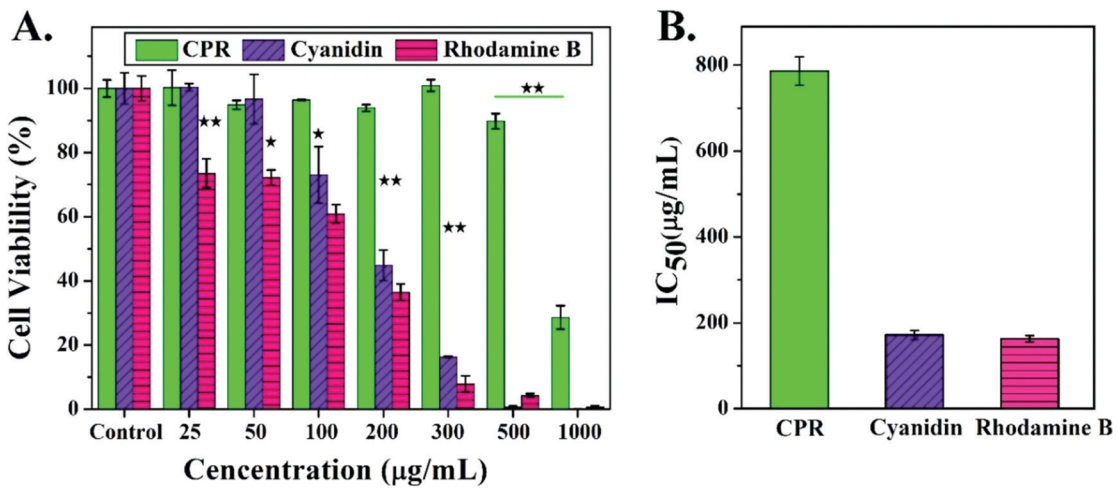

Fig. 6 (A) Cytotoxicity of CPR, cyanidin chloride and rhodamine B base toward NIH-3T3 cells incubated for 24 h. (B) Comparison of the IC50 values of CPR, cyanidin chloride and rhodamine B base in NIH-3T3 cells. *$P < 0.05$ and **$P < 0.01$.

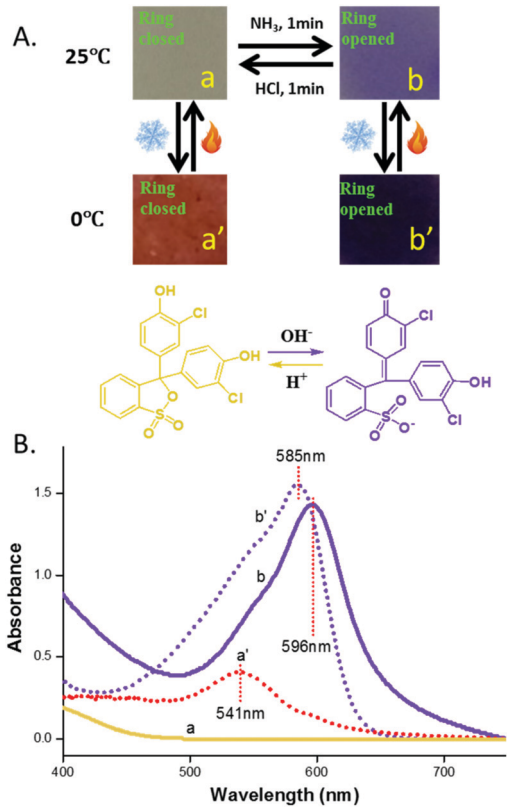

Fig. 7 (A) Digital pictures of CPR–MDD binary system with a concentration of 0.07 mol% after being treated with ammonium hydroxide or hydrochloride vapour for 1 minute at 25 °C and corresponding solids at 0 °C. (B) The corresponding UV-vis spectra of sample a, a′, b and b′ and ring-closed or ring-opened molecular structures of CPR.

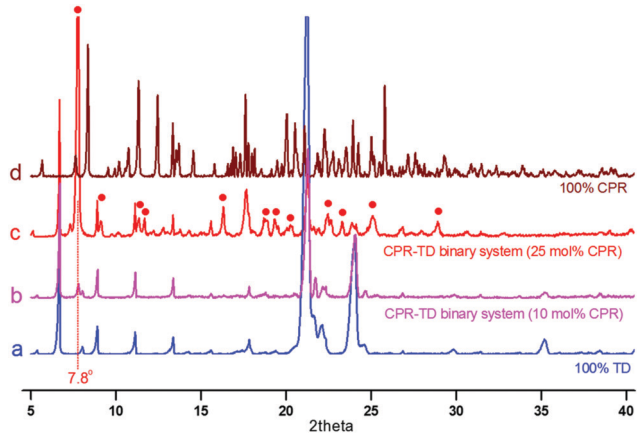

Fig. 8 XRD patterns of pure (a) 100% solid TD, (b) CPR–TD solid binary system with 10 mol% CPR, (c) CPR–TD solid binary system with 25 mol% CPR and (d) 100% solid CPR powder.

(CPR–MDD, Fig. 7a) was treated with basic ammonium hydroxide vapor (aq. NH_4OH, 25 °C) for 1 min. The material became purple in appearance with λ_{max} = 596 nm (Fig. 7b) and, upon cooling, led to a stronger purple colour with λ_{max} = 585 nm (Fig. 7b′). The CPR–MDD solution returned to a pale-yellow solution (Fig. 7a) after being re-acidified with hydrochloric acid vapor (aq. HCl, 25 °C) for 1 min and formed a red solid (Fig. 7a′) upon cooling. This is in contrast to the thermochromic colour change observed by the solid CPR–solvent binary systems (Fig. 3B, 4B and 7B) with an absorbance peak of around λ_{max} = 541 nm (Fig. 7a′) in the UV-vis spectra. In other words, ring-closed CPR resulted in a unique absorbance peak at 541 nm, while that of the ring-opened CPR shifted from 596 nm to 585 nm after solidification. Therefore, for reversible thermochromism, CPR must not remain in the ring-opened state. Further evidence of the CPR structure in our binary thermochromic system comes from FTIR analysis (Fig. S4 of ESI†). FTIR measurements indicated that the binary system of CPR–TD (10 mol%) as both hot liquid (70 °C) or cold solid (25 °C) showed similar peaks attributed to the sulfone group at 1345 and 1191 cm^{-1}, which indicates a ring-closed CPR structure[21] at both temperatures and different colours. After treatment with base however, peaks at 1180 and 1630 cm^{-1} due to the benzene sulphonate and *p*-quinoid groups appear,[53,54] respectively, which are consistent with the ring-opened structure of CPR. This evidence confirms that the thermochromic mechanism of this binary system is not related to a ring-opening of the dye molecule and that reversible thermochromism only occurs when the dye remains in the ring-closed state.

Furthermore, the XRD patterns of the solid CPR–TD binary system (Fig. 8) indicate that CPR is crystallized in its agglomeration. Compared to TD (Fig. 8a), the pattern of the CPR–TD binary system with 10 mol% CPR (Fig. 8b) exhibits an extra small diffraction peak at 7.8°. As CPR is concentrated to 25 mol%, this diffraction peak dominates the XRD pattern (Fig. 8c) and is seen along with the appearance of other peaks (●). However, the peaks from CPR agglomeration do not match the peaks of pure CPR powder (Fig. 8d). Therefore, CPR molecules within the solid mixture agglomerate into another crystalline form, different from that of pure CPR. Macroscopically, this is consistent with the fact that CPR agglomeration appears red rather than greenish-brown, reported for pure CPR powder.[55]

Proton NMR was used to further elucidate the molecular structure of CPR in the binary system. Analysis was performed on mixtures of CPR dissolved in d_3-methanol at 10^{-4}, 0.1 and 2 mol% (sample α–γ in Fig. 9). As shown in Fig. 9A, the colour of the methanol solution became darker and changed colour with an increase in CPR concentration. The ^{1}H NMR spectra of CPR at increasing concentrations in d_3-methanol showed an exclusive up-field shift of the aromatic hydrogens (Fig. 9B, signals a, b, b′ and c) connected to the sulfoxide ring. This effect is attributed to aromatic electron shielding and is always observed in π–π stacking of conjugated planar molecules.[26,30,56–58] It is well-established that electron withdrawing groups attached to aromatic rings enhance π–π stacking.[59,60] In the case of sulfonephthalein dyes, the electron withdrawing sulfoxide (SO_3^-) group connected to the benzene ring leads to an increase in the π–π stacking and increased intensity due to the agglomeration of the dye molecules.

The UV-vis absorption spectrum of CPR in methanol at low concentration (Fig. 9A: α: 0.1 mmol%) shows an insignificant shift in wavelength between the liquid and solid states. Also, at a high concentration of CPR (Fig. 9A: γ: 2 mol%), no peak shift

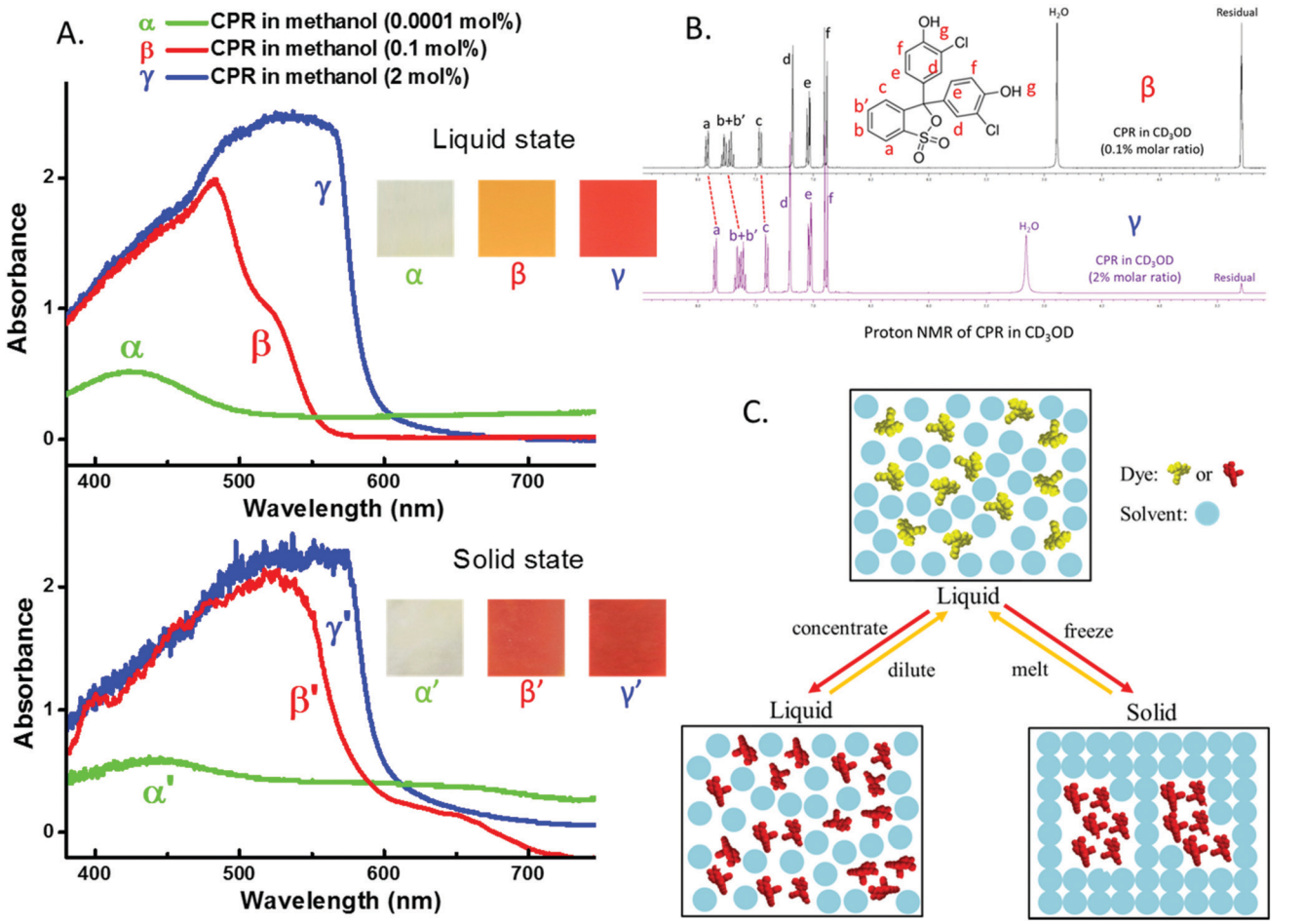

Fig. 9 (A) The photographic images of CPR–methanol samples with a concentration of (α) 0.0001 mol%, (β) 0.1 mol% and (γ) 2 mol% at 25 °C and −196 °C. The corresponding UV-vis absorption spectra indicate only sample β shows thermochromism. (B) ^{1}H NMR spectra of CPR (0.1 mol% and 2 mol%) in CD_3OD showing an upfield shift for peaks a, b, b′ and c. (C) A schematic representation of CPR molecules in solvent in a diluted liquid state, concentrated liquid state and diluted solid state.

in wavelength is observed. In both of these cases, no thermochromism is observed upon solidification and the CPR molecules remain either homogeneously dissolved or completely aggregated in both solid and liquid states. The UV-vis spectrum of CPR in methanol at medium concentration (Fig. 9A: β: 0.1 mol%) shows a significant shift in wavelength between the solid and liquid states, with an obvious thermochromism being observed for the sample. At this concentration, CPR is fully solubilized in the liquid methanol and is insoluble enough in the solid methanol to lead to π–π stacking and thermochromism.

This observation is analogous to the thermochromism seen for the binary systems of dye and long chain hydrophobic solvents shown earlier. The UV-vis absorption spectra of red solid CPR–HA, CPR–MH, CPR–HD, CPR–TD and CPR–DD in Fig. 3 or Fig. 4 show the peak at 541 nm. Although the UV-vis absorption peaks in the spectra of liquid and solid CPR–methanol (2 mol%) and solid CPR–methanol (0.1 mol%) are broad due to the high absorbance intensity, their locations are still around 541 nm (Fig. 9A). Therefore, CPR shows a similar colour change and the same UV-vis spectral changes in both methanol and long chain hydrophobic solvents. Here, the dye structures agglomerate between the regions of the solvent crystal boundaries. The schematic diagram in Fig. 9C illustrates the proposed mechanism of thermochromism in solution: (1) a low concentration of dye molecules are surrounded by solvent molecules and show the colour of a diluted liquid solution; (2) with an increase in dye molecules, they agglomerate in solution resulting in a stronger colour; and (3) dye molecules are excluded from the solvent crystal structure as the solvent solidifies and form agglomerated structures at the solvent crystal boundaries.

To further illustrate the π–π stacking mode of CPR in the binary system, molecular dynamics (MD) simulations were used to model the preferential alignment of the CPR molecules in methanol at 25 °C and −196 °C. The eight CPR molecules quickly (within a few picoseconds) approach each other forming a rather compact cluster at −196 °C (Fig. S5B at 10 ns, ESI†), contrary to the case at room temperature where CPR molecules are dispersed in methanol (Fig. S5A at 10 ns, ESI†). Fig. S6A (ESI†) shows a snapshot of the benzene rings connected to the sulfoxide group (highlighted pink atoms) of eight CPR molecules in 200 methanol molecules at −196 °C. Three pairs of

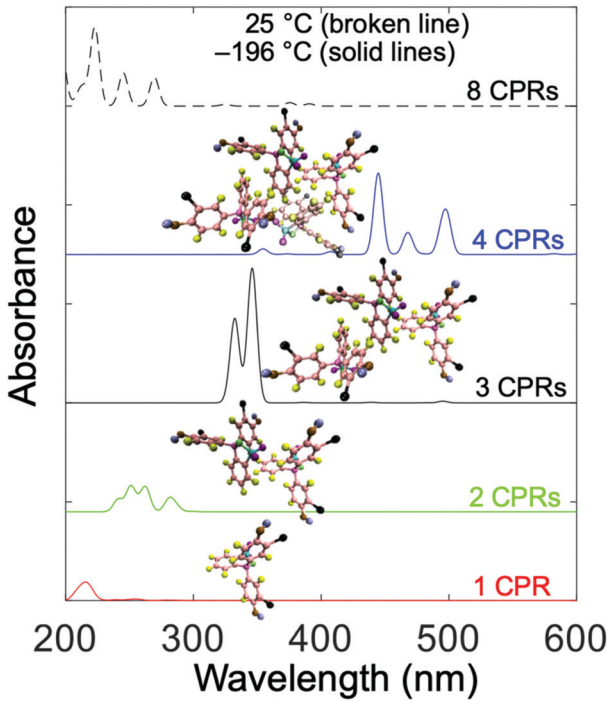

Fig. 10 Absorbance spectra of 1 (red solid line), 2 (green solid line), 3 (black solid line) and 4 CPR molecules (blue solid line) at −196 °C and 8 CPR molecules at 25 °C (black broken line).

benzene rings are shown, two of which (rings 1 & 2 and rings 2 & 3) exhibit edge-to-face π–π stacking.[61] Specifically, at t = 10 ns, the geometric centres of the planes of rings 1 & 2 have a distance of 4.94 Å and interplanar angle of 65.2° (Fig. S6B: green line, ESI†), while those of rings 2 & 3 are 4.96 Å and 85.4°, respectively (Fig. S6B: black line, ESI†). Even though rings 2 and 4 (Fig. S6B: red line, ESI†) have a shorter plane-to-plane distance of 4.75 Å, they do not form π–π stacks as their interplanar angle is 48.9°.[61] In fact, the π–π stacking formation is maintained throughout the simulation (t > 0 ns), as evidenced by the time evolution of the interplanar distance and angle (Fig. S6B, ESI†) of the pairs of rings 1 & 2 (green diamonds) and 2 & 3 (black circles).

Additionally, the π–π stacking formation is also confirmed by the calculated UV-vis absorption spectra (Fig. 10) of CPR molecules at 25 °C (broken line) and −196 °C (solid lines). At −196 °C, increasing the number of CPR molecules from 1 (Fig. 10: red line) to 4 (Fig. 10: blue line) causes a red-shift in the absorbance from 215 nm to 400–500 nm, respectively, due to the increasing length of π-electron conjugation.[62] At 25 °C, however, the 8 CPR molecules are dispersed in methanol (Fig. S5A at 10 ns, ESI†), acting as single molecules that result in absorption peaks between 200–300 nm in the UV-vis spectrum (Fig. 10: broken line).

In summary, thermo-induced solvent phase change results in agglomeration or dis-agglomeration of sulfonephthalein molecules and is accompanied with changes in the localised concentration of dye molecules, both combining to affect a strong colour change of the samples. Unlike other thermochromic π–π stacking systems, sulfonephthaleins do not conjugate uniformly on a plane and are further enhanced by aggregachromic changes. The solvent crystal boundaries during crystallisation of the binary system provide limited space for dye π–π stacking, which enables it to be reversed upon melting, a reduction in π–π stacking, a reversal of the colour and full homogenous solvation of the dye molecules.

4. Conclusions

In conclusion, a new class of reversible and nontoxic dye–solvent binary thermochromic materials is reported. These binary systems with sulfonephthaleins as dyes and linear chain esters, acids or alcohols as solvents show clear colour changes from the solid to liquid states. The colour change is attributed to changes in π–π stacking, caused by different dye solubilities in the liquid or solid solvent. Contrary to the mechanism associated with pH indicator dyes, this binary system involves ring-closed sulfonephthaleins exhibiting an aggregachromic phenomenon. The relative low toxicity and concentration of the sulfonephthalein dyes make this system promising for real commercial food or health care product packaging applications, where thermochromic observations can be utilized. Although the fabrication is simple and rapid, incorporating this binary system into a processable sealed film will be the next challenge for further study.

5. Experimental section

Materials

Chlorophenol red (CPR, indicator grade, Aldrich), bromothymol blue (BTB, 99%, Ajax Finechem), bromocresol purple (BCP, 99%, Ajax Finechem), bromocresol green (BCG, 99%, Chem-supply), bromophenol blue (BPB, 99%, Ajax Chemicals), thymol blue (TB, 99%, Sigma-Aldrich), crystal violet lactone (CVL, 97%, Sigma-Aldrich), dimethyl yellow (DMY, 98%, Sigma-Aldrich), crystal violet (CV, 99%, Sigma-Aldrich), methyl green (MG, 85%, Sigma-Aldrich), cyanidin chloride (98%, BOC Sciences, USA), rhodamine B Base (97%, Aldrich), 32 wt% hydrochloric acid solution (Ajax Finechem), aqueous ammonium hydroxide solution (28 w/w%, Sigma-Aldrich), methanol (99.8%, Chem-supply), deuterated methanol (CD_3OD, 99.8 atom %D, Aldrich), dodecanoic acid (98%, Sigma-Aldrich), 1-dodecanol (98%, Sigma-Aldrich), 1-tetradecanol (97%, Aldrich), methyl dodecanoate (98%, Sigma-Aldrich), methyl hexadecanoate (97%, Sigma-Aldrich), hexadecanoic acid (99%, Sigma) and 1-hexadecanol (99%, Aldrich) were used as received without further purification.

Instrumentation

Differential scanning calorimetry (DSC). Full heat flow curves were measured on a PerkinElmer Differential Scanning Calorimeter 8500 under a nitrogen atmosphere. Melting points or freezing points were taken at the intersection of the extrapolated baseline and the tangent to the heat flow curve at the inflection point of the appropriate side of the peak[63] when the heating or cooling rate is 1 °C min^{-1}.

Fourier transform infrared (FTIR-ATR) spectroscopy. FTIR spectra were recorded on a Bruker TENSOR II FTIR-ATR spectrometer at a resolution of 4 cm^{-1} over the range of 4000 cm^{-1} to 400 cm^{-1}. Measurements were determined at both 25 °C and 70 °C controlled by a Specac ATR assembly.

X-ray diffraction (XRD). XRD patterns of the samples were recorded at 25 °C on a Bruker D8 Advance diffractometer with Cu Kα radiation (40 kV, 40 mA) and a nickel filter, and the samples were exposed at a scanning rate of $2\theta = 0.020\ ^\circ \cdot s^{-1}$ in the range of 5°–85°.

^{1}H nuclear magnetic resonance (NMR) spectroscopy. ^{1}H NMR spectroscopy was carried out at 25 °C on a Varian Unity 400 MHz spectrometer, using deuterated methanol (CD_3OD) as solvent. CPR (0.1 mol% in CD_3OD) ^{1}H NMR (400 MHz): δ 7.92 (d, J = 7.6 Hz, 1H), 7.77 (t, J = 7.6 Hz, 1H), 7.71 (t, J = 7.6 Hz, 1H), 7.46 (d, J = 8 Hz, 1H), 7.18 (d, J = 2.4 Hz, 2H), 7.04 (dd, J = 8.8, 2.4 Hz, 2H), 6.89 (d, J = 8.8 Hz, 2H). CPR (2 mol% in CD_3OD): ^{1}H NMR (400 MHz): δ 7.85 (d, J = 7.6 Hz, 1H), 7.66 (t, J = 7.6 Hz, 1H), 7.60 (t, J = 7.6 Hz, 1H), 7.40 (d, J = 7.6 Hz, 1H), 7.20 (d, J = 2.4 Hz, 2H), 7.03 (dd, J = 8.8, 2.4 Hz, 2H), 6.89 (d, J = 8.4 Hz, 2H).

Chromaticity. Photographs of bulk samples were calibrated for white balance using Adobe Photoshop CS6 as Camera Raw format.[64] The x and y coordinates of the CIE chromaticity were determined by conversion from RGB values of the colour balanced images.[65]

Ultraviolet visible (UV-vis) spectroscopy. UV-vis absorption analysis was performed on a Shimadzu UV-1800 spectrophotometer combined with an Ocean Optics DH-2000 optical fibre light source and Flame UV-vis-ES miniature spectrometer. The thickness of the quartz cuvette containing samples for analysis was 1 mm.

Light microscope. Optical microscope images and videos were captured using an Olympus CKX41 microscope with AnalySIS getIT software.

UV-vis kinetic analysis

The sample chamber of a Pharmacia LKB Novaspec II spectrometer connected to a thermostatic water bath was kept at 35 °C. A quartz cuvette (optical path length of 1 mm) containing the sample was pre-heated at 70 °C for 30 min prior to being placed rapidly into the thermostatted spectrometer chamber. The absorbance was recorded every 0.5 s at a single wavelength of 541 nm.

Dye toxicity study. Normal NIH-3T3 cells were maintained in Dulbecco's modified Eagle's medium (DMEM) supplemented with 10% fetal bovine serum (FBS), GlutaMAX™ (2 mM), and penicillin (100 units per mL). Cells were passaged every 3–4 days using 0.25% trypsin–EDTA at subconfluence and incubated at 37 °C, 5% CO_2, and 90% humidity. Cell passages 5–15 were used for cell experiments.[66] The cell viability tests were analyzed by the standard cell counting kit-8 (CCK-8) assay method. NIH-3T3 cells were seeded into 96-well plates (1×10^4 cells per well) in cell culture medium. After 12 hours, the medium was replaced with 100 μL of fresh medium containing various concentrations of dyes (0–1000 μg mL^{-1}) and incubated for a further 24 h. The cells were then washed three times with PBS and incubated with 110 μL of fresh medium containing 10 μL of CCK-8 solutions for a further 3 hours. Finally, the medium was removed and the absorbance at 460 nm was measured using a microplate reader (TECAN M200 infinite Pro). Note that all experiments were conducted in triplicate, and error bars represent the standard error of independent experiments. The cell viability (%) was calculated by the following formula, where $[A]$ is the average absorbance:

$$\text{Cell viability (\%)} = \frac{[A]_{460(\text{sample})} - [A]_{460(\text{blank})}}{[A]_{460(\text{control})} - [A]_{460(\text{blank})}}$$

Statistical analysis. Data are shown as averages and standard deviations. The student's t tests were used to analyze the statistical differences between samples for cytotoxicity and were considered significant at $p < 0.05$.

Computational methods

Molecular dynamics (MD) simulations were used to model the preferential alignment of the CPR molecules in methanol at 25 °C and −196 °C. Eight CPR molecules were placed at the centre of a 30 × 30 × 30 Å simulation cell surrounded by 200 methanol molecules (initial configuration is shown at the top of Fig. S5A and B of the ESI†). The equations of motion are integrated by the velocity-Verlet algorithm[67] with a timestep of 1 fs in the *NVT* (constant number, volume, and temperature) ensemble using the polymer consistent force field (PCFF). The MD simulations were performed on the University of Melbourne's High-Performance Computing system for up to 10 ns using the LAMMPS MD code.[68] The UV-vis absorption spectra were calculated using ORCA's UV-vis spectra simulator.[68–70]

Conflicts of interest

There are no conflicts to declare.

Acknowledgements

We thank the Australian Research Council (ARC), The University of Melbourne and Mondelez Australia for providing funding through Industrial Transformation Research Hub (ITRH, Project ID: IH120100053). Special thanks to Jiaxi Zhang, Chuan He and Shilin Yu for their assistance.

Notes and references

1 E. Reinitzer, *Chemie*, 1889, **4**, 462–472.
2 Y. Cheng, X. Zhang, C. Fang, J. Chen and Z. Wang, *J. Mater. Sci. Technol.*, 2018, **34**, 2225–2234.
3 Y. Guan, L. Zhang, D. Wang, J. L. West and S. Fu, *Mater. Des.*, 2018, **147**, 28–34.
4 T. J. White, M. E. McConney and T. J. Bunning, *J. Mater. Chem.*, 2010, **20**, 9832–9847.
5 W. Wang, G. P. Wang, W. Zhang and D. Zhang, *Nanophotonics*, 2018, **7**, 217–227.

6 D. I. Uhlenhaut, P. Smith and W. Caseri, *Adv. Mater.*, 2006, **18**, 1653–1656.
7 A. N. Bourque and M. A. White, *Can. J. Chem.*, 2014, **93**, 22–31.
8 H. Guo, J. Zhang, D. Porter, H. Peng, D. W. Löwik, Y. Wang, Z. Zhang, X. Chen and Z. Shao, *Chem. Sci.*, 2014, **5**, 4189–4195.
9 F. Donati, A. Pucci, C. Cappelli, B. Mennucci and G. Ruggeri, *J. Phys. Chem. B*, 2008, **112**, 3668–3679.
10 M. C. Chiappelli and R. C. Hayward, *Adv. Mater.*, 2012, **24**, 6100–6104.
11 A. Seeboth, J. Kriwanek and R. Vetter, *J. Mater. Chem.*, 1999, **9**, 2277–2278.
12 S. Pirra, *Waste & Resources Action Programme (WRAP) - Final Report, Thermochromic inks and reducing household food waste*, Oxon, UK, 2013, http://www.wrap.org.uk.
13 D. C. MacLaren and M. A. White, *J. Mater. Chem.*, 2003, **13**, 1695–1700.
14 K. Bašnec, L. S. Perše, B. Šumiga, M. Huskić, A. Meden, A. Hladnik, B. B. Podgornik and M. K. Gunde, *Sci. Rep.*, 2018, **8**, 5511.
15 S. Yi, S. Sun, Y. Deng and S. Feng, *J. Text. Inst.*, 2015, **106**, 1071–1077.
16 K. Yoshikawa, H. Fukuo and J. Kuroda, *US Pat.*, 4620941, Washington, DC, 1986.
17 T. De Meyer, K. Hemelsoet, V. Van Speybroeck and K. De Clerck, *Dyes Pigm.*, 2014, **102**, 241–250.
18 A. Seeboth, J. Kriwanek and R. Vetter, *Adv. Mater.*, 2000, **12**, 1424–1426.
19 W. Y. Chung, S. M. Lee, S. M. Koo and D. H. Suh, *J. Appl. Polym. Sci.*, 2004, **91**, 890–893.
20 C. Wanihsuksombat, V. Hongtrakul and P. Suppakul, *J. Food Eng.*, 2010, **100**, 427–434.
21 W. Zhang, X. Ji, C. Zeng, Y. Yin and C. Wang, *Color. Technol.*, 2019, **135**, 97–102.
22 Y. Wang, N. Archambault, A. M. Belcher, D. Busse, D. B. Damon, A. Mills, A. E. Riddle, I. J. Samardjiev, B. L. Lucht and W. B. Euler, *Macromolecules*, 2008, **41**, 7115–7121.
23 C. R. G. Grenier, W. Pisula, T. J. Joncheray, K. Müllen and J. R. Reynolds, *Angew. Chem., Int. Ed.*, 2007, **46**, 714–717.
24 P. Naumov, S. C. Lee, N. Ishizawa, Y. G. Jeong, I. H. Chung and S. Fukuzumi, *J. Phys. Chem. A*, 2009, **113**, 11354–11366.
25 Y. Morita, S. Suzuki, K. Fukui, S. Nakazawa, H. Kitagawa, H. Kishida, H. Okamoto, A. Naito, A. Sekine, Y. Ohashi, M. Shiro, K. Sasaki, D. Shiomi, K. Sato, T. Takui and K. Nakasuji, *Nat. Mater.*, 2008, **7**, 48.
26 M.-S. Yuan, D.-E. Wang, P. Xue, W. Wang, J.-C. Wang, Q. Tu, Z. Liu, Y. Liu, Y. Zhang and J. Wang, *Chem. Mater.*, 2014, **26**, 2467–2477.
27 M. W. Urban, *Handbook of stimuli-responsive materials*, John Wiley & Sons, 2011.
28 R. E. Hughes, S. P. Hart, D. A. Smith, B. Movaghar, R. J. Bushby and N. Boden, *J. Phys. Chem. B*, 2002, **106**, 6638–6645.
29 F. Würthner, C. Thalacker, S. Diele and C. Tschierske, *Chem. – Eur. J.*, 2001, **7**, 2245–2253.
30 Z. Chen, A. Lohr, C. R. Saha-Möller and F. Würthner, *Chem. Soc. Rev.*, 2009, **38**, 564–584.
31 A. Pucci, R. Bizzarri and G. Ruggeri, *Soft Matter*, 2011, **7**, 3689–3700.
32 B. R. Crenshaw and C. Weder, *Adv. Mater.*, 2005, **17**, 1471–1476.
33 A. Pucci, F. Signori, R. Bizzarri, S. Bronco, G. Ruggeri and F. Ciardelli, *J. Mater. Chem.*, 2010, **20**, 5843–5852.
34 A. Pucci, F. Donati, S. Nazzi, G. U. Barretta, G. Pescitelli, L. D. Bari and G. Ruggeri, *React. Funct. Polym.*, 2010, **70**, 951–960.
35 B. R. Crenshaw, J. Kunzelman, C. E. Sing, C. Ander and C. Weder, *Macromol. Chem. Phys.*, 2007, **208**, 572–580.
36 C. E. Sing, J. Kunzelman and C. Weder, *J. Mater. Chem.*, 2009, **19**, 104–110.
37 F. Donati, A. Pucci, L. Boggioni, I. Tritto and G. Ruggeri, *Macromol. Chem. Phys.*, 2009, **210**, 728–735.
38 F. Donati, A. Pucci and G. Ruggeri, *Phys. Chem. Chem. Phys.*, 2009, **11**, 6276–6282.
39 J. Kunzelman, B. R. Crenshaw, M. Kinami and C. Weder, *Macromol. Rapid Commun.*, 2006, **27**, 1981–1987.
40 G. Sharma, W. Wu and E. N. Dalal, Color Research & Application: Endorsed by Inter-Society Color Council, The Colour Group (Great Britain), Canadian Society for Color, Color Science Association of Japan, Dutch Society for the Study of Color, The Swedish Colour Centre Foundation, Colour Society of Australia, *Centre Français de la Couleur*, 2005, **30**, 21–30.
41 A. Marini, A. Munoz-Losa, A. Biancardi and B. Mennucci, *J. Phys. Chem. B*, 2010, **114**, 17128–17135.
42 S. Bian, X. Sun, A. Bai, C. Zhang, L. Li, K. Enjyoji, W. G. Junger, S. C. Robson and Y. Wu, *PLoS One*, 2013, **8**, e60184.
43 D. A. Hinckley and P. G. Seybold, *J. Chem. Educ.*, 1987, **64**, 362.
44 K. Takaoka, S. Maeda, H. Miura, K. Endo and D. P. Chong, *Bull. Chem. Soc. Jpn.*, 1998, **71**, 807–816.
45 S. Yumiko, T. Satoshi, G. Takeshi and S. Kenji, *Chem. Lett.*, 2007, **36**, 1010–1011.
46 X. Shi and Y. Liu, *US Pat.*, 15578815, 2018.
47 N. Kuno and T. Mizutani, *J. Toxicol. Environ. Health, Part A*, 2005, **68**, 1431–1444.
48 A. Seeboth, D. Lötzsch and R. Ruhmann, *J. Mater. Chem. C*, 2013, **1**, 2811–2816.
49 O. G. Fitzhugh, P. J. Schouboe and A. A. Nelson, *Toxicol. Appl. Pharmacol.*, 1960, **2**, 59–67.
50 R. Elder, *J. Am. Coll. Toxicol.*, 1987, **6**, 321–401.
51 M. a. P. Xavier, B. Vallejo, M. a. D. Marazuela, M. a. C. Moreno-Bondi, F. Baldini and A. Falai, *Biosens. Bioelectron.*, 2000, **14**, 895–905.
52 K. A. Halberg and N. Møbjerg, *J. Exp. Biol.*, 2012, **215**, 497–507.
53 K. Zheng, C. Lai, L. He and F. Li, *Sci. China Chem.*, 2010, **53**, 1398–1405.
54 I. Fleming and D. H. Williams, *Spectroscopic methods in organic chemistry*, New York: McGraw-Hill, 1966, p. 160.
55 W. C. Harden, *J. Am. Chem. Soc.*, 1930, **52**, 4611.
56 P. R. Mitchell, B. Prijs and H. Sigel, *Helv. Chim. Acta*, 1979, **62**, 1723–1735.

57 P. Mitchell and H. Sigel, *J. Am. Chem. Soc.*, 1978, **100**, 1564–1570.
58 W. Wang, J. J. Han, L.-Q. Wang, L.-S. Li, W. J. Shaw and A. D. Li, *Nano Lett.*, 2003, **3**, 455–458.
59 F. Cozzi, M. Cinquini, R. Annuziata and J. S. Siegel, *J. Am. Chem. Soc.*, 1993, **115**, 5330–5331.
60 M. J. Rashkin and M. L. Waters, *J. Am. Chem. Soc.*, 2002, **124**, 1860–1861.
61 V. Sivaramakrishnan, M. Ilamathi, K. Ghosh, S. Sathish, T. Gowda, B. Vishwanath, K. Rangappa and B. Dhananjaya, *J. Mol. Recognit.*, 2016, **29**, 22–32.
62 Y.-C. Huang, T.-C. Lu and C.-I. Huang, *Polymer*, 2013, **54**, 6489–6499.
63 A. A. Mammoli and C. Brebbia, *Materials Characterisation IV: Computational Methods and Experiments*, WIT Press, 2009.
64 G. R. Gossweiler, G. B. Hewage, G. Soriano, Q. Wang, G. W. Welshofer, X. Zhao and S. L. Craig, *ACS Macro Lett.*, 2014, **3**, 216–219.
65 H. Chen, F. Yang, Q. Chen and J. Zheng, *Adv. Mater.*, 2017, **29**, 1606900.
66 S. J. Shirbin, K. Ladewig, Q. Fu, M. Klimak, X. Zhang, W. Duan and G. G. Qiao, *Biomacromolecules*, 2015, **16**, 2463–2474.
67 W. C. Swope, H. C. Andersen, P. H. Berens and K. R. Wilson, *J. Chem. Phys.*, 1982, **76**, 637–649.
68 S. Plimpton, *J. Comput. Phys.*, 1995, **117**, 1–19.
69 F. Neese, *Wiley Interdiscip. Rev.: Comput. Mol. Sci.*, 2012, **2**, 73–78.
70 B. Tejerina, *UV/Vis Spectra simulator*, https://nanohub.org/resources/uvspec., 2014, DOI: 10.4231/D3GH9B964.

Supporting Information

A Nontoxic Reversible Thermochromic Binary System via π-π Stacking of Sulfonephthaleins

Bingxin Liu, Hadi Ranji-Burachaloo, Paul A. Gurr, Eirini Goudeli, Greg G. Qiao

Contents

Table S1. The freezing points of CPR-DA binary systems with different concentration

Concentration of CPR (mol%)	0.07	0.03	0.02	0.01	0.007
T_f (°C)	41.78 ±0.01	41.77 ±0.34	41.73 ±0.30	41.68 ±0.10	41.60 ±0.24

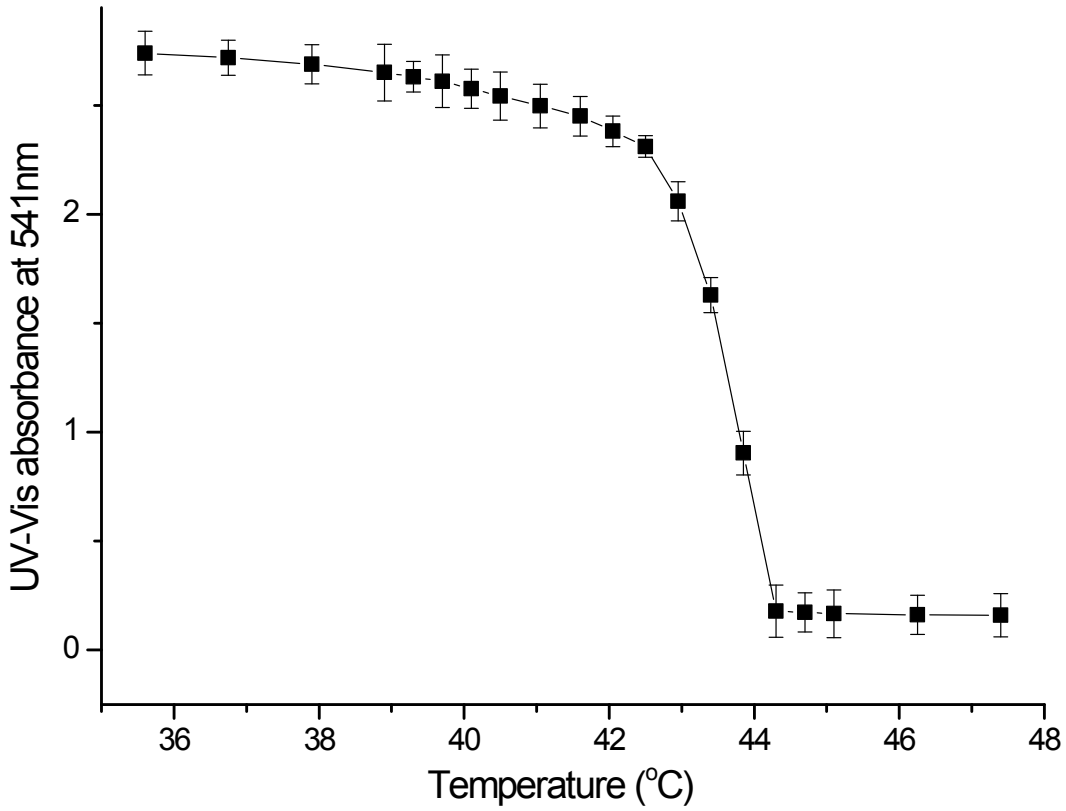

Figure S1. Plot of UV-Vis absorbance at 541nm of CPR-DA (0.07 mol%) vs. temperature upon heating from 35°C to 48°C.

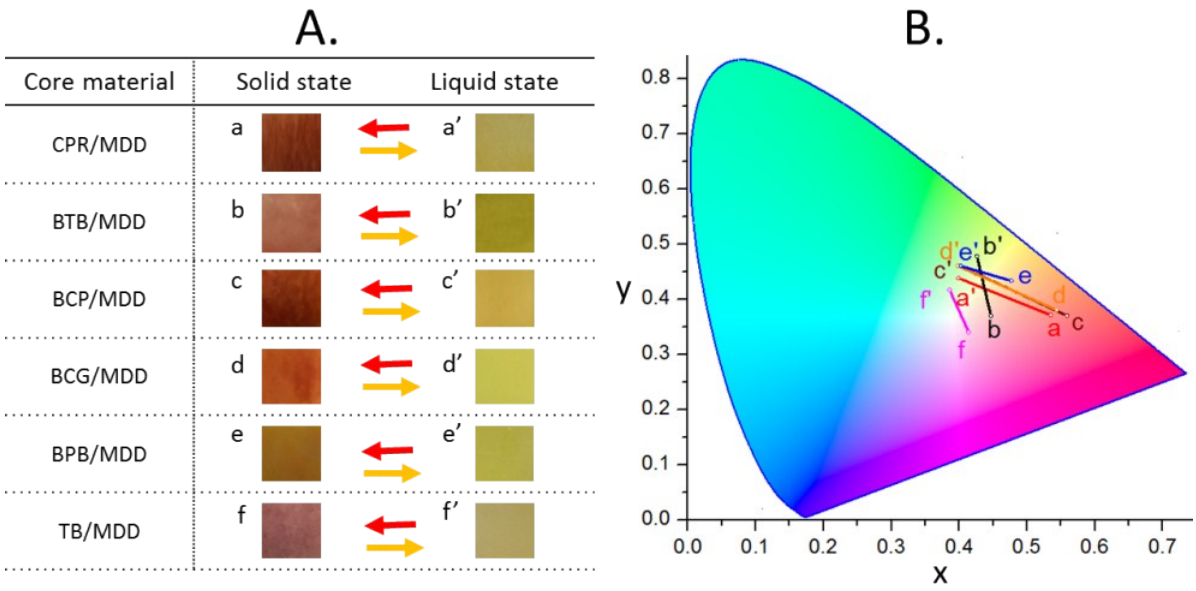

Figure S2. (A) Photographic images of the colour change between solid (0°C) and liquid (25°C) state of six sulfonephthalein dyes (0.07 mol%) in MDD (B) Standard CIE 1931 chromaticity chart showing the x-y values in colour transition between solid (0°C) and liquid (25°C) state of sample a-f.

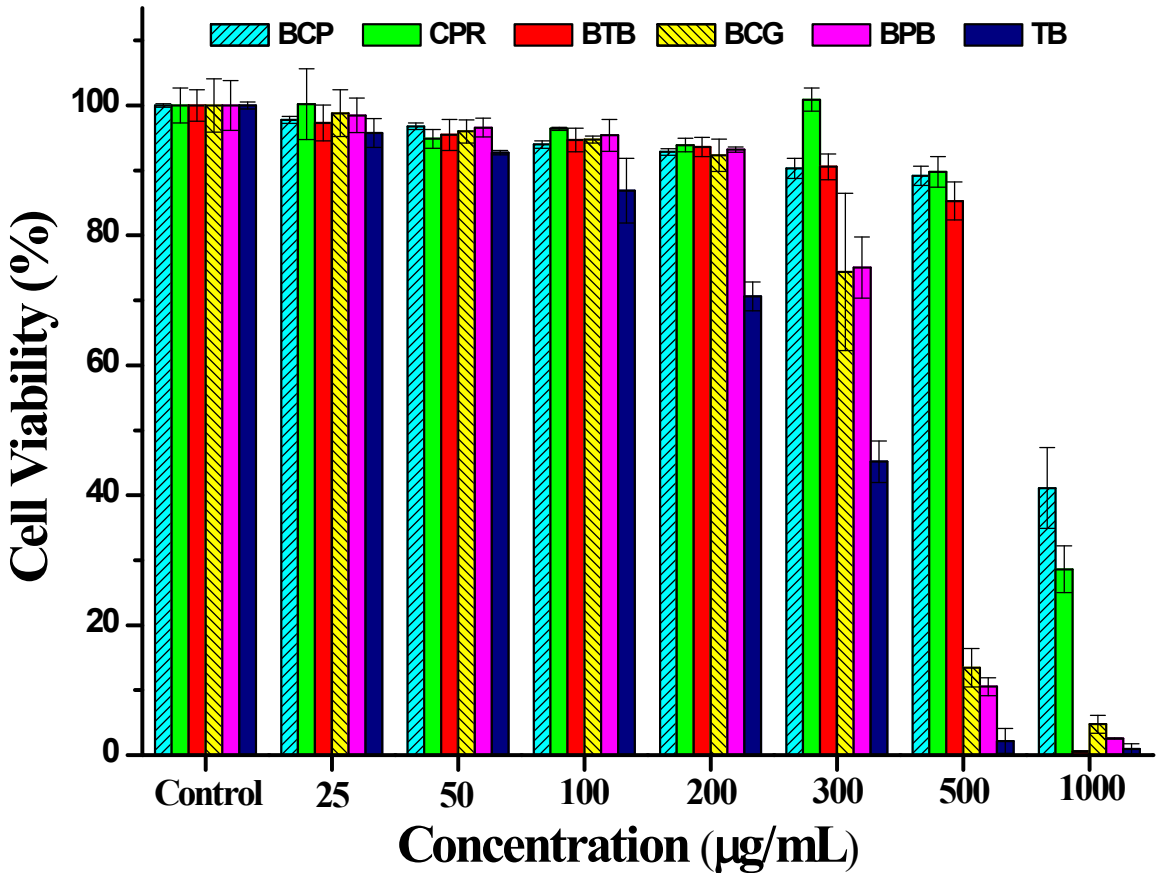

Figure S3. Cytotoxicity of BCP, CPR, BTB, BCG, BPB and TB toward NIH-3T3 cells incubated for 24 hours.

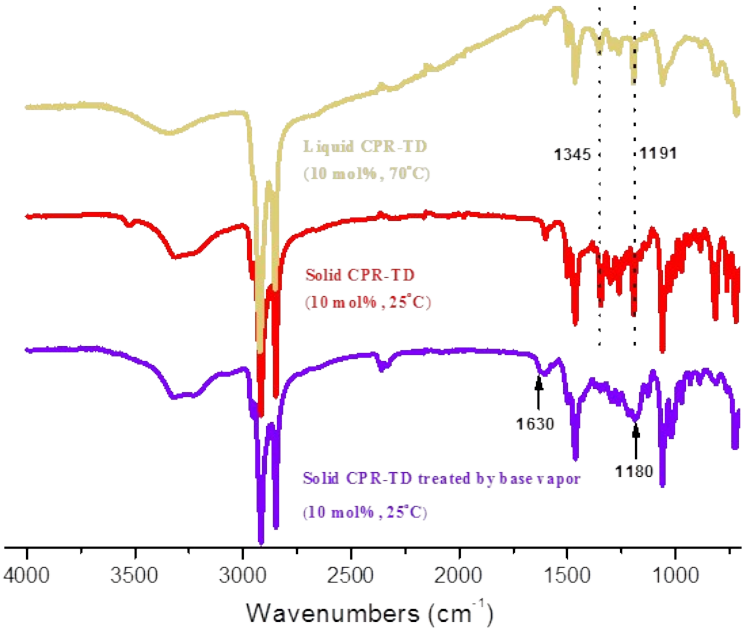

Figure S4. FTIR spectra of CPR-TD (10 mol%) liquid sample at 70°C, solid sample at 25°C and base vapour (aq. NH_4OH) treated solid sample at 25°C.

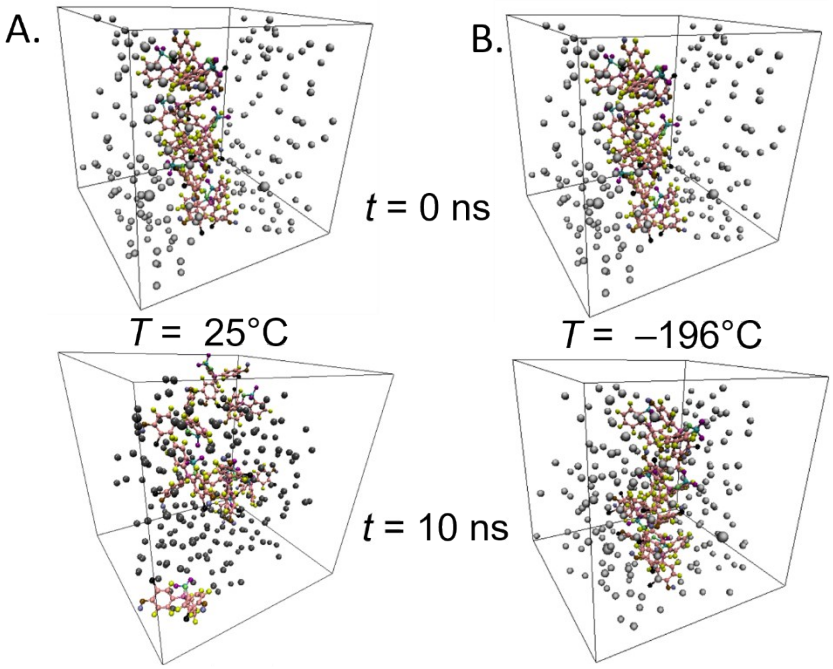

Figure S5. Initial (t = 0 ns) configuration (top) of the 8 CPR molecules dispersed in 200 methanol molecules (depicted by grey spheres) simulated in the NVT ensemble at (A) 25°C and (B) –196°C.

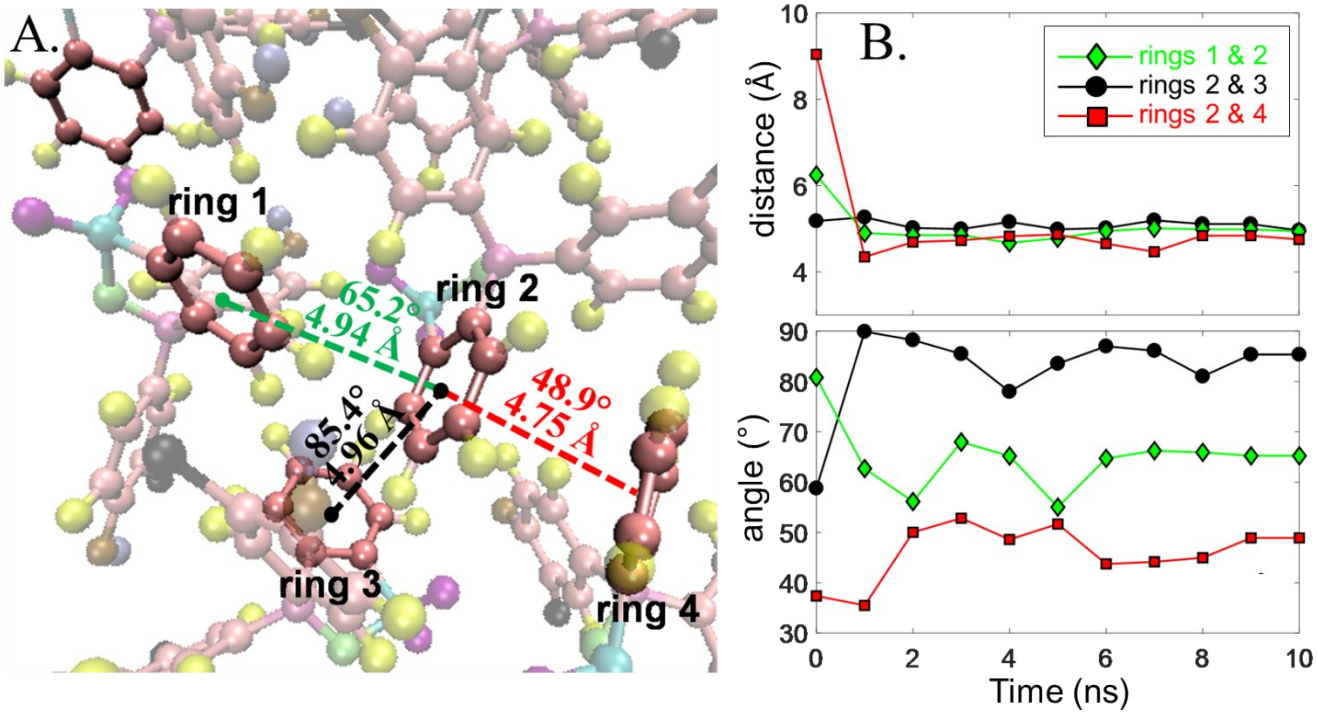

Figure S6. A) Snapshot of benzene rings connected to the sulfoxide group (highlighted pink atoms) obtained by MD simulations of eight CPR molecules in 200 methanol molecules at –196 °C. Three pairs of benzene rings are shown. B) The interplanar distance and angle of the three pairs.

Chapter 3. Reversible Nontoxic Thermochromic Microcapsules

3.1 Chapter perspective

To make this new thermochromic binary system we developed in **Chapter 2** more broadly applicable, microencapsulation of the binary system into a practical and workable medium is necessary. However, creating nontoxic microcapsules containing thermochromic materials for applications in ink and film materials is historically challenging. Due to the systems developed in **Chapter 2** have hydrophilic dyes and hydrophobic solvents, making encapsulation become difficult. In this chapter, we will firstly develop a binary system with both hydrophilic dye and solvent. Chlorophenol red-water binary system will be developed to demonstrate the thermochromic performance then be used as the core part in the formation of core-shell structured microcapsules. Cell toxicity tests of the obtained microcapsules towards NIH-3T3 cells will be also conducted. The thermochromic behaviour of these microcapsules used as inks for screen-printing or additives in film will be further investigated.

This chapter is an article published in *ACS Applied Materials & Interfaces*, 2020, 12, 9782

3.2 Main text

Reversible Nontoxic Thermochromic Microcapsules

Bingxin Liu†, Alicia Rasines Mazo†, Paul A. Gurr†, Greg G. Qiao†*

†Polymer Science Group, Department of Chemical Engineering, The University of Melbourne, Parkville, VIC 3010, Australia

*Corresponding author: gregghq@unimelb.edu.au

ABSTRACT

Thermochromic materials exhibit colour change in response to a change in temperature. Creating nontoxic microcapsules containing thermochromic materials for applications in ink and film materials is historically challenging. In this study, we developed a nontoxic chlorophenol red (CPR)-water thermochromic system and its microcapsules with silicone shells via reaction between water and octadecyltrichlorosilane (OTS) at the interface of a w/o emulsion. The obtained microcapsules exhibited clear colour change with full reversibility and were successfully used as inks by screen printing and as additives in films. Nontoxicity of both microcapsules and films were demonstrated through cell cytotoxicity assays. These features make these novel materials applicable for the next generation of intelligent food packaging materials.

Key words: nontoxic, thermochromic, ink, reversible, print

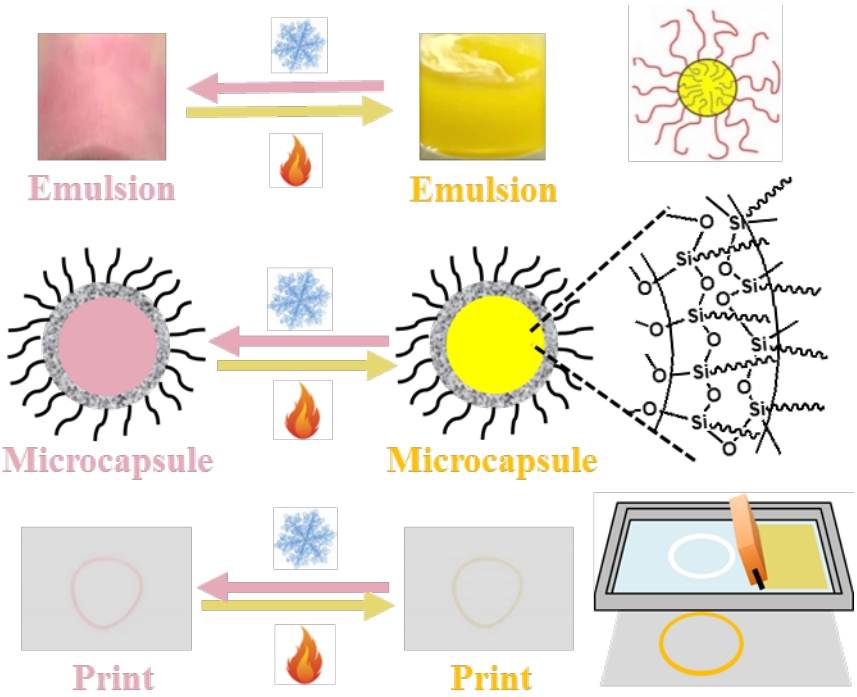

Introduction

Smart responsive materials change their properties in response to external stimuli, such as temperature, pressure, light, pH, magnetic and electric fields or exposure to moisture and chemical compounds.[1] Thermochromic materials change their colour as a response to a change in temperature and typically include materials made from liquid crystals,[2] leuco dye systems,[3] gold or silver nanoparticles,[4] quantum dots[5] or dye-polymer blends.[6] The most commonly used types are liquid crystals and leuco dyes.[7] The change in wavelength of reflected light of thermochromic liquid crystals relies on a variation in the internal spiral pitch length at different temperatures.[2] However, the commercial applicability of liquid crystals towards thermochromic products is greatly hampered by their high cost and weak colour changing effects.[7] In contrast, leuco dye systems have been more successfully applied in commercial applications such as colour changing automotive paints, costumes, packaging materials, hair dyes and nail polish. Their introduction in these products has been widely accepted by consumers and has been shown to increase customer appeal.[8] However the food industry is reluctant to use leuco dyes, due to concerns about the potential for leaching of toxic components.

Leuco dye systems contain three components: dye, developer and long chain solvent. Briefly, the dye interacts with the developer to form one colour when the solvent is in the solid form, while upon heating and melting of the solvent, this interaction is lost forming an alternate colour. Thus, the colour change of the leuco dye system is controlled by the melting or crystallisation of the long chain solvent. Leuco dyes and developers are usually toxic, which has led to their use being limited to non-food applications or food packaging articles with significant barriers, such as glass, metal or thick plastic layers so that direct food contact is avoided.[9] Furthermore, to make them amenable to printing, leuco dye systems are typically microencapsulated by crosslinked polymeric shells, using either melamine–formaldehyde resin, acrylic-based or styrene-based polymers, some of which also pose food safety concerns.[10] Methods of microencapsulation include emulsion polymerization, suspension polymerization, interfacial polymerization, *in-situ* polymerization, complex coacervation, sol-gel and spray drying.[11] Microencapsulation of leuco dye systems is carried out employing oil in water (o/w) emulsions via crosslinking of the hydrophilic shell material, typically by condensation of a urea-formaldehyde solution.[12]

As an alternative to the toxic leuco dye systems, we have recently reported the first nontoxic binary thermochromic system comprised of a hydrophilic sulfonephthalein dye and a hydrophobic aliphatic solvent (long chain ester, acid or alcohol).[13] The colour change of this binary system is controlled by the melting/crystallisation of the solvent, without the need for developer. This system has the benefits of a non-toxic nature and reversible thermochromism. To make this new material more broadly applicable, encapsulation of the binary system into a practical and workable medium is necessary. However, protection of this system by encapsulation is inherently difficult due to the components being both hydrophobic (solvent) and hydrophilic (dye) in nature and microencapsulation of both hydrophilic and hydrophobic components is difficult. To address this challenge, we investigated the use of water as the solvent in the binary system, which maintains the nontoxicity but importantly replaces the hydrophobic solvent with water, making the emulsification of the binary system possible. The microencapsulation of our binary hydrophilic system is carried out from a water in oil (w/o) emulsion, via reaction between the shell material and water. Crosslinked silicone polymers have been chosen as they are commonly applied as medical materials due to their human compatibility.[14]

In this work, we firstly developed a nontoxic thermochromic system with both components hydrophilic (chlorophenol red (CPR)-water). The thermochromic performance of this novel binary system and corresponding microcapsules were then investigated. The obtained microcapsules were further developed as inks in screen printing and as additives in films. The cell toxicity of the microcapsules towards NIH-3T3 (noncancerous fibroblasts) cells was further examined.

Results and discussion

New thermochromic emulsions

To test the hypothesis of a thermochromic system using CPR and water, we first prepared aqueous solutions of CPR at concentrations of 10^{-2}, 10^{-3}, 10^{-4} and 10^{-5} M, respectively (Figure 1). We then encapsulate them into microcapsules using a water in oil (w/o) emulsion approach where a crosslinked silicon polymer shell is formed.

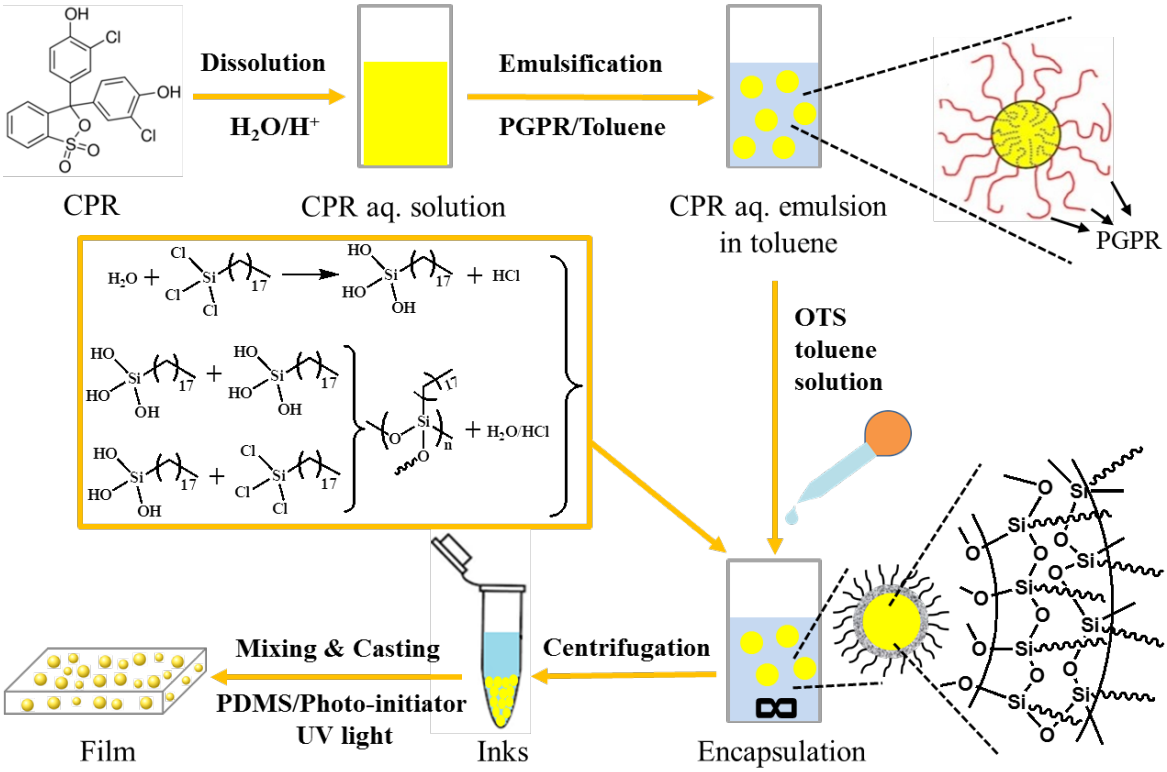

Figure 1. The schematic diagram of the fabrication of CPR-water based microcapsules with crosslinked silicone shells and their application in crosslinked PDMS films.

Liquid aqueous solutions containing CPR dye at 25 °C show colours ranging from dark orange, pale orange, dark yellow to bright yellow as the concentration of dye is decreased (Figure 2).

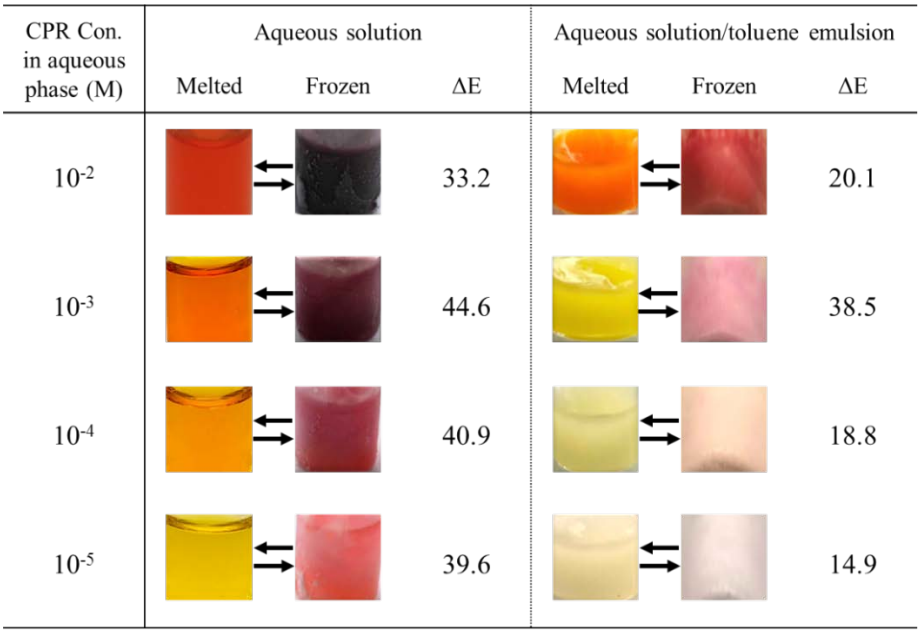

Figure 2. Photographic images of aqueous CPR solutions at different concentrations (10^{-2} M, 10^{-3} M, 10^{-4} M and 10^{-5} M) and their w/o emulsions in toluene (volume ratio of 1:10) at melted (25 °C) and frozen states (-196 °C). The colour differences between melted and frozen states are evaluated by ΔE according to CIE2000.

Upon cooling these liquid solutions to solids, clear colour changes were observed with different colours exhibited at different concentrations (Figure 2). Quantification of the colour change (ΔE values, which can be used to quantitatively evaluate the colour difference according to CIE2000[15]) indicates all liquid-solid transitions show very distinctive contrast in colour. This confirms that the sulfonephthalein-water binary systems (with both hydrophilic components) exhibit thermochromism, similar to our previous observations (with binary systems containing one hydrophilic dye and one hydrophobic solvent).[13] The binary system was then emulsified in toluene into microdroplets which showed lighter colours corresponding to the original CPR concentrations, ranging from orange, bright yellow, pale yellow to milky white (Figure 2). The reduced colours in the emulsions are likely due to dilution in toluene. Upon cooling, the thermochromic nature of the binary system was maintained in emulsion, with similar colour changes occurring, having ΔE values ranging from 14.9 to 38.5. It was found that at the concentration of 10^{-3} M CPR, both solution and droplets exhibited the highest ΔE value. The UV-Vis absorption spectra of the emulsions in melted and frozen state are shown in Figure S1. We have previously shown that the bathochromic shift of the absorption peak is the result of agglomeration of CPR, leading to the emergence of a pink colour in the frozen state.[13] When the CPR concentration is too low or too high, no thermochromism would be observed upon solidification due to CPR molecules remain either homogeneously dissolved or completely aggregated in both liquid and solid states. Therefore, there is an optimal concentration value for CPR to show the most noticeable thermochromism. Since the concentration of CPR at 10^{-3} M showed the greatest ΔE, core materials used in the subsequent encapsulation were performed at this concentration.

DSC analysis was additionally performed on the binary system to determine its thermal properties (Figure S2). During the heating cycle (5 °C/min) endothermic peaks corresponding to the melting of the aqueous CPR solution with a melting point (T_m) of -0.6±0.2 °C (Table S1) were observed. This is marginally lower than 0 °C, due to the

solution vapor pressure being lower than that of the pure solvent, when non-volatile solute is added. The cooling cycles showed very sharp exothermic peaks at their freezing points around -18 °C, which are much lower than for their melting point. Furthermore, the freezing point shifts in each thermal cycle and this phenomenon in the crystallization process is very common and is related to supercooling, crystal seed formation and growth.[16] The lowest temperature reported at which water can be cooled before freezing to ice is 225K (-48.15 °C). Therefore, the freezing point of the core solution will unlikely be below -49 °C.

Thermochromic microcapsule formation

One monomer used in the formation of silicone polymers is alkyltrichlorosilane, which spontaneously hydrolyses with water at the hydroxylated surface of the substrate to form hydroxysilane, which can condense to form Si–O–Si bonds. The condensation reaction not only occurs between the Si–OH groups and the –OH groups on the hydroxylated surface but also with the neighbouring silanol groups to form stable crosslinked networks.[17] In particular, the monomer octadecyltrichlorosilane (OTS) has been extensively reported in the formation of self-assembled monolayers on the surface of a wide range of substrates[18] and at the interfaces of air/water,[19] semiconductor/dielectric,[17] and nematic/water[20]. Importantly, OTS has also been used as a shell material for microencapsulation of aqueous core systems.[21] For this reason OTS was chosen to generate a crosslinked shell for the newly designed hydrophilic binary systems in a (w/o) emulsion (Figure 1).

Stable microcapsule formation is dependent on the core to shell ratio, too little shell material will result in leaching of the core material or collapse of the particle, while too much shell material will result in aggregation of the particles or suppression of the dye's colour intensity upon cooling.[12b] With aqueous CPR solutions as core material and OTS as the shell precursor for the microencapsulation (Figure 1), the feed core-shell mass ratios of 320:1, 40:1, 20:1 and 10:1 were prepared and evaluated (Figure 3 BX_1-BX_4). The amount of encapsulated core material initially increased with increasing shell material, then plateaued into a constant value from 20:1 ratio (Figure 3). The formation of the microcapsule shell occurs at the surface of the CPR/water droplets, which continually grows in thickness, by the reaction of OTS with water at the toluene-water interface (Figure 1). The reaction continues until the shell is completely sealed and no further water molecules can react with the external OTS, or until the OTS has been completely consumed in the toluene solution. In general, if the ratio of the core is too high, less core material is incorporated into the microcapsules with only ~75% being encapsulated. Conversely, if the feed amount of OTS is too low, thin shells are formed and they are not robust enough to enclose the core materials.

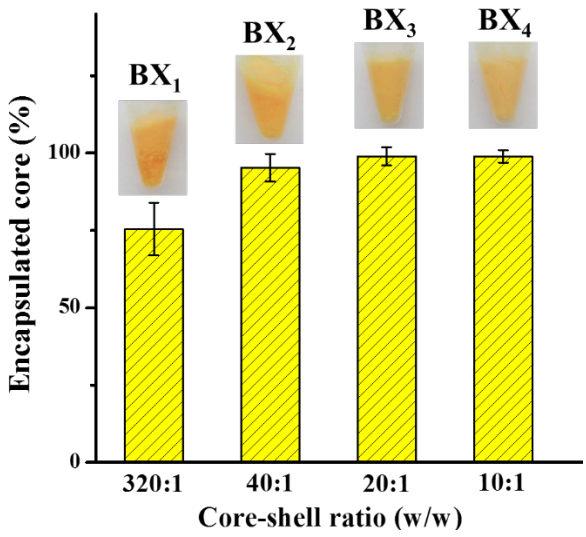

Figure 3. Encapsulation percentage of encapsulated core part of sample BX_1, BX_2, BX_3 and BX_4 with different core-shell feed mass ratios (320:1, 40:1, 20:1 and 10:1) when core is CPR aqueous solution and shell material is OTS and corresponding photographic images of capsules in tubes.

The chemical composition of the microcapsules and unreacted aqueous CPR solution were determined by FTIR analysis (Figure 4). Prior to encapsulation, analysis of the CPR-water solution showed characteristic broad peaks at 3250 cm^{-1} and 1625 cm^{-1} associated with water.[22] No signals resulting from CPR were observed, due to concentration of CPR falling below the FTIR detection limit. Spectral analysis of the core-shell microcapsules showed the presence of unreacted and enclosed water within the shells. Additionally, signals resulting from the shell structure were observed, including a peak at 2956 cm^{-1} corresponding to the asymmetrical stretching vibration of $-CH_3$ groups and strong peaks at 2915 cm^{-1} and 2850 cm^{-1} corresponding to the asymmetrical and symmetrical stretching vibrations of $-CH_2-$ groups of the aliphatic chains.[23] In addition, a sharp peak at 1467 cm^{-1} was also observed, attributed to the deformation vibration of $-CH_2-$ groups. The FTIR absorptions from 1010 cm^{-1} to 1110 cm^{-1} and from 850 cm^{-1} to 940 cm^{-1} are attributed to the stretching vibration of -Si-O-Si- groups, which are evidence of the formation of crosslinked silicone shells.[24]

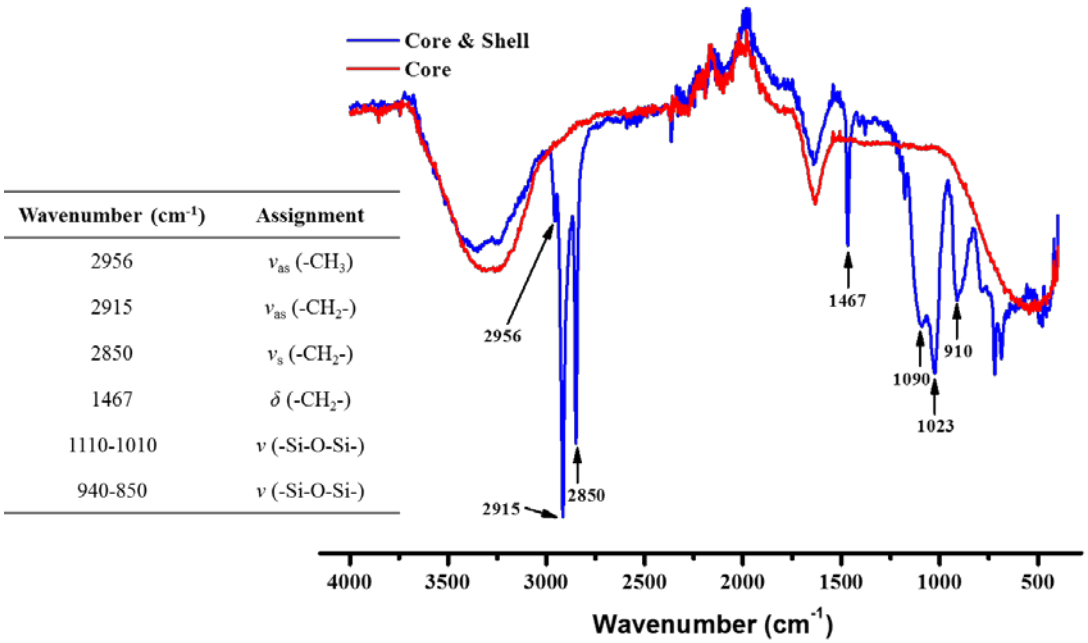

Figure 4. ATR-FTIR spectra of core CPR aqueous solutions and core-shell microcapsules at 25 °C.

For microcapsules intended to be used in ink applications, the size range needs to be well controlled.[25] Thermochromic pigments including encapsulated leuco dye systems and liquid crystals are approximately micron sized.[26] For printing applications, their size is typically around several microns, which is 10-times larger than ordinary non-thermochromic pigment particles.[27] Smaller microcapsules have better mechanical properties and can bear high shearing forces so that they are more favoured as offset inks, while larger ones have better thermochromic performance and are more suited for screen printing.[25, 28] An optical microscopic image of core-shell capsules from BX_3 is shown in Figure 5A. The size distribution calculated by ImageJ analysis software based on the optical microscopic image shows the size of core-shell microcapsules ranges from 0.6 μm to 3.0 μm (Figure 5C), with the majority of the microcapsules having diameters from 1.0 μm to 1.2 μm. The size distribution analysed by dynamic light scattering (DLS) reveals a similar size distribution with a mean diameter of 1.1±0.1 μm (Figure 5D). DLS is a more accurate method for determining size when particles are below sub microns,[29] and it provides a reference of overall size distribution of these microcapsules. The size distributions of BX_1 to BX_4 (Table 1) indicate all of these microcapsules have similar mean sizes around 1 μm making them suitable for printing applications.

Most reported thermochromic microcapsules with crosslinked polymeric shells are spherical in shape owing to their preparation method.[7, 10d] However, in this case, the microcapsules have a rough surface, due to the heterogeneous nature of the hydrolysis reaction in the capsule formation. During the water-toluene mixing process, the w/o emulsion was formed, accompanied with partial air and water solvation in the toluene phase. Initially, a portion of the OTS molecules spontaneously hydrolyse with the dissolved water in the organic phase (Figure 1). As the unreacted OTS and reacted molecules migrate to the surface of the aqueous microdroplets, three-dimensional and two-dimensional polymerization processes occur simultaneously to form heterogeneous yet stable shells with non-uniform thicknesses. A scanning electron microscopy (SEM) image of microcapsule BX_3 shows a rough and irregular surface morphology (Figure 5B). This phenomenon has been previously reported.[30]

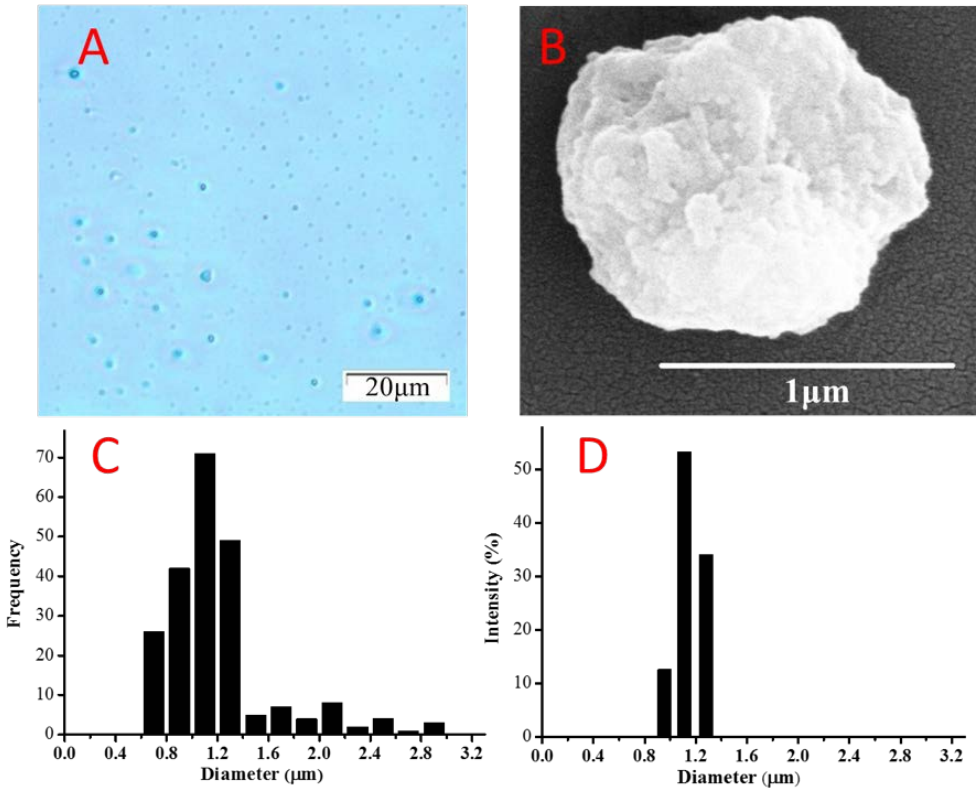

Figure 5. A) The optical microscopic image of core-shell microcapsules from BX_3. B) The scanning electron microscopic image of core-shell microcapsule from BX_3. C) The size distribution of core-shell microcapsules calculated by ImageJ analysis software based on the optical microscopic image. D) The size distribution of core-shell microcapsules analysed by dynamic light scattering.

Table 1. Summary of microcapsules showing feed mass ratio of core (CPR/Water) and shell materials (OTS), size distributions calculated by DLS and colour contrasts (ΔE) between 25 °C and -80 °C of BX_1 to BX_4.

Sample	Feed ratio (core: shell by weight)	Mean size (μm)	Standard deviation σ (μm)	ΔE
BX_1	320:1	0.993	±0.099	36.5±1.4
BX_2	40:1	1.006	±0.090	33.4±1.5
BX_3	20:1	1.148	±0.107	29.9±0.6
BX_4	10:1	1.237	±0.123	28.7±1.9

DSC analysis of microcapsules BX_3 shows the melting point (T_m) is -2.8±0.3 °C (Figure 6B & Table S1), which is lower than the melting point of the initial core CPR aqueous solution. This phenomenon is caused by the size-dependent melting point depression of small particles due to their surface-to-volume ratios being larger than in bulk materials. As the size of particle decreases, the proportion of water molecules occupying on the surface or interface increases. These molecules are more loosely bound, which facilitates melting. The first round of cooling cycle shows the freezing point is around -20 °C (Figure 6B). Based on the analysis of melting and freezing points, microcapsules at 25 °C and -80 °C have undergone melting and freezing processes, respectively. Therefore, the thermochromic behaviour of the microcapsules at these temperatures was examined and is shown in Figure 6A.

The microcapsules showed distinct colour changes between yellow and pink when the temperature altered between 25 °C and -80 °C. The chromaticity coordinates in the CIE chromaticity chart (i & i' in Figure 6) visually confirm the obvious thermochromism of the microcapsules. The ΔE values of BX_1 to BX_4 are summarized in Table 1, where the colour of each sample at 25 °C was set as the reference. The results indicate that the thermochromic effect of the microcapsules decreases as the core-shell mass ratio is lowered. This is attributed to the fact that the thermochromic properties are imparted by the core solution, and a lower core-shell mass ratio results in denser and thicker shells which interferes the colour that can be observed from the core solution. Based on the considerations of both yield and optimal colour contrast in thermochromism, a core-shell feed mass ratio of 20:1 was found to be the most suitable for the microcapsule fabrication. As a result, BX_3 microcapsules were used in subsequent investigations for film formation.

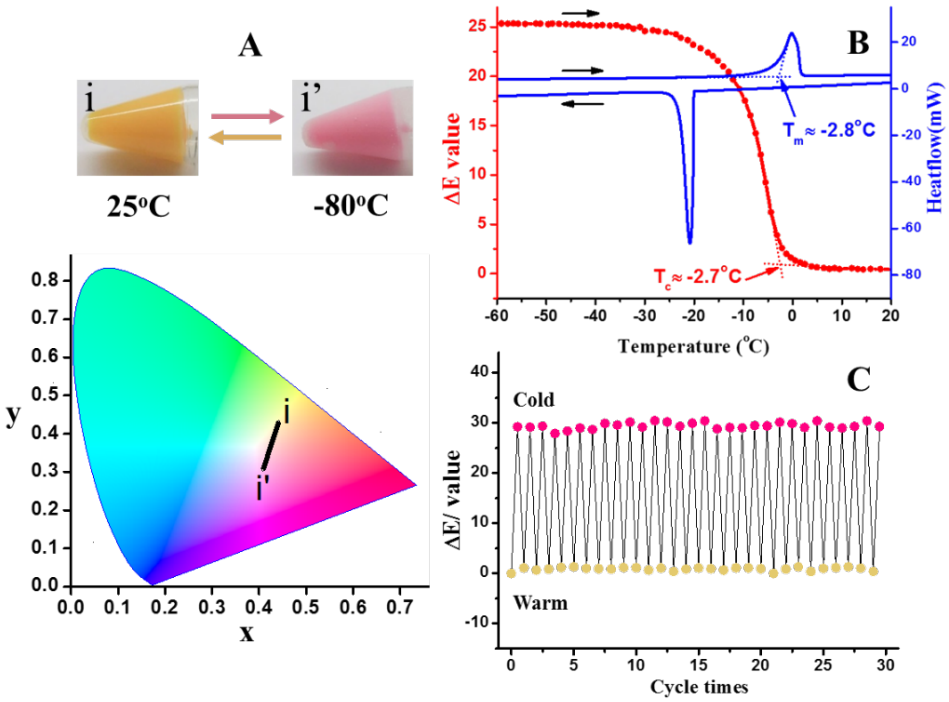

Figure 6. A) Photographic images of core-shell microcapsules from BX_3 in centrifuge tubes at i) 25 °C and i') -80 °C and their corresponding x-y coordinates represented in the standard CIE 1931 chromaticity chart. B) DSC heat flow curves (5 °C/min, blue) and ΔE value-temperature curve (red) of BX_3 microcapsules in temperature range between -60 °C and 20 °C when colour of microcapsules at 25 °C is set as reference. C) ΔE values of BX_3 microcapsules over 30 thermal cycles between 25 °C (●) and -80 °C (●).

The temperature-induced colour change of microcapsules BX_3 in heating process was quantified using ΔE and was correlated to the observed phase change from DSC analysis. Figure 6B (red) shows the gradual colour change beginning at approximately -25 °C and finishing at -2.7 °C. The heating cycle of DSC curve in figure 6B (blue) shows a similar phase change behaviour with the melting point (T_m) occurring at -2.8 °C. These results indicate the microcapsules fully change colour into yellow at approximately -2.7 °C (T_c) with a complete melting of the core material. To investigate the reversibility of the microcapsule thermochromism, ΔE values were recorded over 30 heating and cooling cycles as shown in Figure 6C. Upon cooling to -80 °C from an initial temperature of 25 °C

in the first cycle, colour changes from yellow to pink with ΔE of 29.4±0.6 were observed; these correspond to an obvious colour contrast to the naked eye. In addition, the sample returned to its original colour upon heating to 25 °C, *i.e.* ΔE=0.9±0.3, showing preservation of the reversible thermochromism. Thus, successful encapsulation has been verified.

Thermochromic microcapsules as ink

To test the potential of these microcapsules as inks, a paste of microcapsules in hexane (0.6 g/mL) was cast into a 3D-printed mould (Figure 7A). The mould was printed on a 3D-printer using a UV-curable commercial resin, followed by being washed and post-cured under a UV lamp at dry condition. After evaporation of hexane, the microcapsules stacked in the 'PSG' logo that consisted of grooves showed reversible thermochromic behaviour between 25ºC and -80ºC. The yellow colour at 25ºC and pink colour at -80ºC are similar to the microcapsules alone in a tube shown before in Figure 6A. To demonstrate its applicability as a printing ink, the same paste of microcapsules was screen printed onto paper showing a 'ring' image (Figure 7B). The screen printing was conducted on a fine fabric mesh with open apertures forming a 'ring' stencil. The ink could transfer onto the paper beneath only through the open apertures to form the corresponding image when a blade was moving across the screen. The 'ring' image on paper after evaporation of hexane also clearly exhibited similar reversible thermochromic behaviour between 25ºC and -80ºC (Figure 7B). Therefore, the test demonstrated the potential applicability of CPR-water microcapsules as ink materials for printing.

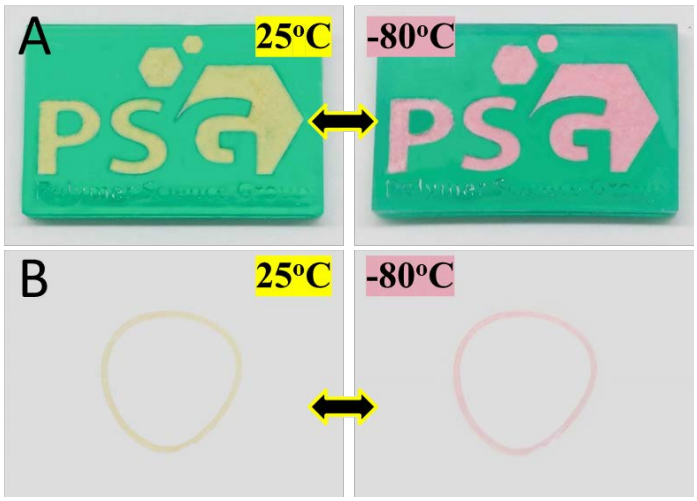

Figure 7. Thermochromic prototypes prepared from BX_3 microcapsules A) cast into a 3D-printed mould and B) screen printed as ink onto paper.

Thermochromic microcapsules as film additives

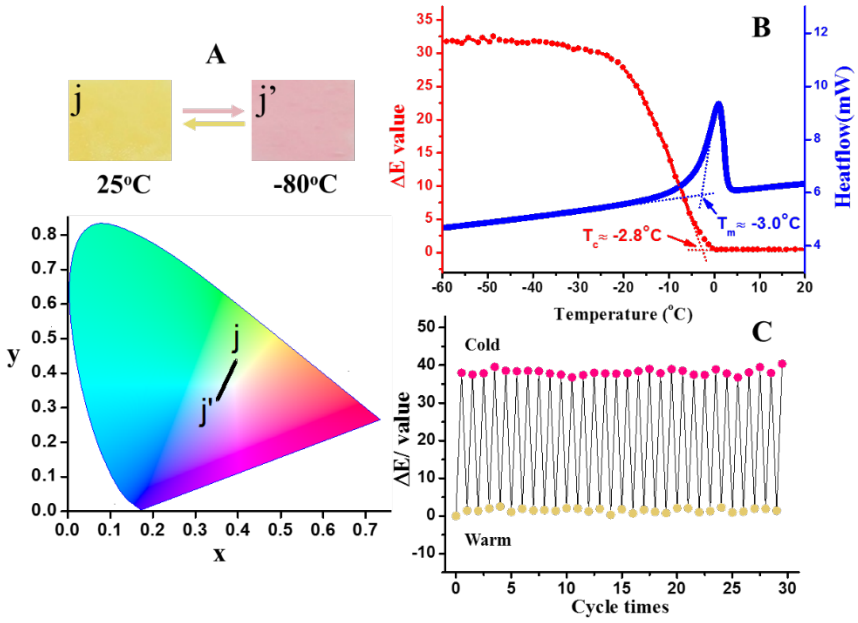

Figure 8. A) Photographic images of film at j) 25 °C and j') -80 °C and corresponding x-y coordinates represented in standard CIE 1931 chromaticity chart. B) DSC heat flow curves (5 °C/min, blue) and ΔE value-temperature curve (red) of film in temperature range between -60 °C and 20 °C when colour of film at 25 °C is set as reference. C) ΔE values of film over 30 thermal cycles between 25 °C (●) and -80 °C (●).

The applicability of the thermochromic microcapsules as additives was demonstrated by their incorporation into a film. Due to the transparency, flexibility and nontoxicity of poly(dimethylsiloxane) (PDMS),[14c, 31] a vinylmethylsiloxane-dimethylsiloxane copolymer resin (Vinyl-PDMS) mixed with BX_3 microcapsules was cast onto polyethylene terephthalate (PET) plastic film before being crosslinked by UV light (Figure 1). The DSC curve of the obtained film sample in figure 8B (blue) shows the melting point (T_m) is -3.0±0.3 °C (Table S1). This value is similar to the one from the microcapsules, indicating the core solution did not leak out from the shells within the film. The thermochromic behaviour of the film was examined at 25 °C and -80 °C (Figure 8A) and showed distinct colour change between yellow and pink respectively, as also indicated by the shift of chromaticity coordinates in the CIE chromaticity chart (j & j' in Figure 8). Overall, it was observed that processing of the microcapsules into films did not affect the thermochromic properties. As already described, the film was yellow at temperatures ≥-2.8 °C (T_c), a value in close agreement with the T_m displayed in the DSC heat flow curve (Figure 8B). Thus, the thermochromic behaviour of the microcapsules or film is only dependent on the internal phase change of aqueous CPR solution and demonstrates the stability of the microcapsules inside the silicone matrix after crosslinking. The ΔE values of film undergoing temperature alternates indicate the thermochromism of the film is also fully reversible during 30 thermal cycles (Figure 8C). The colour of the film remains pink at -18 °C, which is the temperature at which household freezers operate, demonstrating the film's potential use as an indicator for the transportation or storage of frozen food products.

Toxicity study

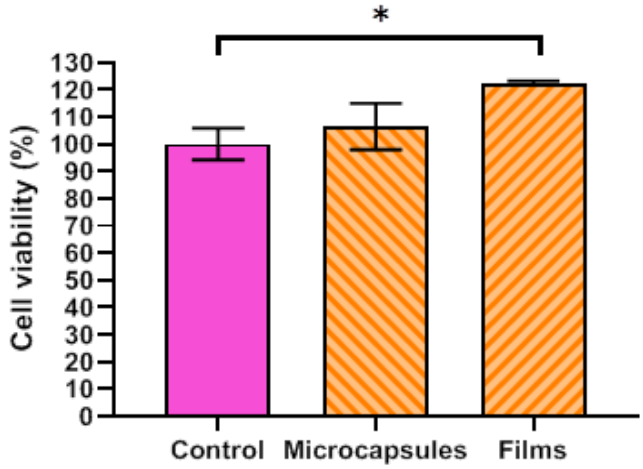

Figure 9. Cytotoxicity of microcapsules (2 mg/mL) or films (20 wt.% microcapsules in film) toward NIH-3T3 cells incubated for 24h. *P <0.05. The cells were incubated only with fresh medium in the control samples.

The relative cytotoxicity of microcapsules BX_3 and their processed films was examined using the CCK-8 assay (Figure 9). No statistical differences in formazan absorbance were observed between control and microcapsules or microcapsules and films ($P > 0.05$) using student t-test. In all cases, examination of the NIH-3T3 cells (Figure S3) under the microscope showed a nearly confluent layer. The nearly confluent well surface indicates that the tested samples are nontoxic and do not exert any soluble cytotoxicity with the cells, as the cells maintained their viability. Cells exposed to film samples also grew to confluency, despite the high concentrations of microcapsules (20 wt.%) which were used in forming the film. The higher absorbance values observed compared to the control may indicate that the PDMS surface provides a better cell growth environment.

Conclusion

In conclusion, a nontoxic CPR-water binary system was developed, which showed clear and reversible thermochromic performance. This binary system was further emulsified and microencapsulated by stable silicone shells generated from the hydrolysis and crosslinking reaction of OTS. The core-shell structure of the obtained microcapsules was confirmed by ATR-FTIR. The formed microcapsules also exhibited clear and reversible thermochromic performance upon cooling or heating. Results of microscopic and DLS analyses revealed the size distribution of these microcapsules was approximately 1 micron, a dimension suitable for ink applications. A pattern generated from screen printing using these microcapsules showed thermochromic behaviour. When the microcapsules were used as additives to form a PDMS film, the resultant film also showed reversible thermochromic behaviour. Cell cytotoxicity tests of both microcapsules and film confirmed they were nontoxic. The thermochromic microcapsules developed in this work provide a novel material design concept with potential applications in intelligent food packaging.

Experimental

Materials

Chlorophenol red (CPR, indicator grade, Merck), aq. hydrochloric acid (32 wt.%, Ajax FineChem), anhydrous toluene (99.8%, Merck), polyglycerol polyricinoleate (PGPR-4125, Palsgaard), octadecyltrichlorosilane (OTS, ≥ 90%, Merck), acetone (AR, Chem-Supply) and 1-hydroxycyclohexyl-1-phenyl methanone (Irgacure 184, Merck) were used as received without further purification. Vinylmethylsiloxane-dimethylsiloxane copolymer (Vinyl-PDMS) was purchased from Gelest (USA) and used as received.

Methods

Preparation of microcapsules

An aqueous solution of CPR (1 mM) was prepared and adjusted to pH 3 with the addition of aq. HCl (1 M). The w/o emulsion was then prepared by stirring at 33000 rpm for 5 min (Dremel mini-drill, Model 3000) of a mixture of aq. CPR soln. (3 mL, 1mM) and surfactant PGPR (60 mg) in anhydrous toluene (30 mL). Toluene solutions (4 mL) containing various concentrations of OTS (6 mM, 48 mM, 96 mM and 192 mM respectively) were added dropwise into the emulsion, while the emulsion was stirred using a magnetic stirrer bar at 2500 rpm, and then continued stirring for 5 hours. The resulting microcapsules were collected by centrifugation, separation of the mother liquor, then washed with hexane and dried *in vacuo* at -80 ℃ for 10 minutes (Figure 1).

Film Preparation

In a typical fabrication, a homogeneous PDMS mixture of Irgacure 184 (0.02 g, 1.6 wt%) in Vinyl-PDMS (1.0 g, 78.7 wt%) was formed by sonication and the solution kept at 25℃ prior to use. Previously prepared microcapsules (0.25 g, 19.7 wt%) were mixed into the PDMS solution and the suspensions cast between two commercial films of PET, which were then exposed to UV light (λ =366 nm, 1 hour, MINERALIGHT® lamp UVGL-58). The solid PDMS-based films were obtained after removal of the outer PET films (Figure 1).

Design and formation of the 3D printed mould

The mould used for casting the thermochromic microcapsules was modelled in TinkerCAD, a cloud-based computer-aided design (CAD) software by adapting a 3D model from an Adobe Illustrator file of the ‘PSG’ logo into a printable 3D model. The design was exported and converted to a 3D printable file in ANYCUBIC Photon Slicer64 software. Then the mould was printed on a DLP-style 3D printer using UV-curable ANYCUBIC Green Colour Resin (ANYCUBIC Photon). Printing conditions used were layer heights of 50μm with 8 bottom layers at 30 second exposure time and the remaining layers cured at 8 seconds each. The mould was removed from the printer build plate, sonicated in isopropyl alcohol before being blown dry with N_2 and post-cured under a 36W UV lamp for 10 minutes.

Cell Culture and Cytotoxicity

NIH-3T3 noncancerous fibroblast cells were obtained from American Type Culture Collection (ATCC). The cells were cultured according to standard procedure. NIH-3T3 cells were maintained in DMEM medium (DMEM, Gibco, Invitrogen, U.S.A.) supplemented with 10% FBS (FBS, Gibco, Invitrogen, U.S.A.), 1% GlutaMax (Gibco, Invitrogen, U.S.A.), and 1% penicillin-vancomycin (Gibco, Invitrogen, U.S.A.). The cells were cultured at 37 °C in a humidified 5% CO_2 atmosphere. The culture medium was changed every other day. The cultures were passaged at 80% confluence and lifted using 0.25% trypsin–EDTA (1×, Gibco). For the cell viability tests, cells at passage 10 were used employing CCK-8 assay. NIH-3T3 cells (4×10^4 cells/well, 500 µL) were incubated in a flat bottomed 24 well plate for 24 hours. Subsequently, the cell medium was aspirated, replaced with fresh medium and 2 mg/mL microcapsules or films (20 wt.% microcapsules in film) were added in triplicate and the well plate was further incubated for 24h. After this time, the samples contained in the wells were removed and the cell medium was replaced with 300 µL of fresh medium, to which 30 µL of CCK8 reagent was added to each well. The plate was incubated for 2h before analysing the cell viability using a microplate reader (TECAN M200 infinite Pro) at wavelength of 460 nm.

Instrumentation

Differential Scanning Calorimetry (DSC). Heat flow curves were recorded on a Perkin Elmer Differential Scanning Calorimeter 8500 under a nitrogen flowing at a rate of 20 ml/min with a heating or cooling rate of 5 °C/min. Melting points or freezing points were taken at the intersection of the extrapolated baseline and the tangent to the heat flow curve at the inflection point of appropriate side of the peak.

Fourier Transform Infrared Spectroscopy (FTIR). ATR-FTIR spectra were measured on a Bruker TENSOR II FTIR-ATR spectrometer over the range of 4000 cm^{-1} to 400 cm^{-1} at a resolution of 4 cm^{-1} at 25 °C.

Ultraviolet visible (UV-Vis) Spectroscopy. UV-Vis absorption spectra were performed on a Flame UV-VIS-ES miniature spectrometer equipped with an Ocean Optics DH-2000 optical fibre light source.

Light Microscopy: Optical microscopic images were captured by using an Olympus CKX41 microscope with AnalySIS getIT software.

Particle size analysis. The particles sizes were evaluated on Malvern Nano-ZS Zeta sizer and optical microscopic images using ImageJ analysis software.

Scanning electron microscopy (SEM). The microstructure of the core-shell microcapsules was examined in FEI Teneo VolumeScope. Microcapsules were suspended in hexane and then the suspensions were dropped onto carbon tape. After hexane evaporating, the samples were precoated with gold onto a silica wafer using a Dynavac Mini Sputter Coater prior to imaging.

Photographs of samples were calibrated for white balance using Adobe Photoshop CS6 in Camera Raw format and colorimetric representations were collected for calculating the colour difference (ΔE CIE 2000) between samples.[15, 32] Larger ΔE values represent larger colour differences between samples.

Colour-temperature correlation measurements

Samples were cooled by placing them in acetone and gradually adding dry-ice to the solution in the cooling processing and were warmed up by ambient air, while monitoring the temperature using a digital thermometer. Digital images were taken relative to time and temperature for analysis.

Percentage of encapsulated core material measurements

After centrifuging reaction systems, toluene solutions, microcapsules and unencapsulated aqueous solutions separated into three layers from top to bottom in the centrifuge tubes. Then the unencapsulated aqueous solutions were taken out with a glass pipette to calculate the percentages of encapsulated core solutions.

Acknowledgement

We thank the Australian Research Council (ARC), The University of Melbourne and Mondelez Australia for providing funding through Industrial Transformation Research Hub (ITRH, Project ID: IH120100053). The authors wish to thank Mr. Tom Pattison for preparation of 3D-printed mould and Mr. Matthew Biviano and Mr. Min Liu for assistance.

Supporting information

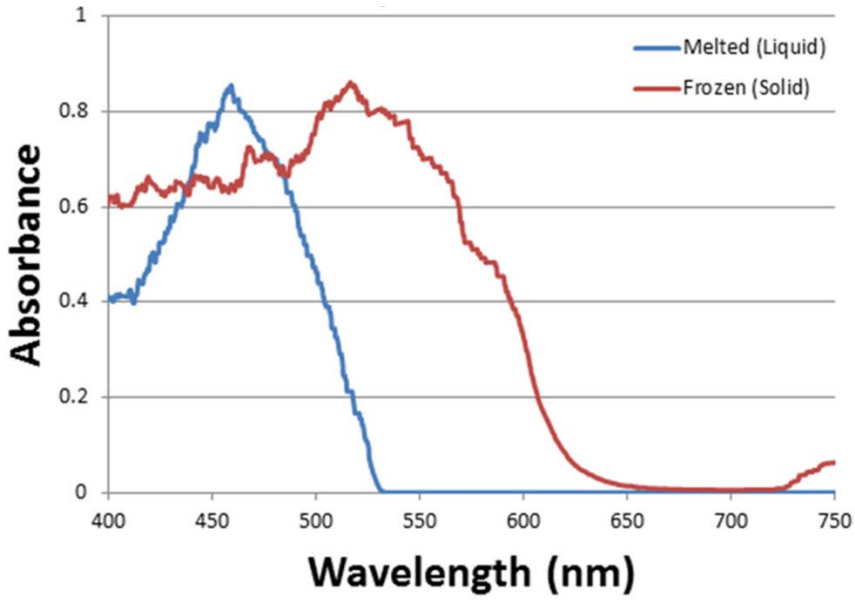

Figure S1. The UV-Vis spectra of w/o emulsion of CPR aqueous solution (10^{-3}M) in toluene (volume ratio of 1:10) at melted (25 °C) and frozen states (-196 °C).

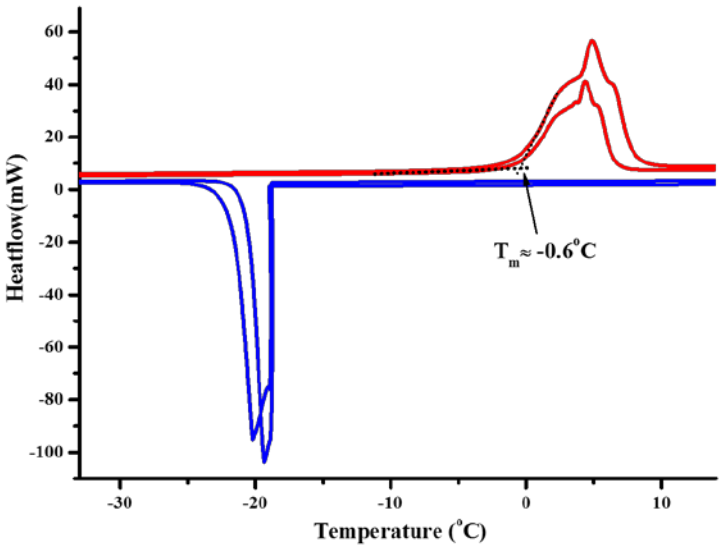

Figure S2. The DSC heat flow curve of CPR aqueous solution (0.001M) in heating and cooling processes between -60 °C and 20 °C (5 °C/min).

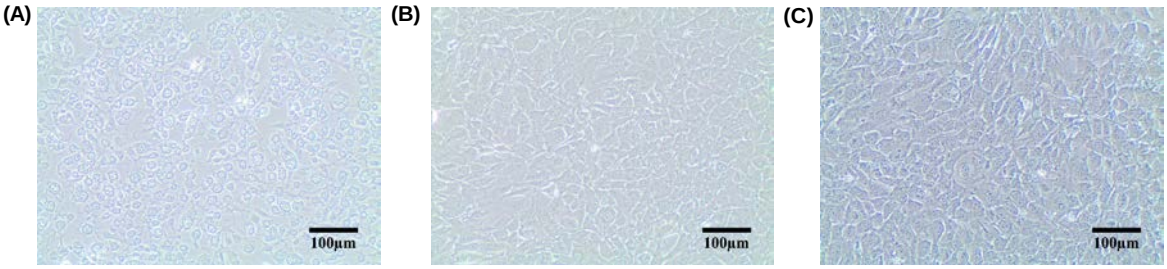

Figure S3. Optical microscopy images of NIH-3T3 fibroblast cells (A) control, (B) incubated with 2 mg/mL microcapsules after 24h and (C) incubated with films (20 wt.% microcapsules in film) after 24h.

Table S1

Thermal parameters of core solution, microcapsules and incorporated film.

Samples	T_m (°C)
Core CPR solution	-0.6±0.2
Microcapsules	-2.8±0.3
Film	-3.0±0.3

References

[1] a) Q. Li, Y. Li, J. Ma, Google Patents, 2015; b) Y.-S. Yang, Y. Zhou, F. B. Y. Chiang, Y. Long, *RSC Advances* **2017**, 7, 7758; c) W. Qiu, P. A. Gurr, G. da Silva, G. G. Qiao, *Polymer Chemistry* **2019**, 10, 1650; d) M. Bengisu, M. Ferrara, *Materials that Move: Smart Materials, Intelligent Design*, Springer, **2018**; e) B. Liu, H. Ranji-Burachaloo, P. A. Gurr, E. Goudeli, G. G. Qiao, *Journal of Materials Chemistry C* **2019**, DOI: 10.1039/C9TC02071C; f) W. Sun, H. Li, H. Wang, S. Xiao, J. Wang, L. Feng, *Talanta* **2015**, 143, 127; g) C. Jarumaneeroj, K. Tashiro, S. Chirachanchai, *Macromolecular rapid communications* **2014**, 35, 1397.

[2] I. Sage, *Liquid crystals* **2011**, 38, 1551.

[3] K. Bašnec, L. S. Perše, B. Šumiga, M. Huskić, A. Meden, A. Hladnik, B. B. Podgornik, M. K. Gunde, *Scientific Reports* **2018**, 8, 5511.

[4] M. Mitsuishi, Y. Koishikawa, H. Tanaka, E. Sato, T. Mikayama, J. Matsui, T. Miyashita, *Langmuir* **2007**, 23, 7472.

[5] H. Tamaki, H. Watanabe, S. Kamiyama, Y. Oaki, H. Imai, *Angewandte Chemie International Edition* **2014**, 53, 10706.

[6] A. Seeboth, J. Kriwanek, R. Vetter, *Journal of Materials Chemistry* **1999**, 9, 2277.

[7] Y. Zhang, Z. Hu, H. Xiang, G. Zhai, M. Zhu, *Dyes and Pigments* **2019**, 162, 705.

[8] D. D. Torrico, S. Fuentes, C. G. Viejo, H. Ashman, P. A. Gurr, F. R. Dunshea, *LWT* **2018**, 89, 475.

[9] W. R. A. P. Report, Waste & Resources Action Programme, Oxon, United Kingdom 2013.

[10] a) K. Pielichowska, K. Pielichowski, *Progress in materials science* **2014**, 65, 67; b) N. Sarier, E. Onder, *Thermochimica Acta* **2012**, 540, 7; c) W. Li, X.-X. Zhang, X.-C. Wang, J.-J. Niu, *Materials Chemistry and Physics* **2007**, 106, 437; d) M. S. Tözüm, S. A. Aksoy, C. Alkan, *Fibers and Polymers* **2018**, 19, 660.

[11] X. Geng, W. Li, Y. Wang, J. Lu, J. Wang, N. Wang, J. Li, X. Zhang, *Applied energy* **2018**, 217, 281.

[12] a) X. Geng, W. Li, Q. Yin, Y. Wang, N. Han, N. Wang, J. Bian, J. Wang, X. Zhang, *Energy* **2018**, 159, 857; b) H. Fukuo, T. Onoguchi, U.S. Patent, US4753759A, **1988**.

[13] B. Liu, H. Ranji-Burachaloo, P. A. Gurr, E. Goudeli, G. G. Qiao, *Journal of Materials Chemistry C* **2019**, 7, 9335.

[14] a) K. F. Mueller, P. Harisiades, Google Patents, 1995; b) F. Abbasi, H. Mirzadeh, A. A. Katbab, *Polymer International* **2001**, 50, 1279; c) Z. Zhang, J. Wang, Q. Tu, N. Nie, J. Sha, W. Liu, R. Liu, Y. Zhang, J. Wang, *Colloids and Surfaces B: Biointerfaces* **2011**, 88, 85.

[15] G. Sharma, W. Wu, E. N. Dalal, *Color Research & Application: Endorsed by Inter-Society Color Council, The Colour Group (Great Britain), Canadian Society for Color, Color Science Association of Japan, Dutch Society for the Study of Color, The Swedish Colour Centre Foundation, Colour Society of Australia, Centre Français de la Couleur* **2005**, 30, 21.

[16] a) E. B. Moore, V. Molinero, *Nature* **2011**, 479, 506; b) P. G. Debenedetti, *Journal of Physics: Condensed Matter* **2003**, 15, R1669.

[17] D. Liu, Q. Miao, *Materials Chemistry Frontiers* **2018**, 2, 11.

[18] a) Y. Liu, L. K. Wolf, M. C. Messmer, *Langmuir* **2001**, 17, 4329; b) P. Fontaine, D. Goguenheim, D. Deresmes, D. Vuillaume, M. Garet, F. Rondelez, *Applied physics letters* **1993**, 62, 2256; c) H. Finklea,

L. Robinson, A. Blackburn, B. Richter, D. Allara, T. Bright, *Langmuir* **1986**, 2, 239; d) Y. Wang, M. Lieberman, *Langmuir* **2003**, 19, 1159; e) J. Huang, X. Liu, X. Qiu, L. Xie, B. Yan, X. Wang, Q. Huang, H. Zeng, *The Journal of Physical Chemistry B* **2017**, 121, 3151.

[19] K. Kojio, A. Takahara, T. Kajiyama, *Colloids and Surfaces A: Physicochemical and Engineering Aspects* **2000**, 169, 295.

[20] A. D. Price, D. K. Schwartz, *The Journal of Physical Chemistry B* **2007**, 111, 1007.

[21] A. Shukla, P. Degen, H. Rehage, *Journal of the American Chemical Society* **2007**, 129, 8056.

[22] I. Fleming, D. H. Williams, Spectroscopic Methods in Organic Chemistry, McGraw-Hill, **1966**.

[23] S. Mirji, *Surface and Interface Analysis: An International Journal devoted to the development and application of techniques for the analysis of surfaces, interfaces and thin films* **2006**, 38, 158.

[24] G. Steiner, H. Möller, O. Savchuk, D. Ferse, H. Adler, R. Salzer, *Journal of Molecular Structure* **2001**, 563, 273.

[25] Y. Guan, L. Zhang, D. Wang, J. L. West, S. Fu, *Materials & Design* **2018**, 147, 28.

[26] a) X. Zhu, Y. Liu, Z. Li, W. Wang, *Scientific reports* **2018**, 8, 4015; b) S. S. Lee, B. Kim, S. K. Kim, J. C. Won, Y. H. Kim, S. H. Kim, *Advanced Materials* **2015**, 27, 627.

[27] a) R. Kulčar, M. K. Gunde, M. Friškovec, *Dyes and Pigments* **2010**, 86, 271; b) K. Fujita, K. Senga, U.S. Patent, US6494950B1, **2002**.

[28] R. Kulčar, M. Klanjšeg Gunde, N. Knešaurek, *Acta graphica: znanstveni časopis za tiskarstvo i grafičke komunikacije* **2012**, 23, 25.

[29] Report, Micromeritics Instrument Corporation, AZoM Materials, **2018**, https://www.azom.com/article.aspx?ArticleID=16800.

[30] J. van Wijk, T. Heunis, E. Harmzen, L. M. Dicks, J. Meuldijk, B. Klumperman, *Chemical Communications* **2014**, 50, 15427.

[31] a) R. Dufour, M. Harnois, Y. Coffinier, V. Thomy, R. Boukherroub, V. Senez, *Langmuir* **2010**, 26, 17242; b) Q. Liang, S. A. Hsie, C. P. Wong, *ChemPhysChem* **2012**, 13, 3700.

[32] G. R. Gossweiler, G. B. Hewage, G. Soriano, Q. Wang, G. W. Welshofer, X. Zhao, S. L. Craig, *ACS Macro Letters* **2014**, 3, 216.

Chapter 4. A Nontoxic Dual Thermochromic and Halochromic Sensor

4.1 Chapter Perspective

In **Chapter 2**, we developed a new class of non-toxic binary thermochromic materials. We found that a change in pH (*i.e.* the addition of acid or base), can also change the colour of these material, known as halochromism. Taking advantage of this characteristic, we will investigate a dual sensor with thermochromic and halochromic properties in this chapter. Specifically, sulfonephthalein-fatty acid thermochromic particles will be incorporated into a gas-permeable polymer matrix to form a nontoxic sensor that shows obvious thermochromism and halochromism. The thermochromic behaviour of the obtained sensor will be checked over heating and cooling cycles. The halochromic behaviour of this sensor will be investigated in ammonia or bio-amine vapour. The potential of this sensor to be used as a time-temperature indicator (TTI) based on its thermochromic behaviour will be further studied.

This chapter is an article to be submitted to *ACS Sensors*

4.2 Introduction

As outlined in Chapter 1, Traditional food packaging affords many benefits to suppliers, retailers and consumers during the transportation, storage and prior to the end use of food products. Currently, the food packaging industry is facing new challenges, such as counterfeited food products, wider food distribution leading to longer transport times and the consumers' requirement to monitor food quality and safety.[1] These challenges have led to the emergence of intelligent food packaging concepts. Intelligent food packaging, which provides information about the food or the inner environment surrounding the food, are based on different techniques including thermochromic labels, radio-frequency identification (RFID) devices[2, 3], quick response (QR) codes or two-dimensional (2D) barcodes[4], gas sensors[5, 6], freshness sensors[7-9], time-temperature indicators (TTIs)[10] and holograms[11]. Unexpected food deterioration occurs during inappropriate shipping or storage temperatures. Different from freshness or gas sensors or digital techniques of RFID and QR codes, thermochromic labels and TTIs attached to packages show food quality to consumers by directly focusing on the thermal history of food products.[10, 12-14]

As the most commonly used intelligent indicators, TTIs provide a simple and visual response towards an accumulative result of time and temperature.[15] The function of TTIs can be based on different mechanisms, such as through the redox reaction,[16] polymerization,[17] chemical diffusion,[18] enzymatic reaction[19] and surface plasmon resonance.[20] Given the importance of toxicity when used in food products, not every TTI can be applied to intelligent food packaging. For instance depending on exposure levels, anthraquinones used in redox reaction based TTIs are harmful to human cells,[10] silver nanoparticles in TTIs could damage organisms by generating reactive oxygen species in mitochondria,[21] and diacetylene compounds in polymerization based TTIs are toxic to human fibroblasts.[10] TTIs have also been prepared with irreversible thermochromic materials, however, none of them is nontoxic.[22-24]

Thermochromic products have been applied to nail polishes, hair dyes and textiles. However, the potential toxicity of thermochromic materials is the main problem inhibiting their application to food packaging. Leuco dye systems, the most widely used thermochromic system, are only applied to food packages using glass, metal or thick plastic substrate to avoid direct food contact.[25] This approach whether valid or perceived is driven by the fear of consumer concerns about toxic chemicals, and reluctance of the industries to test these markets. Other reports about thermochromic materials, such as liquid crystals,[26, 27] nanoparticles,[28] polydiacetylene derivatives[29] and photonic crystals,[30] have rarely mentioned toxicity studies. The limited nontoxic examples involve a polylactide sheet mixed with anthocyanidin dyes, fatty acids and dodecyl gallate, but shows reversible thermochromism.[31, 32]

In **Chapter 2**, we discussed a series of nontoxic sulfonephthalein-solvent binary systems that show clear and reversible colour change upon melting and freezing.[33] In **Chapter 3**, these materials were incorporated into stable microcapsules which were shown to be fully reversibly thermochromic. This system was shown to have potential applications in temperature indicators for food products to indicate the food was at the correct temperature for transportation, storage and consumption, *e.g.* ice cream, fish or meat. In this chapter, we will discuss the use of this same binary system in a format that will allow for irreversible thermochromism as well as be more susceptible to chemical changes from the surrounding environment. This type of sensor would have very

different applications such as thermal sensors on soft packages or TTIs as well as a spoilage indicator. It was envisaged that if this binary system was dispersed evenly throughout a polymeric film, it would potentially migrate more homogeneously upon each heating and cooling cycle, as well as gradually change colour due to exposure to gas released from the food during gradual spoilage. In this area, spoilage sensors based on lactic acid, carbon dioxide, ethanol, biogenic amines or volatile nitrogen compounds generated from food have been used to monitor the shelf life of food products.[34] Biogenic amines have been reported to be important indicative gases given off by perishable meat or fish products.[35, 36] Sulfonephthaleins have been used in these sensors due to their halochromic nature.[37-40] Chlorophenol red (CPR), one of sulfonephthaleins, is nontoxic and has been used in freshness sensors.[33, 41-43] It has also been reported that one of the components of the binary system reported in Chapter 2, dodecanoic acid (DA) is nontoxic.[44, 45]

In this chapter we aimed to prepare a nontoxic dual sensor that shows irreversible colour change both towards temperature and bio-amines, by incorporating the binary system detailed in Chapter 2, into a gas permeable matrix. Due to its transparency, flexibility, biocompatibility and nontoxicity, polydimethylsiloxane (PDMS) and its derivatives have been used as matrix materials for biological, microfluidic and electric sensors.[46-50] Importantly, dense PDMS film has moderate permeability to ammonia gas[51] and as such has been chosen as the film component. Here, CPR-DA binary thermochromic system will be dispersed as particles into crosslinked non-toxic PDMS films. The colour change performance of the obtained film towards temperature and base will be investigated. The potential of this film as a TTI will also be presented.

4.3 Results and discussion

4.3.1 Film formation

Either commercial liquid (methacryloxypropyl)methylsiloxane-dimethylsiloxane copolymer resin (methacrylate-PDMS, RMS-083, Gelest) or vinylmethylsiloxane-dimethylsiloxane copolymer resin (vinyl-PDMS, VDT-5035, Gelest) were mixed with the (CPR-DA) particles and cast onto polyethylene terephthalate (PET) plastic film before being crosslinked by UV light (Figure 4.1). The obtained films were classified as F_1 to F_6 according to different PDMS material and dispersed particle size (Table 4.1).

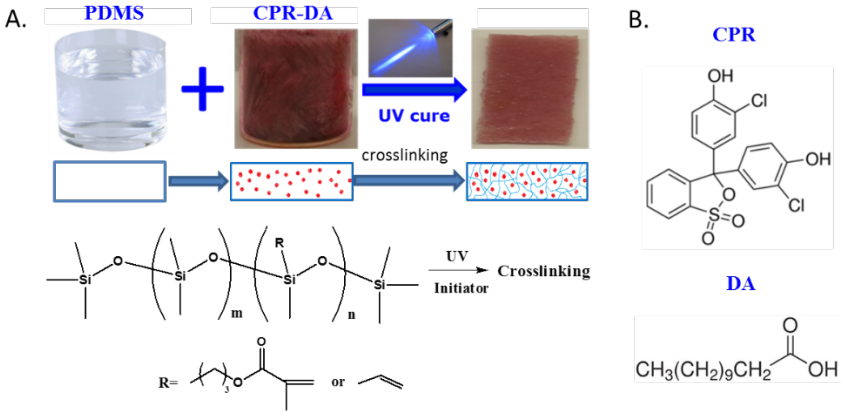

Figure 4.1 A) Preparation scheme of the hybrid film with PDMS as the polymeric medium and dispersed chlorophenol red-dodecanoic acid (CPR-DA) binary system as the functional particles. B) The molecular structures of CPR and DA.

Table 4.1

The polymeric materials and CPR-DA particles with different sizes used in the film samples.

Sample	Polymeric material	Particle size
F_1	vinyl-PDMS	<90 µm
F_2	vinyl-PDMS	90-425 µm
F_3	vinyl-PDMS	>425 µm
F_4	methacrylate-PDMS	<90 µm
F_5	methacrylate-PDMS	90-425 µm
F_6	methacrylate-PDMS	>425 µm

The photographic images of the CPR-DA binary system alone and subsequent film samples (F_1-F_6) are shown in Figure 4.2. As the size of the distributed particles increases, the uniformity of the obtained film deteriorated. The melting points (T_m) and freezing points (T_f) of the CPR-DA binary system and the obtained film samples, measured by differential scanning calorimeter (DSC) at heating cycles of 1 °C/min are listed in Table 4.2. The T_m of the CPR-DA binary system was 43.77 ± 0.33 °C, while its T_f was 41.75 ± 0.01 °C. The T_m or T_f values of film samples (F_1-F_6) are slightly lower than those of CPR-DA binary system. This phenomenon is attributed to the size-dependent melting point depression of small particles due to their surface-to-volume ratios being larger than in bulk materials as discussed in **Chapter 3**.

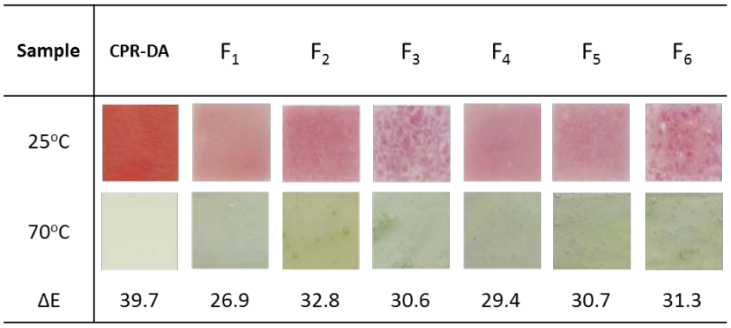

Figure 4.2 Photographic images CPR-DA binary system and film samples (F_1 to F_6) at 25 °C and 70 °C. ΔE values indicate the colour difference of samples between 25 °C and 70 °C.

Table 4.2

The melting points (T_m) and freezing points (T_f) of CPR-DA binary system and film samples.

Sample	CPR-DA	F_1	F_2	F_3	F_4	F_5	F_6
T_m (°C)	43.77 ±0.03	42.31 ±0.05	42.18 ±0.02	42.16 ±0.04	42.53 ±0.02	42.74 ±0.03	42.10 ±0.04
T_f (°C)	41.75 ±0.01	39.5 ±0.30	40.35 ±0.09	40.18 ±0.26	40.82 ±0.05	40.27 ±0.08	40.54 ±0.20

4.3.2 Irreversible thermochromic sensor

All film samples (F_1-F_6) showed a pink colour at 25 °C where the CPR-DA particles were solid (Figure 4.2). The pink colour as shown in **Chapter 2**, is due to the pi-pi stacking of CPR in the solid CPR-DA binary system. Upon heating to 70 °C, all samples changed colour to pale yellow, as the binary system melted within the matrix (Figure 4.2). The corresponding UV-Vis absorption spectra of these samples at 25 °C and 70 °C are shown in Figure 4.3.

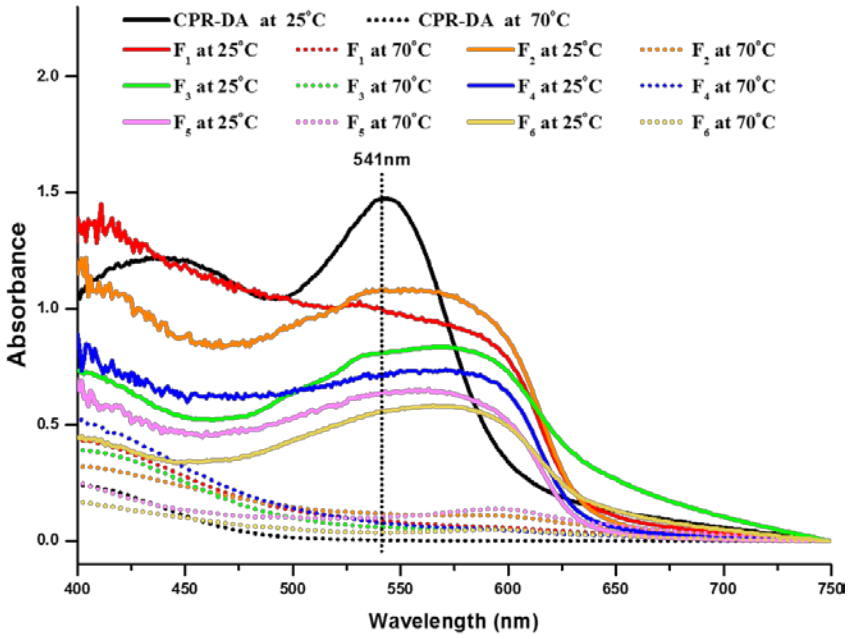

Figure 4.3 UV-Vis absorption spectra of CPR-DA binary system and film samples at 25 °C and 70 °C.

Similar to the disappearance of the absorption peak at 541 nm shown for the CPR-DA binary system, the broad absorption peaks between 500 nm and 650 nm of all film samples (F_1-F_6) also reduced during heating. The pale-yellow colour of all film samples (F_1-F_6) is caused by a disruption of the π-π stacking of CPR and full homogenous solvation of CPR in DA as described in **Chapter 2**.

The obvious colour change was quantified by ΔE values to indicate the colour difference at two temperatures according to CIE 2000.[52] The ΔE value of the pure CPR-DA binary system was determined to be 39.7, which is higher than the ΔE values of all the film samples (F_1-F_6) ranging from 26.9 to 32.8. The reduced colour contrast of the films is attributed to the added weight fraction of non-thermochromic PDMS materials. However, the colour change of all of the film samples (F_1-F_6) is significantly high enough to be perceptible to the naked eye (Figure 4.2).

Based on the highest colour contrast in thermochromism and the uniformity of the sample, F_2 was chosen for subsequent investigations. Different applications require thermochromic materials to have different response times varying from seconds to days.[29, 32, 53] Here, the response time for thermochromism was defined as the duration time for the sample to fully change in colour. Since the absorption peak at 541nm firmly relates to the red colour of CPR-DA binary system, it is easy to examine the thermochromic response time by measuring the absorbance change at 541nm as temperature changes. The absorbance (at 541nm) vs. time correlation curves of CPR-DA binary system show a steep increase in absorbance during cooling and decrease in absorbance during heating to constant values (Figure 4.4).

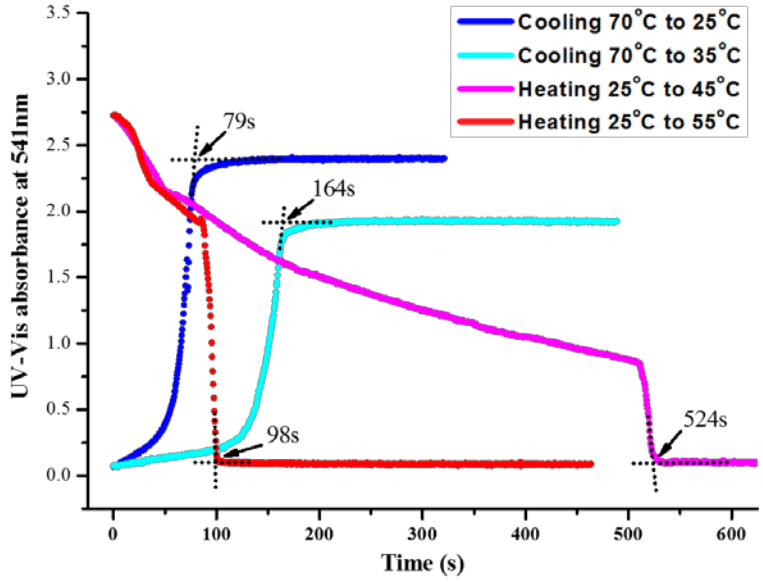

Figure 4.4 The UV-Vis absorbance change at 541nm of CPR-DA binary system (thickness of 10 mm) as a function of time when binary system cools down (from 70 ºC to 25 ºC or from 70 ºC to 35 ºC) or heats up (from 25 ºC to 45 ºC or from 25ºC to 55 ºC).

The response time is taken as the intersection of the extrapolated baseline and the tangent to the plot at the inflection point. Therefore, the thermochromic response time of the pure CPR-DA binary system from 70 ºC to 25 ºC or from 70 ºC to 35 ºC is approximately 79 seconds and 164 seconds, respectively. The thermochromic response time from 25 ºC to 45 ºC or from 25 ºC to 55 ºC is about 524 seconds and 98 seconds, respectively

(Figure 4.4). The thermochromic response time of F_2 was determined in the same manner and compared to the CPR-DA binary system in Figure 4.5.

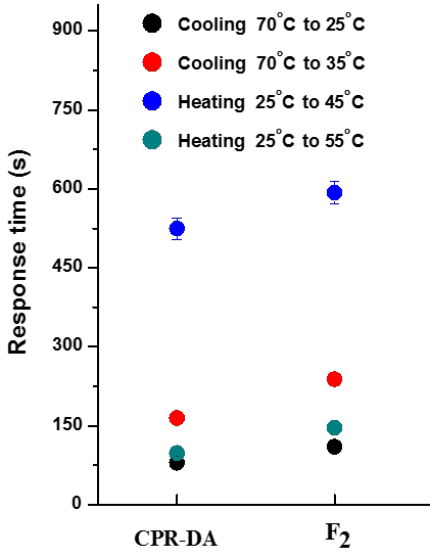

Figure 4.5 Thermochromic response time of CPR-DA binary system and film F_2 in cooling (70 ºC to 25 ºC or 70 ºC to 35 ºC) and heating (25 ºC to 45 ºC or 25 ºC to 55 ºC) process.

The thermochromic behaviour of CPR-DA binary system is firmly related to phase change as described in **Chapter 2**. Therefore, larger temperature difference will lead to shorter thermochromic response time both in heating and cooling process due to faster phase transition. On the other hand, the colour change of F_2 lags behind the CPR-DA binary system under the same conditions due to the fact that the heat has to conduct through the film matrix.

The photographic images of F_2 are compared to the CPR-DA binary system during the first cycle of heating and cooling (from 25 ºC to 70 ºC, then 25 ºC, held for 30 minutes at each temperature) (Figure 4.6A).

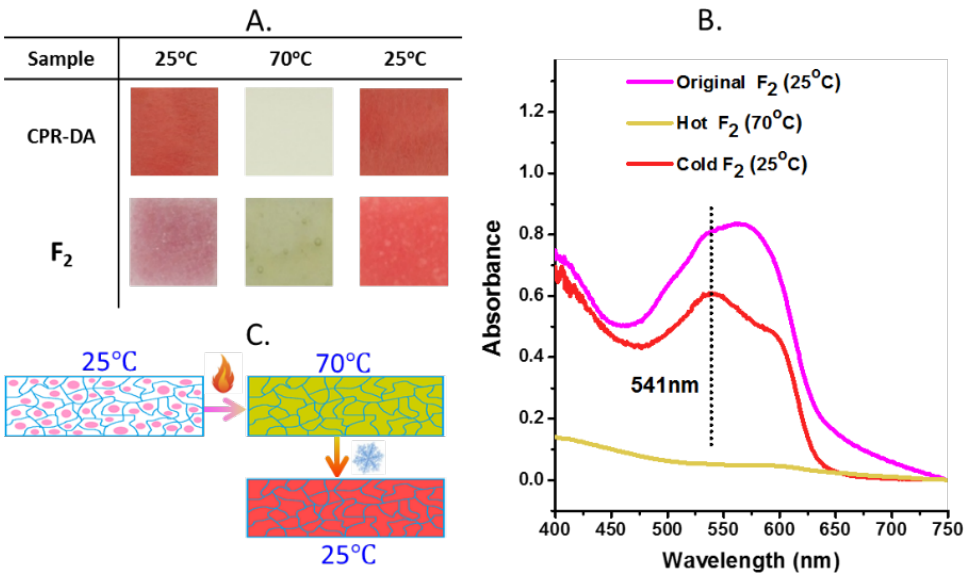

Figure 4.6 A) Photographic images of CPR-DA binary system and F_2 during the first cycle of heating and cooling (25 ºC-70 ºC-25 ºC, 30 minutes at each temperature). B) Corresponding UV-Vis absorption spectra of F_2 during the first cycle of heating and cooling. C) The schematic diagram of F_2 during the first cycle of heating and cooling.

In was shown that the binary system CPR-DA in **Chapter 2**, demonstrated full reversible thermochromism during heating and cooling transitioning between a pale yellow and red colour. However, once combined into a film the system behaves very differently. The pink F_2 changes colour into pale yellow at 70 ^oC with the corresponding absorption peak in UV range (< 400 nm), then changes colour into a red after cooling back to 25 ^oC, with the dominant absorption peak at 541 nm. This is different from the original broad absorption peak between 500 nm and 650 nm (Figure 4.6A&B).

This phenomenon is caused by the difference in the distribution of the CPR-DA particles in the film (Figure 4.6C). In the film formation, the crosslinked PDMS matrix surrounds the CPR-DA particles, with pores void of CPR-DA. The melted CPR-DA binary system flows into the voids at 70 ^oC and solidifies once the temperature returns to 25 ^oC, making the film more homogenous and show red colour similar to the pure CPR-DA binary system with an absorption peak at 541nm.

This irreversible thermochromic behaviour makes this film system amenable to one-off thermochromic sensors, which would indicate the product has been exposed above a certain threshold temperature. The threshold temperature of this sensor could be tuned by adjusting the melting point of long-chain fatty acid/ester/alcohol in the binary system.

As shown in Figure 4.7A, as the cycle of heating and cooling (25 ^oC-70 ^oC-25 ^oC, 30 minutes at each temperature) is repeated, the cooled F_2 gradually transitions to a yellow/orange colour. So that after 50 cycles of heating and cooling, the sample at room temperature no longer appears red (Figure 4.7A). Optical microscopic images of the original F_2 sample and after 10 and 50 cycles of heating and cooling (25 ^oC-70 ^oC-25 ^oC, 30 minutes at each temperature) are shown in Figure 4.7B. The presence of pink particles can clearly be seen in the original F_2 sample, with the particles gradually disappearing and dissolving in the polymer matrix as the heating and cooling cycle proceed (Figure 4.7B).

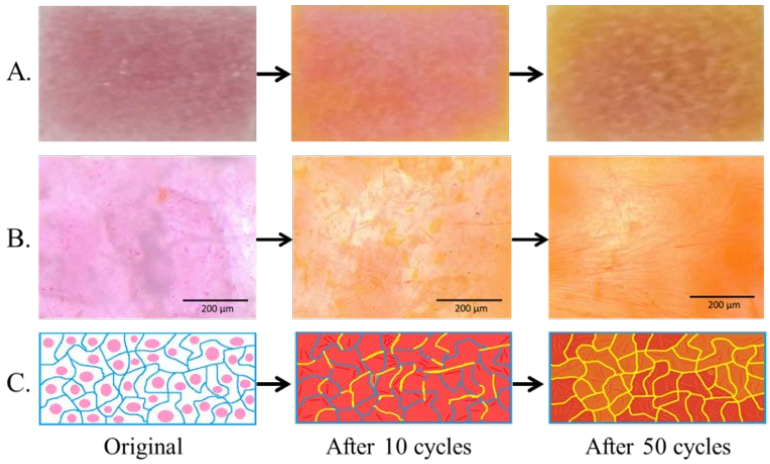

Figure 4.7 A) The photographic image of F_2 (25 ^oC) in original state, after 10 cycles of heating (70 ^oC, 30 mins) and cooling (25 ^oC, 30 mins) and after 50 cycles of heating (70 ^oC, 30 mins) and cooling (25 ^oC, 30 mins). B) The corresponding optical microscopic images of cold F_2 (25 ^oC). C) The schematic diagram of migration of binary system in F_2.

The schematic diagram in Figure 4.7C illustrates the proposed mechanism of yellow colour formation in the film: (1) After the first round of heating and cooling cycle, a portion of the CPR-DA binary system fills the pores within the film; (2) The melted binary system gradually dissolves and diffuses into the crosslinked PDMS, making the

CPR appear yellow colour of the pure dye; (3) Due to the different diffusion rates of CPR and DA in PDMS, the separation of these two components leads to the inability of CPR to form pi-pi stacking; (4) As the heating and cooling cycle continues, more CPR-DA binary system dissolve and diffuse into the PDMS, resulting in a larger area of yellow accumulation and irreversible thermochromism.

4.3.3 Potential as a TTI

To test the potential of this thermochromic film sample as a time-temperature indicator (TTI), the effect of temperature and time was investigated. The sample F_2 was treated in two ways: i) continuous heating at 45 °C for a certain duration before cooling to 25 °C; or ii) intermittent cycles of heating at 45 °C for 30 minutes and cooling at 25 °C for 30 minutes. The ΔE values of each sample F_2 at 25 °C after being continuously heated (**CH**) and intermittently heated (**IH**) are shown in solid red circles and hollow red circles respectively in Figure 4.8A, where ΔE is determined from the original colour of sample F_2 at 25 °C.

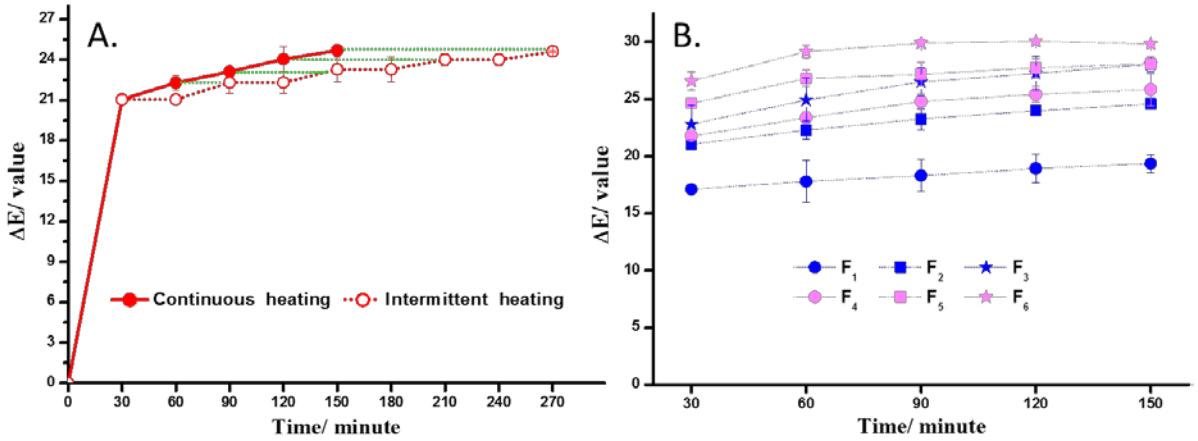

Figure 4.8 A) The ΔE value of cold F_2 (25 °C) after being treated in two different ways: i) continuous heating at 45 °C; ii) intermittent cycles of heating at 45 °C for 30 minutes and cooling at 25 °C for 30 minutes. B) The ΔE values of cold F_1-F_6 (25 °C) after continuous heating at 45 °C.

Due to the diffusion of the CPR-DA system within the polymer matrix the ΔE value of F_2 increases with extended heating time. Importantly, the ΔE values of **IH** samples remained constant during the cooling process, suggesting the dissolution and diffusion of binary system in PDMS at 25 °C is minimal. Furthermore, the ΔE values of **CH** samples are equal to the values of **IH** samples when the cumulative heating durations are the same. Therefore, the ΔE value of F_2 at 25 °C is a result of cumulative dissolution and diffusion of CPR-DA in crosslinked PDMS during heating periods at 45 °C. There are three prerequisites for a label to be used as a TTI: (1) it is temperature sensitive; (2) its colour change is irreversible and is not influenced by the cooling process; (3) its colour change due to multiple exposures above the threshold temperature should be additive.[22] Here it has been shown that this system has the potential as a TTI based on these evaluation criteria.

The effect of polymer matrix on the thermochromism of the samples was also investigated. Two series of samples using either vinyl-PDMS (samples F_1-F_3) or methacrylate-PDMS (samples F_4-F_6) were prepared. The ΔE values of each film were determined after continuous heating cycles at 45 °C with varying heating time (Figure 4.8B). The ΔE values of films using methacrylate-PDMS as the polymeric material (F_4-F_6) were higher than that of films containing particles with same size but using vinyl-PDMS as the polymeric material (F_1-F_3) after being heated for

the same duration. This phenomenon is likely due to the fact that methacrylate-PDMS is less hydrophobic than vinyl-PDMS so that hydrophilic CPR dissolves and diffuses more easily in crosslinked methacrylate-PDMS. Therefore, the colour change sensitivity of this TTI can be adjusted by varying the hydrophobicity of the polymer matrix material.

Although all the ingredients used in the film preparation are relatively nontoxic, leaching studies of the components were determined. CPR is very hydrophilic and easily dissolves in water, therefore a leaching experiment was conducted via stirring sample in water (pH=3) and determining the concentration of dye in the aqueous solution using UV-Vis spectroscopy (calculated upon a standard curve of absorbance *vs.* CPR concentration as shown in Figure 4.9A). The *wt.*% of CPR leached from the sample is presented in Figure 4.9B. According to the data, lamination effectively prevented the migration of CPR from the samples with 3 *wt.*% of CPR leaching from the polymer matrix alone, over 5 days. Lamination of the film for an application as a TTI is therefore required.

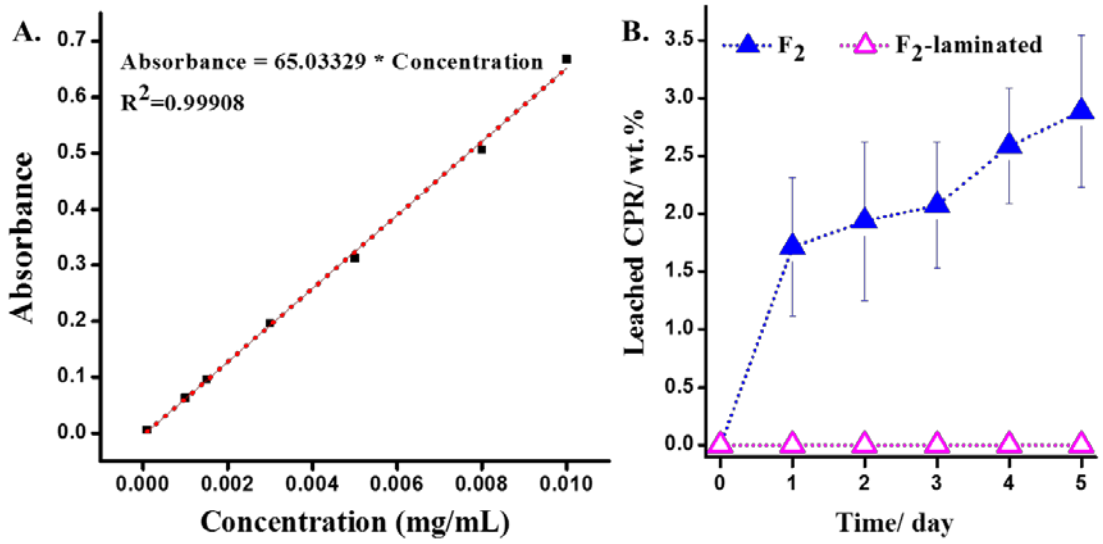

Figure 4.9 A) The standard curve and equation of absorbance at 435nm vs. CPR concentration in aqueous solution (pH=3, light pathway length=10 mm). B) The weight percentage of leached CPR from F_2 and laminated F_2 to water (pH=3) as a function of time.

4.3.4 Irreversible halochromic sensor

It has been previously reported that certain food products such as fish and beef, release basic amines and gases upon degradation.[54, 55] CPR is well known as a pH indicator component, and this halochromic nature is based on the sulfoxide ring opening or closing as a result of an interaction with OH^- or H^+ respectively.[56] To investigate this property further, sample F_2 was treated by ammonia vapor for one minute at 25 ^oC in a sealed vial by the addition of a number of drops of saturated NH_4OH solution. The colour change and corresponding UV-Vis absorption spectra of F_2 before and after being exposed to ammonia vapor are shown in Figure 4.10.

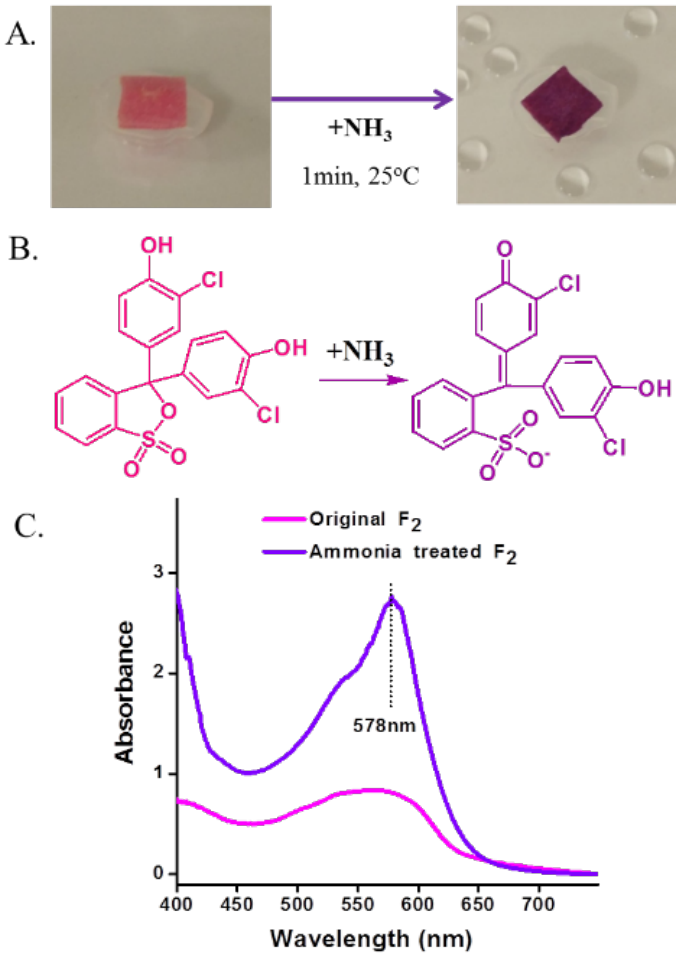

Figure 4.10 A) The photographic images of F_2 before and after being exposed in ammonia vapor (aq. NH_4OH) for one minute at 25 °C. B) Molecular structure change of CPR in the reaction with ammonia. C) Corresponding UV-Vis absorption spectra of F_2 at 25 °C.

The original F_2 sample directly changed colour from pink to dark purple with absorption peak at 578 nm due to the sulfoxide ring opening of CPR. This experiment clearly confirms the ability of sample F_2 to undergo halochromism under basic conditions.

To further investigate the halochromic performance of this film towards bio-amines, samples of F_2 were placed with fresh fish or beef in sealed Petri dishes at 25 °C (Figure 4.11a&a') and -18 °C as a baseline to replicate recommended storage conditions. It can be seen that sample F_2 exposed to fish and beef, which began as a pink indicator, changed over the 4-day period at 25 °C to a dark purple colour (Figure 4.11b&b'). Whereas the indicator samples that were stored at -18 °C for 4 days, remained pink in colour (Figure 4.11c&c').

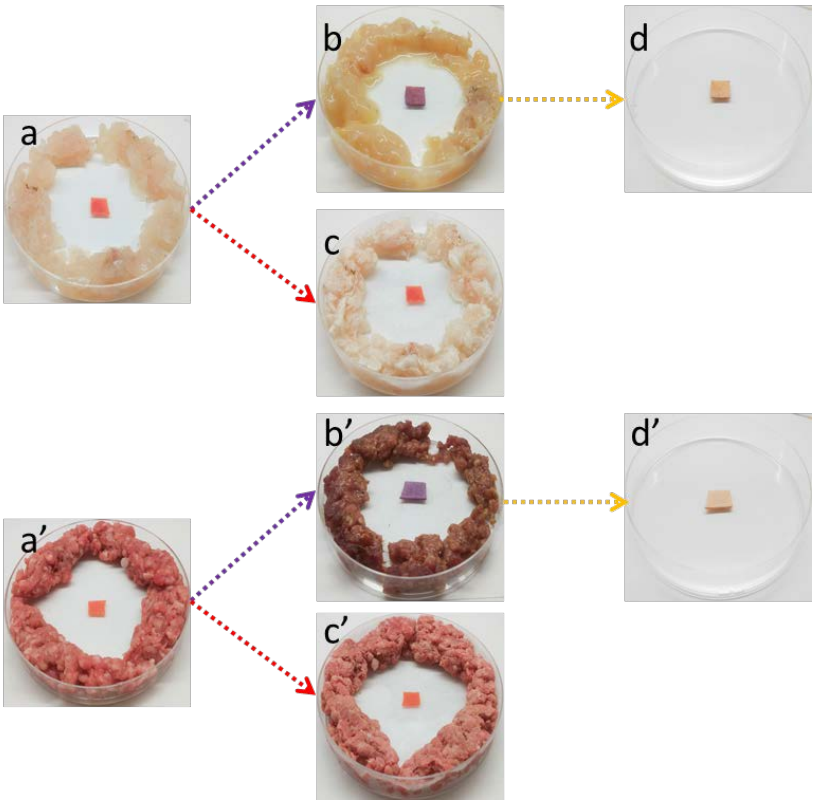

Figure 4.11 Photographic images of F_2 placed with a&a') fresh fish or beef, b&b') fish or beef at 25 °C for 4 days, c&c') fish or beef at -18 °C for 4 days and d&d') sample F_2 after removal of fish or beef then left for 24 hours at 25 °C.

The purple colour which results from the ring-opened CPR is triggered by the bio-amines released as the fish or beef degrades. After removal of the fish or meat, the sample was stored for a further 24 hours at 25 °C. The indicator F_2 was shown change to an orange-yellow rather than original pink colour (Figure 4.11d&d'). This yellow-orange colour that was seen earlier in this chapter, is related to the dissociation of the hydrophilic ring-opened CPR from the hydrophobic DA, leading to a loss of the π-π stacking responsible for the pink colour in the original sample F_2. The control samples kept at -18 °C showed no change in colour after 4 days at the correct storage temperature. Therefore, this film has been demonstrated as a halochromic sensor towards practical bio-amines generated from fish or meat products with an obvious colour change visible to the naked eye (ΔE=21.6 in fish testing while ΔE=29.7 in beef testing). Importantly, the irreversible halochromic nature of this indicator, makes it clear that food degradation or improper storage has occurred, even after separation of the indicator from the food.

4.4 Chapter summary

In conclusion, this chapter has described the first nontoxic food sensor showing both irreversible thermochromism and halochromism. This sensor with PDMS as polymeric matrix and dispersed CPR-DA binary systems as functional particles shows clear and irreversible colour change towards temperature and a basic environment. The irreversible halochromic behaviour of this sensor is ascribed to initial pi-pi stacked structure and the halochromic nature of CPR. The irreversible thermochromic performance of this sensor is attributed to the diffusion of melted particles in film matrix. Therefore, its sensitivity to thermochromism can be adjusted via choosing polymeric film materials of differing hydrophobicity. The colour of cold sensor is related to the duration of time it is exposed above the melting point of the incorporated particles. Therefore, this material can potentially be used as a TTI. The combination of dual functions of thermochromism and halochromism, coupled with the non-toxic nature of the components as well as its ease of preparation, makes this sensor show great potential as a food quality indicator on intelligent packaging.

4.5 Experimental

4.5.1 Chemicals and Materials

Chlorophenol red (CPR), dodecanoic acid (DA) and 1-hydroxycyclohexyl-1-phenyl methanone (Irgacure 184) were purchased from Sigma-Aldrich. Vinylmethylsiloxane-dimethylsiloxane copolymer (vinyl-PDMS, VDT-5035) and (methacryloxypropyl)methylsiloxane-dimethylsiloxane copolymers (methacrylate-PDMS, RMS-083) were purchased from Gelest. All the reagents were used as received with no further purification. Polyethylene terephthalate (PET) packaging film was purchased from Polyplex. Laminating pouches were purchased from GBC.

4.5.2 Preparation of samples

CPR was dissolved into DA with molar ratio of 1:1000 by sonication. The obtained yellow solution was placed into freezer (-18 ℃) to form dark red crystallized solid. Finally, the crystallized solid was grinded into particles, which was then separated by sieving with 90 μm and 425 μm sieves.

Irgacure 184 photoinitiator (0.02 g, 1.3 wt.% of film sample) was dissolved into PDMS (1.0 g, 65.8 wt.% of film sample, vinyl-PDMS or methacrylate-PDMS) liquid by sonication. The clear PDMS solution was preserved in a freezer (-18 ℃) for further usage. CPR-DA particles (0.5g, 32.9 wt.% of film) at three size scales were mixed into cold clear PDMS solution to form homogeneous suspensions by mechanical stirring. These liquid suspensions were casted between two PET films for UV-curing (MODEL UVGL-58 MINERALIGHT® lamp, 366 nm) for 1 hour. After PET films being peeled off, the samples were obtained. The obtained samples could be further laminated on the edge by ACCO Rexel Model LP35HS laminator. The matrix components and the size of particles used in each sample were listed in Table 4.1.

4.5.3 Instrumentation and measurements

Optical microscope images were obtained by using an Olympus CKX41 microscope with AnalySIS getIT software.

Perkin Elmer Differential Scanning Calorimeter 8500 was used to examine the melting points and freezing points of samples under a nitrogen flowing at a rate of 20 ml/min with a heating and cooling rate of 1 ℃/min.

UV-Vis absorbance spectra were measured on a Shimadzu UV-Mini 1240 spectrophotometer with thermostat. The absorbance at single wavelength was measured on a Pharmacia LKB•Novaspec II spectrophotometer with thermostatic water bath. Reflection spectra were measured on a Flame Miniature spectrometer with Ocean Optics DH-2000 UV-VIS-NIR light source.

All digital photographs were white balanced by Photoshop CS6 in Camera Raw file formats.[57] Then colorimetric representations were collected by the same software from the samples in photographs. Colour difference (ΔE CIE 2000) was calculated from the colorimetric representations.[52]

Response time of colour change: Thermochromic particles and films were placed into quartz cuvette in the chamber of Pharmacia LKB•NovaspecII spectrophotometer with a thermostatic water bath. The water bath was

set to 45 ºC or 55 ºC during the heating process of cold samples (T_0 = 25 ºC). Otherwise, the water bath was set to 25 ºC or 35 ºC during the cooling process of hot samples (T_0 = 70 ºC); Absorbance change at single wavelength (541 nm) was computer recorded every 0.5s.

Dye leaching experiment: Standard plot of absorbance vs. concentration of CPR aqueous solution was linear fitted by measuring the absorbance (light pathway length=10 mm) of CPR aqueous solution (pH=3) at 435 nm with concentrations of 0.001 mg/ml, 0.005 mg/ml, 0.010 mg/ml and 0.020 mg/ml respectively. The samples were stirred with water (pH=3) at 100 rpm in a sealed container. The concentration of CPR in water was determined by calculation based on standard plot using absorbance of water at 435nm every 24 hours. The leaking ratio of CPR was calculated according to following equation:

$$L=\frac{C_i \times V_0}{W_0 \times \frac{0.5}{1.52} \times 0.21\%} \times 100\%$$

where C_i means the concentration of CPR in water, V_0 means the volume of water and W_0 means the weight of original sample without any lamination.

4.6 Reference

1. Dainelli, D.; Gontard, N.; Spyropoulos, D.; Zondervan-van den Beuken, E.; Tobback, P., Active and intelligent food packaging: legal aspects and safety concerns. *Trends in Food Science & Technology* **2008,** 19, S103-S112.
2. Trebar, M.; Lotrič, M.; Fonda, I., Use of RFID temperature monitoring to test and improve fish packing methods in styrofoam boxes. *Journal of Food Engineering* **2015,** 159, 66-75.
3. Kumar, P.; Reinitz, H.; Simunovic, J.; Sandeep, K.; Franzon, P., Overview of RFID technology and its applications in the food industry. *Journal of Food Science* **2009,** 74 (8), R101-R106.
4. Ziegler, A., Stand alone product, promotional product sample, container, or packaging comprised of interactive quick response (QR code, MS tag) or other scan-able interactive code linked to one or more internet uniform resource locators (URLs) for instantly delivering wide band digital content, promotions and infotainment brand engagement features between consumers and marketers. U.S. Patent US8261972B2, **2012**.
5. Vu, C. H. T.; Won, K., Novel water-resistant UV-activated oxygen indicator for intelligent food packaging. *Food Chemistry* **2013,** 140 (1), 52-56.
6. Puligundla, P.; Jung, J.; Ko, S., Carbon dioxide sensors for intelligent food packaging applications. *Food Control* **2012,** 25 (1), 328-333.
7. Nopwinyuwong, A.; Trevanich, S.; Suppakul, P., Development of a novel colorimetric indicator label for monitoring freshness of intermediate-moisture dessert spoilage. *Talanta* **2010,** 81 (3), 1126-1132.
8. De Jong, A.; Boumans, H.; Slaghek, T.; Van Veen, J.; Rijk, R.; Van Zandvoort, M., Active and intelligent packaging for food: Is it the future? *Food Additives and Contaminants* **2005,** 22 (10), 975-979.
9. Brockgreitens, J.; Abbas, A., Responsive Food Packaging: Recent Progress and Technological Prospects. *Comprehensive Reviews in Food Science and Food Safety* **2016,** 15 (1), 3-15.
10. Wang, S.; Liu, X.; Yang, M.; Zhang, Y.; Xiang, K.; Tang, R., Review of time temperature indicators as quality monitors in food packaging. *Packaging Technology and Science* **2015,** 28 (10), 839-867.
11. Naydenova, I.; Jallapuram, R.; Toal, V.; Martin, S., In Hologram-based humidity indicator for domestic and packaging applications, Proc. SPIE 6528, Nanosensors, Microsensors, and Biosensors and Systems, **2007**, 652811 (11 April 2007).
12. Torrico, D. D.; Fuentes, S.; Viejo, C. G.; Ashman, H.; Gurr, P. A.; Dunshea, F. R., Analysis of thermochromic label elements and colour transitions using sensory acceptability and eye tracking techniques. *LWT* **2018,** 89, 475-481.
13. Yam, K. L.; Takhistov, P. T.; Miltz, J., Intelligent packaging: concepts and applications. *Journal of food science* **2005,** 70 (1), R1-R10.
14. Siró, I., Active and intelligent packaging of food. *Progress in food preservation* **2011**, 23-48.
15. Poyatos-Racionero, E.; Ros-Lis, J. V.; Vivancos, J.-L.; Martinez-Manez, R., Recent advances on intelligent packaging as tools to reduce food waste. *Journal of Cleaner Production* **2018,** 172, 3398-3409.
16. Galagan, Y.; Su, W.-F., Fadable ink for time–temperature control of food freshness: Novel new time–temperature indicator. *Food research international* **2008,** 41 (6), 653-657.
17. Baughman, R. H.; Hall, L. J.; Kozlov, M.; Smith, D. E.; Prusik, T., Crystallized diacetylenic indicator compounds and methods of preparing the compounds. U.S. Patent US8269042B2, **2012**.

18. Wanihsuksombat, C.; Hongtrakul, V.; Suppakul, P., Development and characterization of a prototype of a lactic acid–based time–temperature indicator for monitoring food product quality. *Journal of Food Engineering* **2010,** 100 (3), 427-434.
19. Meng, J.; Qian, J.; Tang, Y., A solid-state time-temperature indicator used in chilled fresh pork monitoring. *Packaging Technology and Science* **2018,** 31 (5), 353-360.
20. Wang, Y.-C.; Mohan, C.; Guan, J.; Ravishankar, C.; Gunasekaran, S., Chitosan and gold nanoparticles-based thermal history indicators and frozen indicators for perishable and temperature-sensitive products. *Food Control* **2018,** 85, 186-193.
21. Oberdörster, G.; Oberdörster, E.; Oberdörster, J., Nanotoxicology: an emerging discipline evolving from studies of ultrafine particles. Environ Health Perspect **2005**, 113, 823–839.
22. Galliani, D.; Mascheroni, L.; Sassi, M.; Turrisi, R.; Lorenzi, R.; Scaccabarozzi, A.; Stingelin, N.; Beverina, L., Thermochromic Latent-Pigment-Based Time–Temperature Indicators for Perishable Goods. *Advanced Optical Materials* **2015,** 3 (9), 1164-1168.
23. Pucci, A.; Bizzarri, R.; Ruggeri, G., Polymer composites with smart optical properties. *Soft Matter* **2011,** 7 (8), 3689-3700.
24. Crenshaw, B. R.; Weder, C., Phase Separation of Excimer-Forming Fluorescent Dyes and Amorphous Polymers: A Versatile Mechanism for Sensor Applications. *Advanced Materials* **2005,** 17 (12), 1471-1476.
25. Report, W.R.A.P.-F. Thermochromic inks and reducing household food waste. *Waste & Resources Action Programme*: Oxon, United Kingdom, **2013**.
26. Guan, Y.; Zhang, L.; Wang, D.; West, J. L.; Fu, S., Preparation of thermochromic liquid crystal microcapsules for intelligent functional fiber. *Materials & Design* **2018,** 147, 28-34.
27. White, T. J.; McConney, M. E.; Bunning, T. J., Dynamic color in stimuli-responsive cholesteric liquid crystals. *Journal of Materials Chemistry* **2010,** 20 (44), 9832-9847.
28. Uhlenhaut, D. I.; Smith, P.; Caseri, W., Color Switching in Gold—Polysiloxane Elastomeric Nanocomposites. *Advanced Materials* **2006,** 18 (13), 1653-1656.
29. Guo, H.; Zhang, J.; Porter, D.; Peng, H.; Löwik, D. W.; Wang, Y.; Zhang, Z.; Chen, X.; Shao, Z., Ultrafast and reversible thermochromism of a conjugated polymer material based on the assembly of peptide amphiphiles. *Chemical Science* **2014,** 5 (11), 4189-4195.
30. Wang, W.; Wang, G. P.; Zhang, W.; Zhang, D., Reversible thermochromic response based on photonic crystal structure in butterfly wing. *Nanophotonics* **2018,** 7 (1), 217-227.
31. Detlef, L.; Ralf, R.; Arno, S., Thermochromic biopolymer based on natural anthocyanidin dyes. *Open Journal of Polymer Chemistry* **2013,** 3, 43-47.
32. Seeboth, A.; Lötzsch, D.; Ruhmann, R., First example of a non-toxic thermochromic polymer material–based on a novel mechanism. *Journal of Materials Chemistry C* **2013,** 1 (16), 2811-2816.
33. Liu, B.; Ranji-Burachaloo, H.; Gurr, P. A.; Goudeli, E.; Qiao, G. G., A nontoxic reversible thermochromic binary system via π–π stacking of sulfonephthaleins. *Journal of Materials Chemistry C* **2019,** 7 (30), 9335-9345.
34. Arvanitoyannis, I. S.; Stratakos, A. C., Application of modified atmosphere packaging and active/smart technologies to red meat and poultry: a review. *Food and Bioprocess Technology* **2012,** 5 (5), 1423-1446.

35. Pacquit, A.; Lau, K. T.; McLaughlin, H.; Frisby, J.; Quilty, B.; Diamond, D., Development of a volatile amine sensor for the monitoring of fish spoilage. *Talanta* **2006,** 69 (2), 515-520.
36. Kuswandi, B.; Damayanti, F.; Jayus, J.; Abdullah, A.; Heng, L. Y., Simple and low-cost on-package sticker sensor based on litmus paper for real-time monitoring of beef freshness. *Journal of Mathematical and Fundamental Sciences* **2015,** 47 (3), 236-251.
37. Rukchon, C.; Nopwinyuwong, A.; Trevanich, S.; Jinkarn, T.; Suppakul, P., Development of a food spoilage indicator for monitoring freshness of skinless chicken breast. *Talanta* **2014,** 130, 547-554.
38. Sun, W.; Li, H.; Wang, H.; Xiao, S.; Wang, J.; Feng, L., Sensitivity enhancement of pH indicator and its application in the evaluation of fish freshness. *Talanta* **2015,** 143, 127-131.
39. Zaragozá, P.; Fernández-Segovia, I.; Fuentes, A.; Vivancos, J.-L.; Ros-Lis, J. V.; Barat, J. M.; Martínez-Máñez, R., Monitorization of Atlantic salmon (Salmo salar) spoilage using an optoelectronic nose. *Sensors and Actuators B: Chemical* **2014,** 195, 478-485.
40. Huang, X.; Xin, J.; Zhao, J., A novel technique for rapid evaluation of fish freshness using colorimetric sensor array. *Journal of Food Engineering* **2011,** 105 (4), 632-637.
41. Vaikousi, H.; Biliaderis, C. G.; Koutsoumanis, K. P., Development of a microbial time/temperature indicator prototype for monitoring the microbiological quality of chilled foods. *Applied and Environmental Microbiology* **2008,** 74 (10), 3242-3250.
42. Morsy, M. K.; Zór, K.; Kostesha, N.; Alstrøm, T. S.; Heiskanen, A.; El-Tanahi, H.; Sharoba, A.; Papkovsky, D.; Larsen, J.; Khalaf, H., Development and validation of a colorimetric sensor array for fish spoilage monitoring. *Food Control* **2016,** 60, 346-352.
43. Vaikousi, H.; Biliaderis, C. G.; Koutsoumanis, K. P., Applicability of a microbial time temperature indicator (TTI) for monitoring spoilage of modified atmosphere packed minced meat. *International Journal of Food Microbiology* **2009,** 133 (3), 272-278.
44. Fitzhugh, O. G.; Schouboe, P. J.; Nelson, A. A., Oral toxicities of lauric acid and certain lauric acid derivatives. *Toxicology and Applied Pharmacology* **1960,** 2 (1), 59-67.
45. Elder, R., ed, Final report on the safety assessment of oleic acid, lauric acid, palmitic acid, myristic acid, and stearic acid. *J Am Coll Toxicol* **1987,** 6 (3), 321-401.
46. Dufour, R.; Harnois, M.; Coffinier, Y.; Thomy, V.; Boukherroub, R.; Senez, V., Engineering sticky superomniphobic surfaces on transparent and flexible PDMS substrate. *Langmuir* **2010,** 26 (22), 17242-17247.
47. Liang, Q.; Hsie, S. A.; Wong, C. P., Low-Temperature Solid-State Microwave Reduction of Graphene Oxide for Transparent Electrically Conductive Coatings on Flexible Polydimethylsiloxane (PDMS). *ChemPhysChem* **2012,** 13 (16), 3700-3706.
48. Kim, S.-J.; Lee, J. K.; Kim, J. W.; Jung, J.-W.; Seo, K.; Park, S.-B.; Roh, K.-H.; Lee, S.-R.; Hong, Y. H.; Kim, S. J., Surface modification of polydimethylsiloxane (PDMS) induced proliferation and neural-like cells differentiation of umbilical cord blood-derived mesenchymal stem cells. *Journal of Materials Science: Materials in Medicine* **2008,** 19 (8), 2953-2962.
49. Wu, Z.; Hjort, K., Surface modification of PDMS by gradient-induced migration of embedded Pluronic. *Lab on a Chip* **2009,** 9 (11), 1500-1503.

50. Zhang, Z.; Wang, J.; Tu, Q.; Nie, N.; Sha, J.; Liu, W.; Liu, R.; Zhang, Y.; Wang, J., Surface modification of PDMS by surface-initiated atom transfer radical polymerization of water-soluble dendronized PEG methacrylate. *Colloids and Surfaces B: Biointerfaces* **2011,** 88 (1), 85-92.
51. Sürmeli, R. Ö.; Bayrakdar, A.; Çalli, B., Ammonia recovery from chicken manure digestate using polydimethylsiloxane membrane contactor. *Journal of Cleaner Production* **2018,** 191, 99-104.
52. Sharma, G.; Wu, W.; Dalal, E. N., The CIEDE2000 color-difference formula: Implementation notes, supplementary test data, and mathematical observations. *Color Research & Application: Endorsed by Inter-Society Color Council, The Colour Group (Great Britain), Canadian Society for Color, Color Science Association of Japan, Dutch Society for the Study of Color, The Swedish Colour Centre Foundation, Colour Society of Australia, Centre Français de la Couleur* **2005,** 30 (1), 21-30.
53. Kunzelman, J.; Crenshaw, B. R.; Kinami, M.; Weder, C., Self-Assembly and Dispersion of Chromogenic Molecules: A Versatile and General Approach for Self-Assessing Polymers. *Macromolecular rapid communications* **2006,** 27 (23), 1981-1987.
54. Chun, H.-N.; Kim, B.; Shin, H.-S., Evaluation of a freshness indicator for quality of fish products during storage. *Food Science and Biotechnology* **2014,** 23 (5), 1719-1725.
55. Galgano, F.; Favati, F.; Bonadio, M.; Lorusso, V.; Romano, P., Role of biogenic amines as index of freshness in beef meat packed with different biopolymeric materials. *Food Research International* **2009,** 42 (8), 1147-1152.
56. De Meyer, T.; Hemelsoet, K.; Van Speybroeck, V.; De Clerck, K., Substituent effects on absorption spectra of pH indicators: An experimental and computational study of sulfonphthaleine dyes. *Dyes and Pigments* **2014,** 102, 241-250.
57. Gossweiler, G. R.; Hewage, G. B.; Soriano, G.; Wang, Q.; Welshofer, G. W.; Zhao, X.; Craig, S. L., Mechanochemical activation of covalent bonds in polymers with full and repeatable macroscopic shape recovery. *ACS Macro Letters* **2014,** 3 (3), 216-219.

Chapter 5. Conclusions and Future Perspective

5.1 Conclusions

This thesis presented a novel non-toxic sulfonephthalein-solvent binary thermochromic system, which shows obvious thermochromic performance controlled by the melting/freezing process. In Chapter 2, initial studies regarding the thermochromic binary system were reported. Based on the initial binary system, Chapter 3 reported a novel hydrophilic CPR-water system which was encapsulated inside a silicone shell and was demonstrated to be applicable as a non-toxic thermochromic ink or as an additive in film, both of which exhibited fully reversible thermochromism. In Chapter 4, it was reported that further development of the initial CPR-fatty acid binary system could be incorporated directly into a polymer matrix and was shown to have irreversible thermochromism. The findings outlined in this thesis represent a significant advancement in the design of simple and non-toxic thermochromic inks and films, which has the potential for a range of commercial applications such as for the next generation of intelligent food packaging materials.

Chapter 2 reported the first example of a dye-solvent binary system that shows reversible thermochromism at modest temperatures suitable for food applications. The thermochromism was shown to result from the solubility-dependent pi-pi stacked agglomeration of sulfonephthalein dyes controlled by melting/solidifying of the solvent component. The colour change was sufficiently pronounced to be observed by the naked eye. A range of solvents were used including acids, esters and alcohols with the solubility of dye in the solvent being the key factor influencing their thermochromic performance. A cell toxicity study towards NIH-3T3 cells, confirmed the sulfonephthalein dyes used in these binary systems are significantly less toxic than cyanidin chloride, the benchmark of the previously only reported non-toxic food dye, with the thermochromism based on an alternative mechanism. The mechanism of our binary system involves sulfonephthalein being dissolved and mono-dispersed in the liquid state and aggregated via pi-pi stacking in the solid state. Therefore, sulfonephthaleins also exhibited aggregachromism. Importantly, the molecules of sulfonephthalein remain in the ring-closed structural form, achieving thermochromism in solvent.

Chapter 3 presented the first example of a non-toxic thermochromic ink fabricated via a specific encapsulation method which confines the reaction to the surface of the emulsion droplets. Emulsion droplets of CPR/aqueous solutions in toluene showed noticeable thermochromism upon melting/solidifying. Microencapsulation using hydrolysis and crosslinking of OTS, created crosslinked silicone shells surrounding CPR aqueous microdroplets, which was confirmed by ATR-FTIR and SEM analysis. The optimal core-shell feed mass ratio was 20:1 based on considerations of both yield and colour contrast of thermochromism. Analysis results showed this new ink is fully reversible in regard to its thermochromic behaviour and can be screen-printed onto paper as a thermochromic image or used as additives in polymer thin films to form thermochromic sheets. Cell toxicity tests towards NIH-3T3 cells demonstrated these novel materials are non-toxic. The significance of this work is its non-toxicity as well as various forms of which this system can be applied in the next generation of intelligent food packaging materials.

Chapter 4 reported an irreversible thermochromic and halochromic sensor containing the non-toxic amphiphilic CPR-DA binary system of Chapter 2, as dispersed particles in a crosslinked PDMS polymeric film. The thermochromic performance matched the thermochromic nature of CPR-DA binary system however it differed significantly as it was irreversible. The obtained sensor exhibits irreversible thermochromic behaviour and showed potential application as a TTI, due to the gradual dissolution and diffusion of the CPR-DA binary system into the crosslinked structure of PDMS. Therefore, the sensitivity of colour response of this sensor towards temperature can be adjusted via changing the hydrophobicity of the polymeric matrix material. Irreversible halochromic behaviour of this sensor was demonstrated either by chemical addition of ammonia vapour or from bio-amines given off by degrading fish or beef. This mechanism was the result of traditional ring-opening of CPR. Therefore, these colour changing properties make this non-toxic sensor a potential candidate for the monitoring and indication of perishable food quality.

5.2 Future Perspective

In this thesis, the pi-pi stacking of sulfonephthalein in dye-solvent binary system is demonstrated by combined results from UV-Vis absorption spectra, liquid ^{1}H-NMR and molecular dynamic simulations. Direct evidence of pi-pi stacking change of sulfonephthalein between liquid and solid binary system may be provided via the analysis of results from liquid ^{13}C-NMR and solid ^{13}C-NMR. The synthesis of ^{13}C isotopic labelling sulfonephthalein could be conducted. NMR Information from the peak of centred carbon in sulfonephthalein molecule will provide direct evidence of molecular ring-opening or ring-closing during thermochromism. The growth of sulfonephthalein single crystal could be achieved in solution under non-solvent atmosphere. Single crystal analysis by X-ray crystallography may reveal more details of sulfonephthalein molecular stacking. In addition, the sulfonate group attached to a benzene ring in sulfonephthalein is crucial for the pi-pi stacking of sulfonephthalein. Therefore, it could be possible to broaden the category of aggregachromic dyes by using functionalisation strategies to replace the sulfonate group with other electron withdrawing groups.

Many types of hydrophilic components can be microencapsulated via water-in-oil-in-water (w/o/w) double emulsion methods. Therefore, the CPR-water hydrophilic binary system may also be microencapsulated through w/o/w double emulsion methods via using various of shell materials such as chitosan, xanthan gum, cellulose, gum Arabic, poly(ethylene glycol-co-lactide), PLA and PLGA. The reaction conditions need to be optimized. The leaking of core materials through these shell materials should be characterized to determine the desired shell materials. More toxicity tests including animal tests should be conducted before practical application to food packaging area. The obtained microcapsules should also be mixed with solvents, resins, lubricants, solubilizers, surfactants and other materials to be used as real inks. The formulation should be tried systematically. By controlling the size, mechanical properties and thermochromic behaviours of obtained microcapsules, the ink could be suitable for inkjet printing.

Microcapsules containing sulfonephthalein-long chain solvent binary systems may also be an achievable goal for preparation of thermochromic inks that can change colour near or above room temperature. Future work could also involve the study of the correlation between the colour responsiveness of CPR-DA-PDMS sensors and microbial growth of food as it spoils, during storage and or transport.